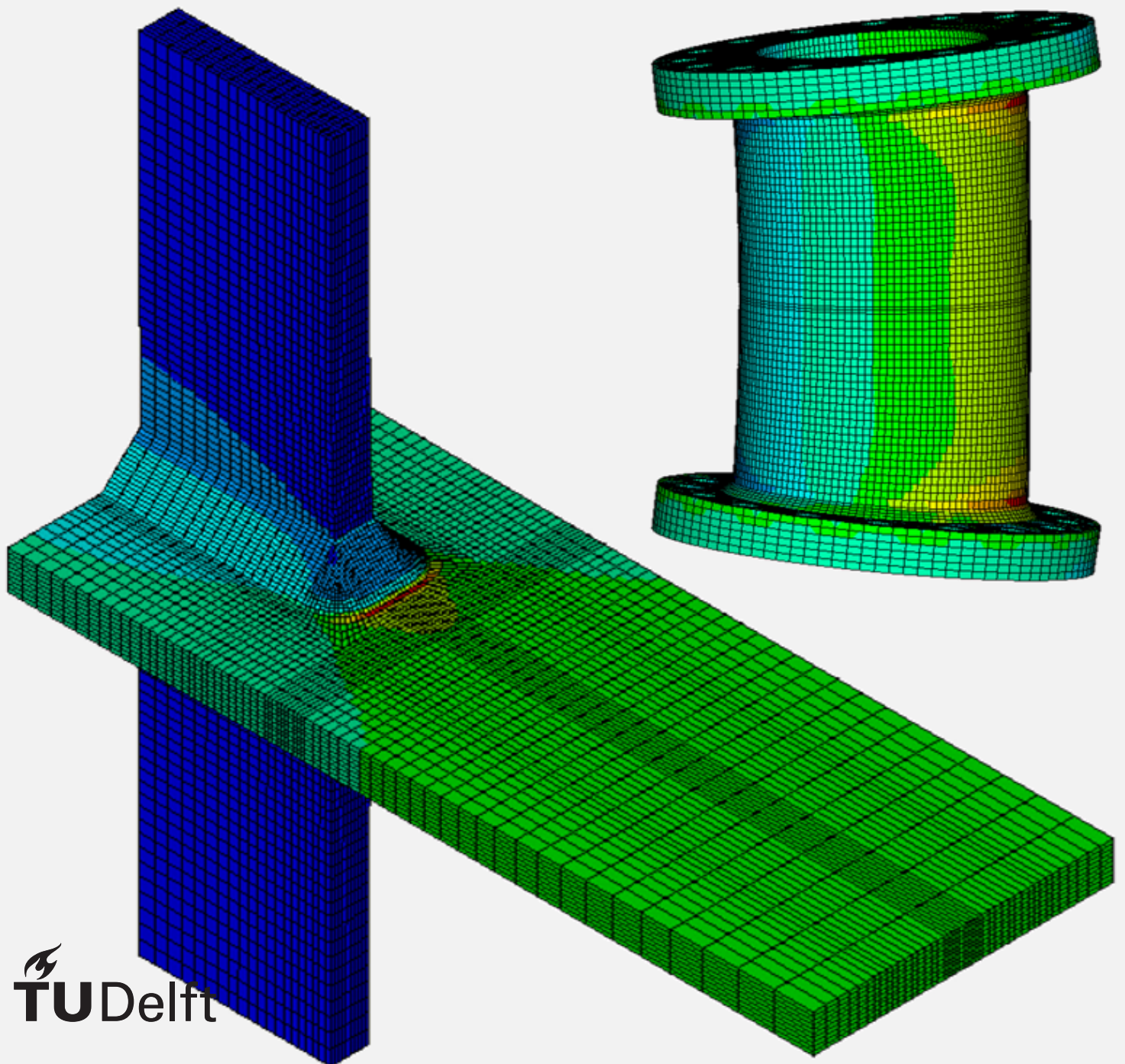


Fatigue of Welded Joints in Steel Marine Structures

Resistance of Double Sided Longitudinal Attachments and Single Sided Butt Joints ~ Design and Testing Considerations

Ho-Seung Seo



Fatigue of Welded Joints in Steel Marine Structures

Resistance of Double Sided Longitudinal Attachments and Single Sided Butt Joints ~ Design and Testing Considerations

by

Ho-Seung Seo

in partial fulfillment of the requirements for the degree of

Master of Science

in Offshore and Dredging engineering

at the Delft University of Technology

to be defended publicly on Monday 6 May, 2019

Student number : 4610059
Thesis committee : Prof. dr. ir. M.L. Kaminski , TU Delft
Dr. ir. J.H. den Besten , TU Delft
Dr. V. Popovich , TU Delft
Ir. Y. Qin , TU Delft

An electronic version of this thesis is available at <http://repository.tudelft.nl>

Contents

Acknowledgment	v
Summary	vii
Nomenclature	ix
Abbreviations	xi
1 Introduction	1
1.1 Fatigue design of double sided longitudinal attachments using a Total Stress Criterion	1
1.2 Fatigue testing of single sided butt joints using a Hexapod	3
2 Theoretical background	5
2.1 Fatigue failure fundamentals	5
2.2 V-shaped notch stress.	6
2.3 Stress intensity	7
2.4 Fatigue assessment	9
2.4.1 Nominal stress concept	9
2.4.2 Structural hot spot stress concept	9
2.4.3 Effective notch stress concept	10
2.4.4 Total stress concept	11
3 Weld notch stress and intensity of DS longitudinal attachment	13
3.1 Weld notch stress distribution	13
3.1.1 Weld load carrying stress.	17
3.1.2 Modification in weld notch stress distribution	20
3.2 Weld notch stress intensity	22
3.2.1 Modification in weld notch stress intensity	23
4 Weld load carrying estimation for DS longitudinal attachment	25
4.1 Double weld element beam model	25
4.1.1 Weld notch stress distribution	32
4.1.2 Weld notch stress intensity.	35
4.2 Parametric method	38
4.2.1 Weld notch stress distribution	40
4.2.2 Weld notch stress intensity.	43
5 Fatigue resistance of DS longitudinal attachment	47
5.1 Nominal stress concept	48

5.2	Structural hot spot stress concept	50
5.3	Total stress concept	52
6	Fatigue testing of single sided butt joints using a Hexapod	55
6.1	Riser response and critical failure location	55
6.2	Loading Condition	56
6.3	Full scale fatigue testing rig	56
6.4	Specimen Design	56
6.4.1	Specimen Design - Option 1	57
6.4.2	Specimen Design - Option 2	72
7	Conclusions	81
	Bibliography	85

Acknowledgment

Foremost, I would like to express my sincere gratitude to my advisor Dr. ir. J.H. den Besten for the continuous support of my study and research, for his patience, motivation, enthusiasm, and immense knowledge. His guidance helped me in all the time of research and writing of this thesis.

My sincere thanks also go to Ir. Y. Qin and S.S. Palkar for advising me. Every discussion with them was always helpful for me and kept motivating me. I also have to say thanks to my thesis committee members Prof. dr. ir. M.L. Kaminski and Dr. V. Popovich. Without them, my graduation could not be managed.

The completion of my master study could not have been accomplished without my best colleague Ir. Trystan van Ommen. We did all the team works together and got satisfying results every time. Also, his encouragement makes me keep moving forward. Thanks to my other foreign and Korean friends as well.

Last but not the least, I would like to give warm and sincere respect to my parents Chang-Min Seo and Seo-Hyun Ahn, for giving birth to me at the first place and supporting me spiritually throughout my life.

Ho-Seung Seo
Delft, May 2019

Summary

Fatigue failure is a governing limit state for marine structures. Marine structures are composed of the numerous structural members connected by the welded joints which are the typically governing fatigue sensitive locations. In this thesis, attention has been paid to fatigue of welded joints from design and from testing perspective. The double sided longitudinal attachment is a common structural detail in marine structures and available resistance information, SN data, has been used to investigate the life time estimate accuracy in case the total stress is adopted as fatigue damage criterion. The single sided butt joint is a common structural detail in marine structures like steel catenary risers and a specimen has been designed for testing using the Hexapod in order to ensure fatigue induced failure at the required location.

Fatigue design of double sided welded longitudinal attachments using a Total Stress criterion

The recently developed total stress concept considers both the weld notch and far field characteristic contributions. The total through-thickness weld notch stress distribution has been adopted to establish the total stress fatigue damage criterion and corresponding fatigue resistance curve. Thanks to a semi-analytical formulation, it is easy to determine the total weld notch stress distribution. The involved weld load carrying stress component is a characteristic one and unique for each weld notch location. A double weld element beam model has been developed to replace the original single weld finite element beam model in order to capture correct estimates for the double sided longitudinal attachments. Alternatively, a parametric has been established as well. The weld notch angle has turned out to be a governing parameter. Evaluation of the fatigue resistance of the welded double sided longitudinal attachment using the Total Stress concept shows a better accuracy in comparison to the nominal stress, hot spot structural stress and effective notch stress concept results. A governing factor for double sided longitudinal attachments is investigated which is the base plate thickness t_b . Although, the IIW classifies the longitudinal attachment based on the attachment length l_a , the base plate thickness t_b is much more dominant.

Fatigue testing of single sided butt joints using a Hexapod

The riser system forms a significant part of the development costs for floating offshore oil production facilities. The SCReen joint industry project aims to optimise the fatigue design and maintenance costs for Steel Catenary Risers (SCR's). Generally, published fatigue resistance data of SCR welded joints are performed using resonance bending tests, which have two major limitations: a very high mean stress state and unrealistic variable amplitude loading. In order to obtain realistic fatigue resistance data, the SCReen project plans to do the fatigue tests with the Hexapod. A dedicated specimen containing the critical single sided butt joint has been designed in order to obtain fatigue failure at the required location, involving two girth welds at the flange-pipe connection and the single sided butt joint at the middle of the specimen. With a post welding improvement, fatigue failure at the intended weld root location can be obtained.

Nomenclature

C	fatigue resistance constant
C_{bb}	weld load carrying stress coefficient under pure bending loading
C_{bm}	weld load carrying stress coefficient under pure membrane loading
C_{bw}	weld load carrying stress coefficient
K	stress intensity factor
\mathcal{L}	log-likelihood
S	stress range
S_n	nominal stress range
S_s	structural hot spot stress range
S_T	total stress range
T_S	scatter range index
Y_f	far field factor
Y_n	notch factor
a	crack size
a_i	initial defect or crack size
a_f	final crack size
f_n	applied normal force
h_w	weld leg height
l_w	weld leg length
l_a	attachment length
m_b	applied bending moment
m_{bb}	bending moment induced weld load carrying bending moment
m_{bm}	membrane force induced weld load carrying bending moment
n	elastoplasticity coefficient
r	radial coordinate
r_l	load ratio
r_s	structural bending stress ratio
t_b	base plate thickness
t_c	connecting plate thickness
t_p	plate thickness
α	half notch angle
β	stress angle
γ	load ratio coefficient
θ	angular coordinate
λ_a	first eigenvalue of anti-symmetry part
λ_s	first eigenvalue of symmetry part
μ_a	stress amplitude of anti-symmetry part
μ_s	stress amplitude of symmetry part
ρ	notch radius
σ	stress / standard deviation
σ_b	structural bending stress component
σ_m	structural membrane stress component
σ_n	weld toe notch stress distribution
σ_{rr}	radial stress component (polar coordinate)
$\sigma_{r\theta}$	shear stress component (polar coordinate)
$\sigma_{\theta\theta}$	tangential stress component (polar coordinate)
σ_s	structural stress
χ_a	first eigenvalue coefficient of anti-symmetry part
χ_s	first eigenvalue coefficient of symmetry part

Abbreviations

AW	as welded
CA	constant amplitude
CI	Confidence interval
DEC	double edge crack
DS	double sided
FAT	fatigue class
FE	finite element
FEA	finite element analysis
FEM	finite element method
FSS	full scale specimen
IIW	International Institute of Welding
LC	load carrying
MCF	medium cycle fatigue, life time range $N = O(10^4 \dots 5 \cdot 10^6)$
MLE	maximum likelihood estimate
NLC	non-load carrying
SCF	stress concentration factor
SCR	steel catenary riser
SEC	single edge crack
SIF	stress intensity factor
SS	single sided
TDP	touch down point
TS	total stress

Introduction

1.1. Fatigue design of double sided longitudinal attachments using a Total Stress Criterion

Fatigue is one of the most common failure mechanisms for the materials and structures. Especially, for the marine structures due to the operating environment (i.e. wind, wave) and even by the operation itself. Marine structures are composed of steel plates, stiffeners, trusses, frames and so on. All these components are welded together to form the marine structures. Consequently, plenty of weld seams are introduced, containing notches a.k.a. stress concentrations. It is hard to consider all the notches in marine structures, and therefore several international codes classified the typical welded joint configurations with corresponding fatigue resistance curves [18, 20]. To achieve accurate fatigue lifetime estimates for welded joints, the weld notch stress distribution is very important. At the same time, having the weld notch stress distributions for each welded joint provides an opportunity to create one fatigue resistance curve for all welded joints.

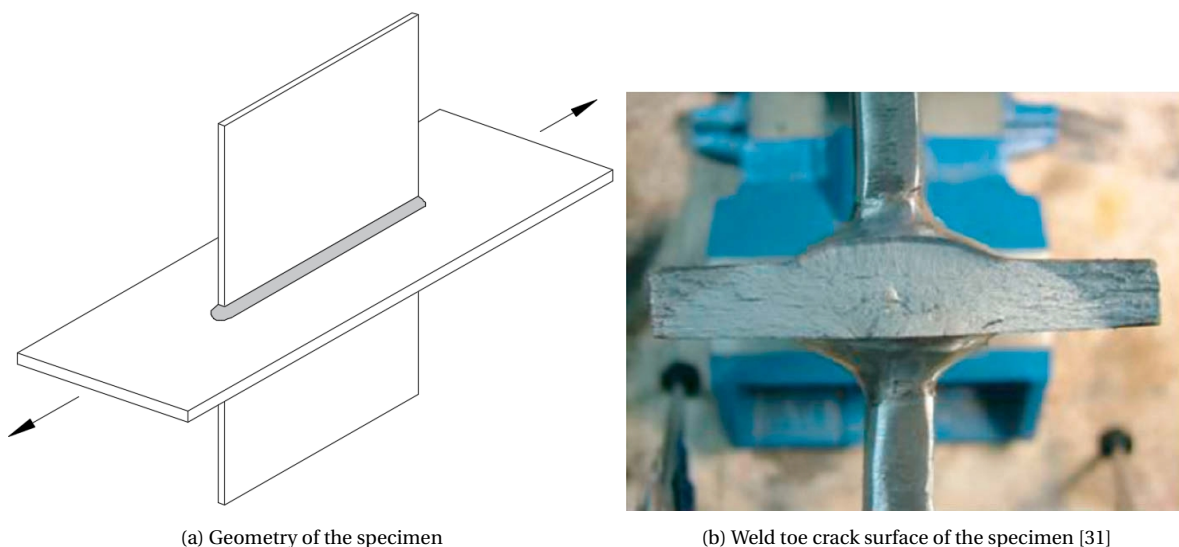


Figure 1.1: Welded double sided longitudinal attachment

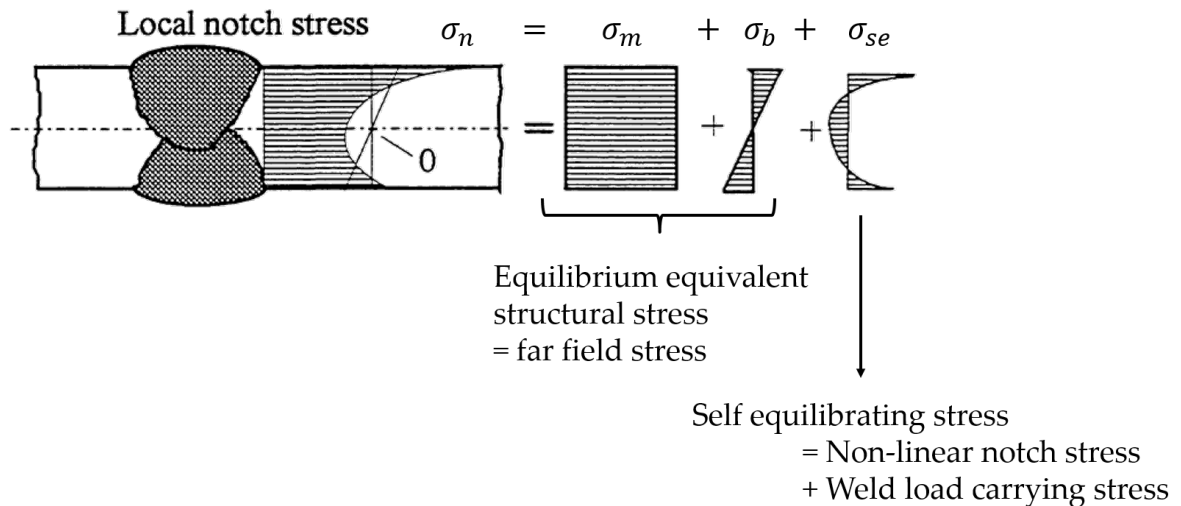


Figure 1.2: Weld notch stress distribution[37]

The weld notch stress is composed of an equilibrium equivalent part (i.e. global far field stress) and a self-equilibrating stress part (V-shaped notch stress component and a weld load carrying stress component). The global far field stress can be obtained using the mechanical loading. A V-shaped notch stress estimate can be obtained using Williams asymptotic solution [56]. Hence, only the weld load carrying stress is unknown. The existence of the weld geometry induces a bending component due to the shift of the local neutral axis. This weld load carrying stress generally affects the stress gradient near the weld notch. Correct weld load carrying stress estimates directly leads to full weld notch stress distribution along the thickness. Of course, using FE solid model could give accurate results but it takes time to build proper FE model and for the computation. Qin et al. presented a double weld element beam model for the double sided T-joint which provides pretty accurate weld notch stress distributions and stress intensity distributions [45]. Recently the governing parameter for the weld load carrying stress is also proposed [44]. In this report, similar work is done for the welded double sided longitudinal attachment; another common structural detail which represents the hot spot type 'a'. The weld load carrying stress result from the simple FE beam model and the parametric study are compared to FE solid model results for reference. Then the weld notch stress distribution and stress intensity can be determined for all different geometric dimensions by using Den Besten's semi-analytical formulations[9]. The fatigue lifetime estimation can be improved with adopting these precise stress distribution and stress intensity by using the recently developed Total Stress concept [9].



(a) Longitudinal stiffener and bracket with toe crack



(b) FPSO topside support

Figure 1.3: Hot spot type 'a' in marine structures [13]

1.2. Fatigue testing of single sided butt joints using a Hexapod

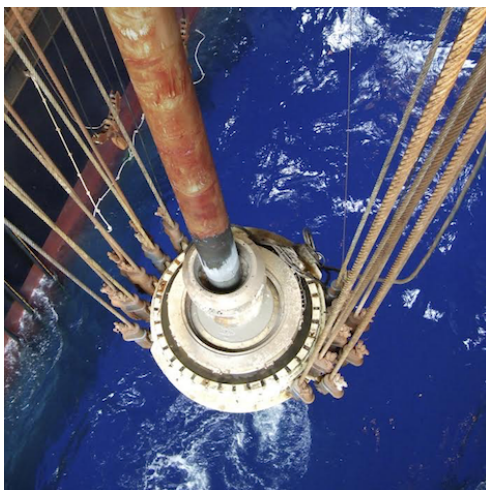
The competitive oil and gas exploration market conditions require lower and optimised project costs. Aim of the SCReen joint industry project is to optimise the costs of the riser system, which forms a significant part of the development costs of the floating production facility.

There are essentially two types of risers: the steel catenary riser (SCR) and the flexible riser. The SCReen project focuses on steel catenary risers due to the better cost-efficiency. The application of a steel catenary riser greatly reduces the production and installation cost of the riser system compared to the flexible riser. The steel catenary riser also has some advantages with respect to high temperature and high pressure applications, in comparison to the flexible riser showing limitations in that respect.

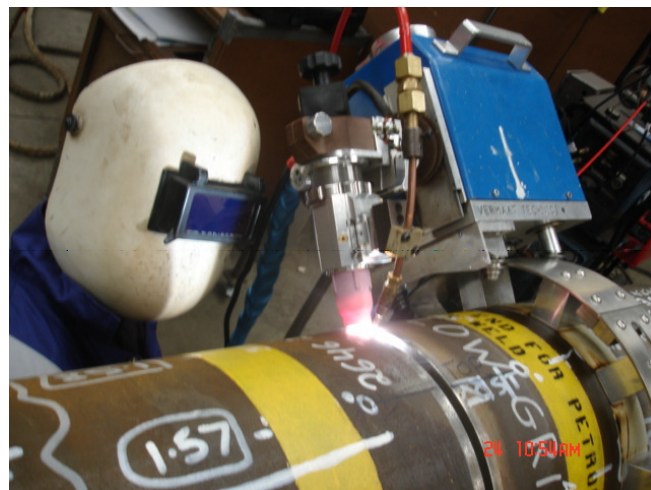
However, an SCR system has a critical drawback compared to the flexible riser system: the critical fatigue resistance. The fatigue behaviour is a governing criterion for the selection of the riser system in the design stage. Hence, the SCR system is limited to deeper water and the shallower water reflecting more rough sea states is predominantly occupied by the more expensive flexible riser system. Apart from the sea state, the type of vessel is also a condition for the selection of the riser system. Because the vessel motions depend on the type of the vessel, ship-shaped floating structures such as an FPSO which has large vessel motions has the higher fatigue loading at the riser system, meaning the use of SCR's is limited for this type of marine structures. Consequently, the SCR is more popular with motion optimized vessels like TLP's and Spars. There are modified SCR configurations like the steep wave, lazy wave etc. providing somewhat reduced fatigue loading, but these configurations require much more cost to install and repair the buoyancy modules. And additional riser length is also needed.

Improving the fatigue life estimation for SCR's will directly expand the application window towards shallower water, in more harsh sea environment and also with large motion vessels. This will be helpful for the lifetime extension of the existing SCR projects. Therefore the goal of the SCReen project is to increase the SCR application window, particularly the free hanging configuration and allow for lifetime extension of the existing SCR's.

The resonance bending test is commonly used for fatigue testing of the governing single sided butt joint of the riser pipe due to the advantage of the high test frequency. However, a resonance bending test has two major limitations: a very high mean stress state and unrealistic variable amplitude loading [40]. In the SCReen project testing with the Hexapod is envisaged, solving the resonance bending test disadvantages. However, a dedicated specimen design is required. In this report, the full scale specimen (FSS) design for the single sided welded joint at the SCR touch down point (TDP) will be proposed and investigated.



(a) Riser pipe with tensioner [1]



(b) Riser girth welding [50]

Figure 1.4: Riser pipe in marine structures

2

Theoretical background

In this chapter, the fundamental theories will be introduced briefly related to main topics of this thesis.

2.1. Fatigue failure fundamentals

The term *fatigue* refers to gradual degradation and eventual failure that occur under loads which vary with time, cyclic in nature, and which are lower than the static strength of the metallic specimen, component or structure concerned [43].

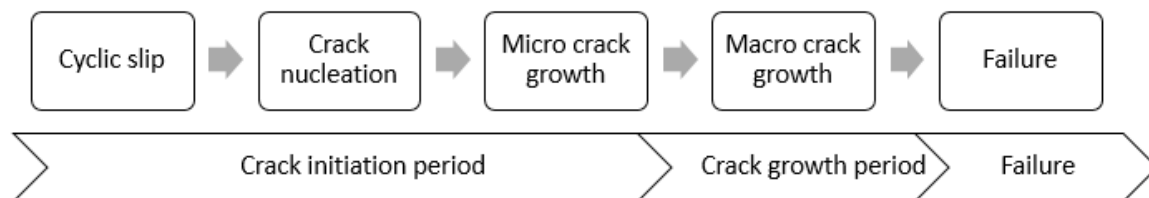


Figure 2.1: Different phases of the fatigue life [47]

The fatigue life is usually split into a crack initiation period and a crack growth period. This is because different mechanisms are dominating for these two stages.

In the crack initiation period, the low cyclic stress which is below the yield stress causes microplasticity in a grain level. Especially a surface has a lower constraint than the material below and micro-plastic deformation preferably occurs at such a location which causes slip on the surface. Due to cyclic loading, the continuous slip occurs and then the cyclic slip band appears which contains intrusions. This intrusion is already a micro stress concentrator for the material and triggers the microcrack nucleation. After microcrack nucleation, the microcrack grows through the grain boundaries. The crack initial period is supposed to be completed when microcrack growth is no longer dependent on the material surface conditions.

The crack growth period starts when the damage process starts to depend on the material bulk property like Young's modulus of material [47]. At the starting stage of the crack growth, the crack grows stable. If the crack growth rate becomes unstable then finally fracture occurs. The typical three crack surface displacements namely mode I (Opening), mode II (Sliding) and mode III (Tearing) are shown as below.

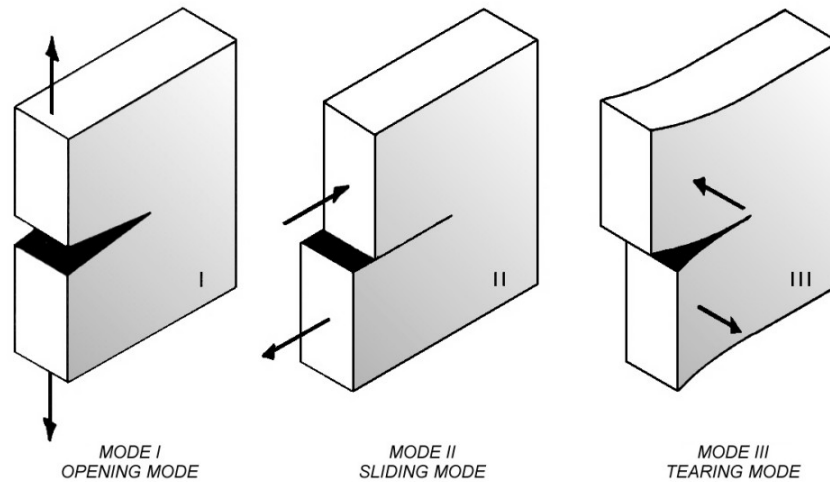


Figure 2.2: Crack surface displacement modes [22]

In reality, the estimation of exact crack initiation and crack growth period is a challenge due to their randomness [10]. The crack initiation is a material surface related phenomenon which often includes initial inclusions, voids, pores, etc. due to various reasons such as welding and imperfect manufacture. The material bulk property is also random for crack growth phenomenon. Consequently, there are still many problems to predict the exact fatigue life of structures.

2.2. V-shaped notch stress

The weld toe geometry of welded joints such as butt joint, T-joint, cruciform joint, etc. can be assumed as V-shaped notch. The linear elastic stress distribution near the V-shaped notch has been introduced by Williams with notch radius $\rho = 0$ [56]. Due to the sharp notch shape, the stress field is singular close to the notch tip, and the singular exponent depends on the notch angle α .

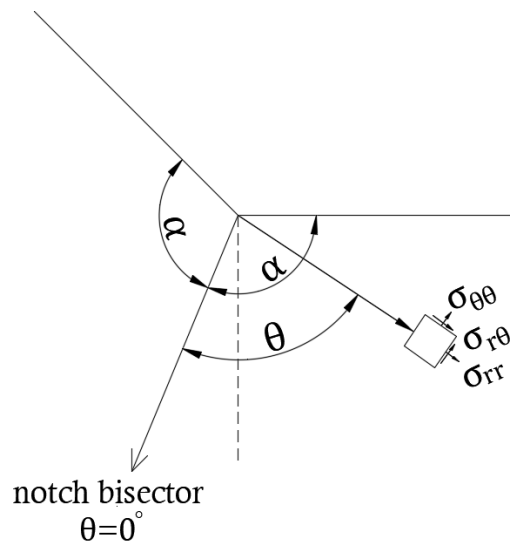


Figure 2.3: V-shaped notch geometry and stress components

The airy stress function with traction free surface boundary conditions are used. Non-trivial solution conditions show that the singular exponent λ is governed by notch angle α .

$$\lambda_s(2\alpha) + \sin(\lambda_s 2\alpha) = 0 \quad (2.1)$$

$$\lambda_a(2\alpha) - \sin(\lambda_a 2\alpha) = 0 \quad (2.2)$$

Index s and a refer to the symmetric (Mode I) and anti-symmetric (Mode II) respectively. Stress components near the V-shaped notch in polar coordinate system are given by [9]:

$$\sigma_{rr} \left(\frac{r}{t_b} \right) = -\sigma_s \left\{ \left(\frac{r}{t_b} \right)^{\lambda_s-1} \mu_s \lambda_s [(\lambda_s + 1) \cos\{(\lambda_s + 1)\theta\} - \chi_s (\lambda_s - 3) \cos\{(\lambda_s - 1)\theta\}] + \right. \\ \left. \left(\frac{r}{t_b} \right)^{\lambda_a-1} \mu_a \lambda_a [(\lambda_a + 1) \sin\{(\lambda_a + 1)\theta\} - \chi_a (\lambda_a - 3) \sin\{(\lambda_a - 1)\theta\}] \right\} \quad (2.3)$$

$$\sigma_{\theta\theta} \left(\frac{r}{t_b} \right) = \sigma_s \left\{ \left(\frac{r}{t_b} \right)^{\lambda_s-1} \mu_s \lambda_s (\lambda_s + 1) [\cos\{(\lambda_s + 1)\theta\} - \chi_s \cos\{(\lambda_s - 1)\theta\}] + \right. \\ \left. \left(\frac{r}{t_b} \right)^{\lambda_a-1} \mu_a \lambda_a (\lambda_a + 1) [\sin\{(\lambda_a + 1)\theta\} - \chi_a \sin\{(\lambda_a - 1)\theta\}] \right\} \quad (2.4)$$

$$\sigma_{r\theta} \left(\frac{r}{t_b} \right) = \sigma_s \left\{ \left(\frac{r}{t_b} \right)^{\lambda_s-1} \mu_s \lambda_s [(\lambda_s + 1) \cos\{(\lambda_s + 1)\theta\} - \chi_s (\lambda_s - 1) \cos\{(\lambda_s - 1)\theta\}] + \right. \\ \left. \left(\frac{r}{t_b} \right)^{\lambda_a-1} \mu_a \lambda_a [(\lambda_a + 1) \sin\{(\lambda_a + 1)\theta\} - \chi_a (\lambda_a - 1) \sin\{(\lambda_a - 1)\theta\}] \right\} \quad (2.5)$$

with symmetric and anti-symmetric eigenvalue coefficients

$$\chi_s = \frac{\cos\{(\lambda_s + 1)\alpha\}}{\cos\{(\lambda_s - 1)\alpha\}}$$

$$\chi_a = \frac{\sin\{(\lambda_a + 1)\alpha\}}{\sin\{(\lambda_a - 1)\alpha\}}$$

The V-shaped notch stress only considers local geometry effect of the sharp notch. Therefore, additional stress components such as far-field stress and weld load carrying stress have to be involved for the accurate stress distribution near the weld toe.

2.3. Stress intensity

The stress intensity concept is related to crack damaged geometry meaning it is important to crack growth analysis. The stress intensity factor (SIF), K , is the factor that indicates magnitudes of crack tip stresses. The SIF is quite different from the SCF. In the case of the SCF, it only depends on local geometry changes while the SIF depends on the loading condition as well. Therefore, there are different SIFs for different modes in Figure 2.2. The point is that the SIF is an excellent parameter to represent crack damaged geometry behaviour.

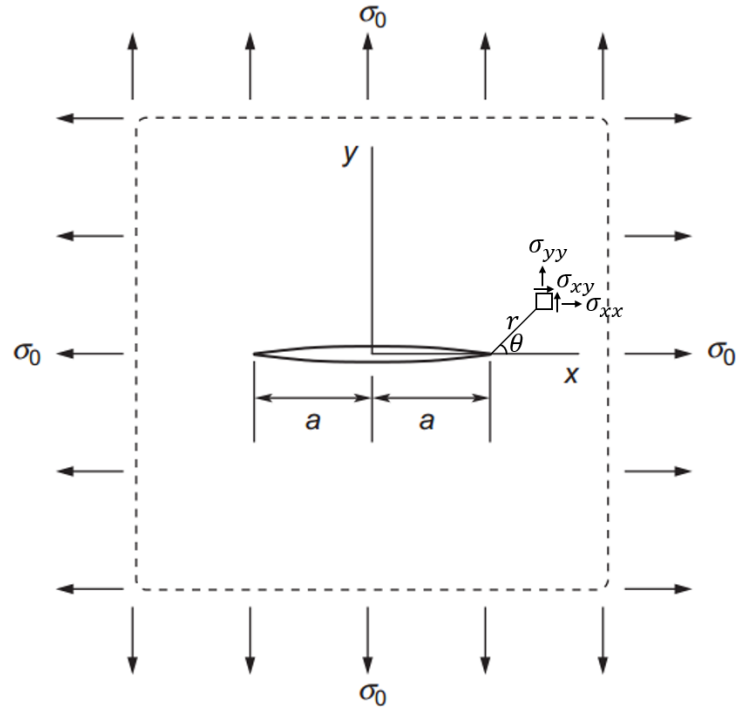


Figure 2.4: A crack in an infinite elastic plane subjected to mode I biaxial tension [51]

Most dominant mode I SIF relating the crack opening is shown as below.

$$K_I = \sigma_0 \sqrt{\pi a} \quad (2.6)$$

$$\sigma_{xx} = \frac{K_I}{\sqrt{2\pi r}} \cos \frac{1}{2}\theta \left(1 - \sin \frac{1}{2}\theta \sin \frac{3}{2}\theta \right) \quad (2.7)$$

$$\sigma_{yy} = \frac{K_I}{\sqrt{2\pi r}} \cos \frac{1}{2}\theta \left(1 + \sin \frac{1}{2}\theta \sin \frac{3}{2}\theta \right) \quad (2.8)$$

$$\sigma_{xy} = \frac{K_I}{\sqrt{2\pi r}} \sin \frac{1}{2}\theta \cos \frac{1}{2}\theta \cos \frac{3}{2}\theta \quad (2.9)$$

From the Equation 2.6, it is easy to see the SIF is a function of far-field stress, σ_0 , and crack length, a , hence the SIF is crack damaged parameter.

There is also a similar concept with SIF called notch stress intensity factor (NSIF) [29, 30]. The NSIF has a difference with SIF by considering notched geometry than cracked geometry. Therefore NSIF can be used as intact geometry parameter of the notched structure such as welded structure which means the predicting crack initiation period could be done with NSIF [3].

2.4. Fatigue assessment

Various fatigue assessment methods have been developed over time. These can be classified according to governing parameters representative for the fatigue behaviour. Typically, three types of the parameter can be adopted: stress, strain or energy. From among these, the most widespread method is the stress based method which is comparing design stress with allowable stresses by means of stress-life curves called S-N curve and also known as Whöller curve [6].

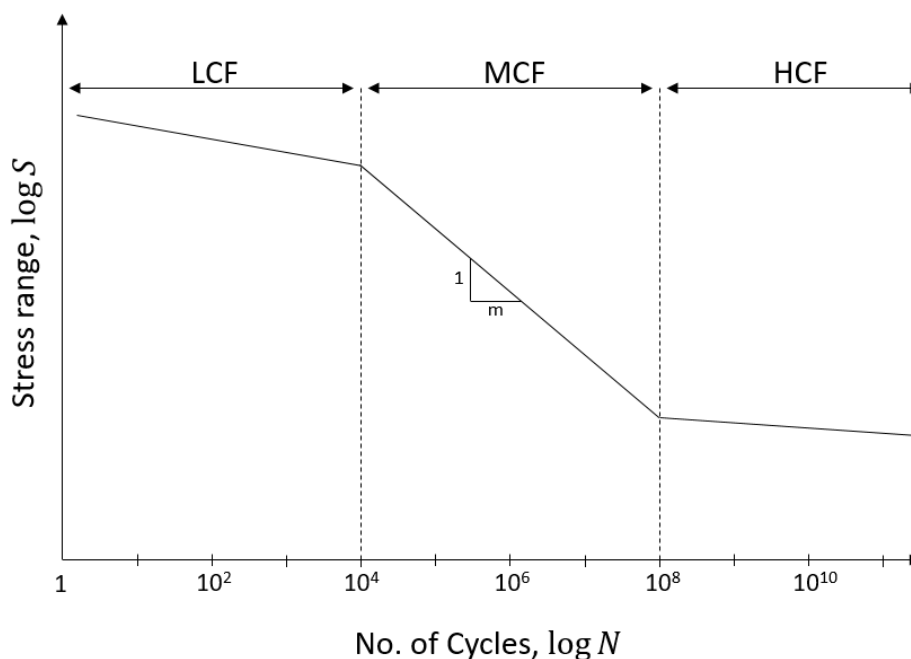


Figure 2.5: Schematic plot of S-N curve

Generally, Basquin type of single slope relation at the medium cycle fatigue(MCF) region is adopted.

$$\log N = \log C - m \log S \quad (2.10)$$

This S-N curve can be based on the various parameters a.k.a damage criteria such as nominal stress, structural hot spot stress, effective notch stress and so on. These parameters generally depend on the level of local information consideration.

2.4.1. Nominal stress concept

Nominal stress is the stress calculated in the sectional area under consideration, disregarding the local stress raising effects of the welded joint, but including the stress raising effects of the macro-geometric shape of the component in the vicinity of the joint e.g. large cutouts [20]. The nominal stress considers only global intact geometry; it presumes global elastic behaviour. Consequently, the nominal stress concept is relatively easy to use but limited to the complex structures. Constant amplitude fatigue resistance information of commonly used structural details can be obtained from international codes for example FATigue classes of IIW recommendation and CATegories of Eurocodes [18, 20].

2.4.2. Structural hot spot stress concept

For the welded structures, attached structural components by the weld induce stress concentrations which are the fatigue sensitive. The structural hot spot stress concept considers these stress concentrations by assuming the major part of a lifetime is related to crack initiation rather than crack growth, i.e. at the weld notch affected region [8, 20, 38]. The concept named as 'hot spot' because of the local temperature rise produced by cyclic plastic deformation prior to crack initiation [46]. There are three types of hot spots in welded structures. The types of hot spots in welded structures are shown in Figure 2.6.

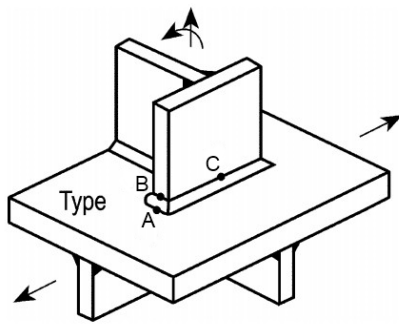


Figure 2.6: Types of hot spots in welded structures [19]

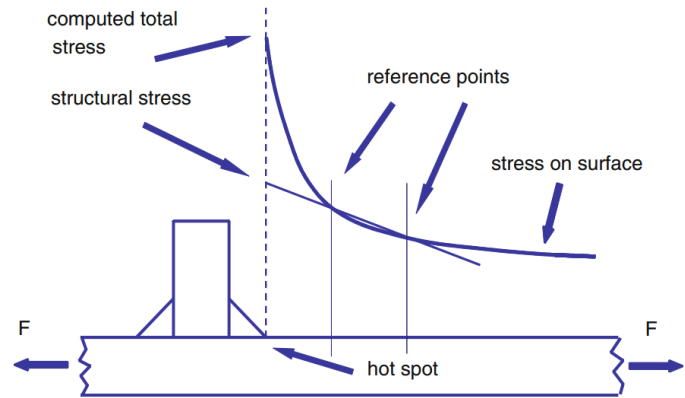


Figure 2.7: Structural hot spot stress by the surface extrapolation method [20]

The structural or geometric stress at the hot spot includes all stress raising effects of a structural detail without consideration of the local weld profile itself [20, 38]. The structural hot spot stress is a combination of membrane and bending stresses and it obeys a linear through-thickness distribution. Since the real hot spot structure is impossible to measure exactly, empirical engineering formulae are used to calculate the structural hot spot stress by taking the results of strain gauges in an experiment or finite element analysis. The engineering formulae are based on extrapolation of the stresses near the hot spot as shown below. However, considering local parameter structural hot spot stress as governing for fatigue life means this concept assumes the major part of a lifetime is related to crack initiation rather than crack growth.

$$\text{Linear extrapolation : } \sigma_{hs} = 1.67\sigma_{0.4t} - 0.67\sigma_{1.0t} \quad (2.11)$$

$$\text{Quadratic extrapolation : } \sigma_{hs} = 2.52\sigma_{0.4t} - 2.24\sigma_{0.9t} + 0.72\sigma_{1.4t} \quad (2.12)$$

From the above equations, t denotes base plate thickness. Depending on the geometry, t can be artificial thickness such as hot spot type B. Linear extrapolation is suitable for non-load carrying geometry and quadratic extrapolation is suitable for load carrying geometry.

Although the surface extrapolation is the most common method to evaluate the structural hot spot stress, it has a weakness of the mesh sensitivity in FE analysis. Hence, other mesh insensitive methods are investigated by researchers. Dong presented mesh insensitive through thickness linearization method and virtual node method [14, 16]. Xiao proposed to use the stress of 1 mm below the surface to calculate the structural hot spot stress [57].

2.4.3. Effective notch stress concept

From the nominal and structural hot-spot stress concepts, some amount of the geometric effect to stress changes are considered but the local notch effect is still not included. The fatigue strength of a structural component depends heavily on its notch effects. Notch effect means both stress concentration and strength reduction due to the existence of notches [46]. In reality, the notched geometry in the structural component is much more frequent than just plane geometry, therefore, the fatigue strength of plane geometry is less critical than the fatigue strength of the notched geometry which depends on shape and size of notches. Also, the theoretical stress concentration is not sufficient to welded geometry, meaning the effective notch stress can show a better result than the previous two concepts.

The as-welded notch radius is close to zero ($\rho \rightarrow 0$), so the singularity makes it impossible to predict proper stress at the notch. Different microstructural notch support hypotheses exist; the stress averaging approach initially proposed by Neuber [36] and the critical distance approach proposed by Peterson [42]. Here the stress averaging approach is considered. Effective notch stress is the total stress at the root of a notch by considering a fictitious notch radius. The fictitious notch radius, ρ_f , is determined considering average stress over micro-structural support length, ρ^* , and microstructural support factor, s , a function of the mode ratio and the notch opening angle [4]. Therefore, effective notch stress concept involves the influence of the stress

gradient at the notch. There are major two reference radii 1.00mm for thickness $t \geq 5\text{mm}$ and 0.05mm for $t < 3\text{mm}$ [48].

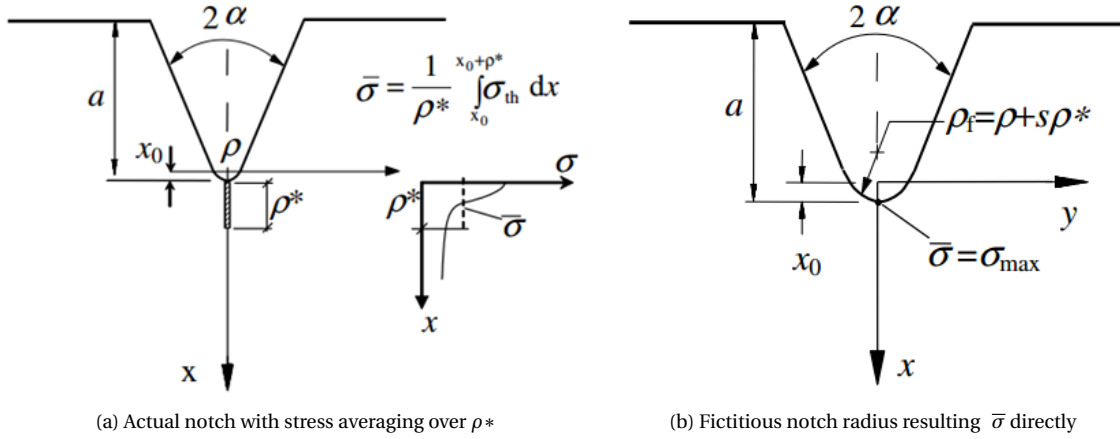


Figure 2.8: Effective notch stress concept [5]

2.4.4. Total stress concept

Den Besten proposed total stress fatigue damage criterion S_T which is an area equivalent line criterion [9]. Welded joint inevitably involves flaws and defects at the weld toe and root notches due to the imperfect welding process. Naturally, the crack growth behaviour governs the fatigue damage at these welded notches. Both the notch affected micro and far-field dominated macro crack growth which are related to the stress intensity also known as the crack driving force are considered in total stress concept. The effective structural stress range $\Delta\sigma_s / (1 - r_l)^{1-\gamma}$ and scaling parameter $t_b^{2-m/2m}$ for the size effect are taken into account as well.

$$S_T = \frac{\Delta\sigma_s}{(1 - r_l)^{1-\gamma} \cdot I_N^{\frac{1}{m}} \cdot t_b^{\frac{2-m}{2m}}} \quad (2.13)$$

with

$$I_N = \int_{\frac{a_i}{t_b}}^{\frac{a_f}{t_b}} \frac{1}{\left\{ Y_n \left(\frac{a}{t_b} \right) \right\}^n \cdot \left\{ Y_f \left(\frac{a}{t_b} \right) \right\}^m \cdot \left(\frac{a}{t_b} \right)^{\frac{m}{2}}} d \left(\frac{a}{t_b} \right) \quad (2.14)$$

The total stress parameter S_T contains more local notch effect than the other concepts. Therefore, it could provide better fatigue resistance estimation. However, it is inevitable that the more local geometric information could give not only more accuracy but also the more complexity.

3

Weld notch stress and intensity of DS longitudinal attachment

For the fatigue analysis, not only the peak stress value but also the stress gradient is required mainly for the size effect[47]. Consequently, the complete stress distribution is essential for precise fatigue life estimation. As previously shown in Figure 1.2, the total stress distribution at the weld notch is assumed to be a linear superposition of the equilibrium equivalent part(i.e. global far field stress) and the self-equilibrating stress part(V-shaped notch stress component and the weld load carrying stress component) [9, 37].

3.1. Weld notch stress distribution

Whatever the amount of weld penetration is and the local geometry is some extent the weld is inevitably load carrying. Therefore evaluating the amount of the weld load carrying stress could help to get correct stress distribution at the weld notches.

The welded double sided longitudinal attachment is a typical welded joint type representing the hot spot type 'a' in marine structures, for instance, a bracket on the longitudinal stiffener. Due to local geometry changes, highly stressed fatigue sensitive locations appear at the weld toe. Base plate loaded situation will be considered meaning the weld toe notches are critical to fatigue failure.

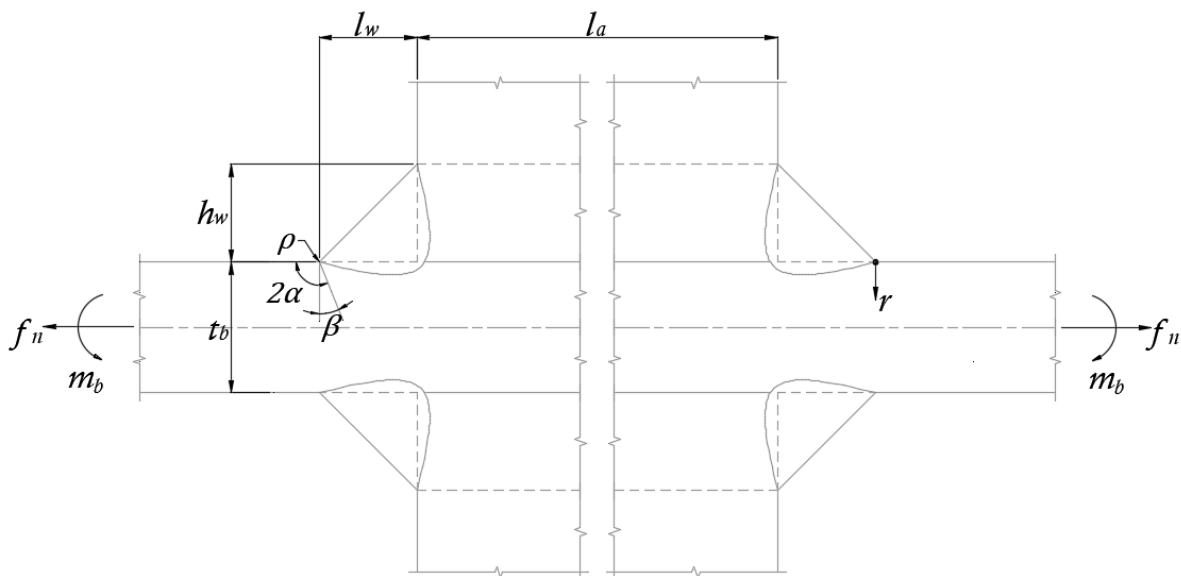


Figure 3.1: DS longitudinal attachment geometry

$$\sigma_n \left(\frac{r}{t_b} \right) = \sigma_s \left(\left[1 - 2r_s \left\{ 1 - f \left(\frac{r}{t_b} = \frac{1}{2} \right) \right\} \right] f \left(\frac{r}{t_b} \right) + r_s \left\{ 2f \left(\frac{r}{t_b} = \frac{1}{2} \right) - 1 \right\} \left[\left\{ 1 - f \left(\frac{r}{t_b} = \frac{1}{2} \right) \right\} - 2 \left(\frac{r}{t_b} \right) \right] \right) \quad (3.1)$$

with

$$f \left(\frac{r}{t_b} \right) = \left(\frac{r}{t_b} \right)^{\lambda_s - 1} \mu_s \lambda_s (\lambda_s + 1) [\cos\{(\lambda_s + 1)\beta\} - \chi_s \cos\{(\lambda_s - 1)\beta\}] + \left(\frac{r}{t_b} \right)^{\lambda_a - 1} \mu_a \lambda_a (\lambda_a + 1) [\sin\{(\lambda_a + 1)\beta\} - \chi_a \sin\{(\lambda_a - 1)\beta\}] + C_{bw} \left\{ 4 \left(\frac{r}{t_b} \right) - 1 \right\} \forall \left\{ 0 \leq \left(\frac{r}{t_b} \right) \leq \frac{1}{2} \right\} \quad (3.2)$$

and

$$f \left(\frac{r}{t_b} = \frac{1}{2} \right) = \frac{(\lambda_a - \lambda_s)(\lambda_s \lambda_a - 2C_{bw})}{\lambda_a(\lambda_a - 1) - \lambda_s(\lambda_s - 1)} + C_{bw} \quad (3.3)$$

The semi-analytic formulas of the weld not stress distribution for the non-symmetric and symmetric geometry are given by Den Besten [9]. Weld notch stress formula for the symmetric welded joint, see Equation 3.1, is composed of symmetric and anti-symmetric V-shaped notch stress term $(r/t_b)^{\lambda_s - 1}(\cdot)$ and $(r/t_b)^{\lambda_a - 1}(\cdot)$ and the weld load carrying stress term $C_{bw}(\cdot)$. Weld load carrying stress $C_{bw}\{4(r/t_b) - 1\}$ contains linear symmetric bending with respect to $t_b/2$. The eigenvalues λ_s and λ_a , the eigenvalue coefficients χ_s and χ_a and the stress angle $\beta = (\alpha - \pi/2)$ are notch opening angle α dependent. Coefficients μ_s and μ_a are determined from the force, moment equilibrium and symmetric condition.

$$\mu_s = \frac{\left(\frac{1}{2} \right) \lambda_a (\lambda_a - 1) + C_{bw}}{C_s [\cos\{(\lambda_s + 1)\beta\} - \chi_s \cos\{(\lambda_s - 1)\beta\}]} \quad (3.4)$$

$$\mu_a = \frac{\left(\frac{1}{2} \right) \lambda_s (\lambda_s - 1) + C_{bw}}{C_a [\cos\{(\lambda_a + 1)\beta\} - \chi_a \cos\{(\lambda_a - 1)\beta\}]} \quad (3.5)$$

with

$$C_s = \left(\frac{1}{2} \right)^{\lambda_s} (\lambda_s + 1) \{ \lambda_a (\lambda_a - 1) - \lambda_s (\lambda_s - 1) \} \quad (3.6)$$

$$C_a = \left(\frac{1}{2} \right)^{\lambda_a} (\lambda_a + 1) \{ \lambda_a (\lambda_a - 1) - \lambda_s (\lambda_s - 1) \} \quad (3.7)$$

and

$$\chi_s = \frac{\cos\{(\lambda_s + 1)\alpha\}}{\cos\{(\lambda_s - 1)\alpha\}} \quad (3.8)$$

$$\chi_a = \frac{\sin\{(\lambda_a + 1)\alpha\}}{\sin\{(\lambda_a - 1)\alpha\}} \quad (3.9)$$

Finite Element model

For reference, FE results are adopted. A 3D geometric effect causes the stress concentration at the weld toe of the DS longitudinal attachments; hot spot type 'a'. However, this 3D effect can be considered with the appropriate SCF, so adopting the 2D plane model is enough.

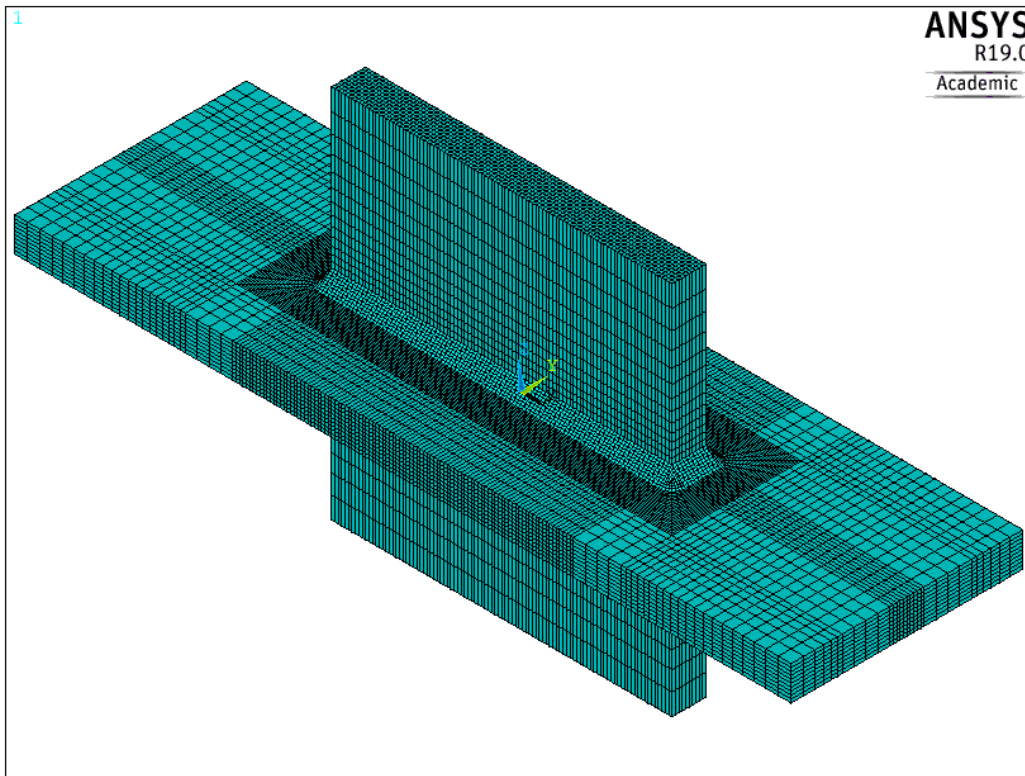


Figure 3.2: FE solid model

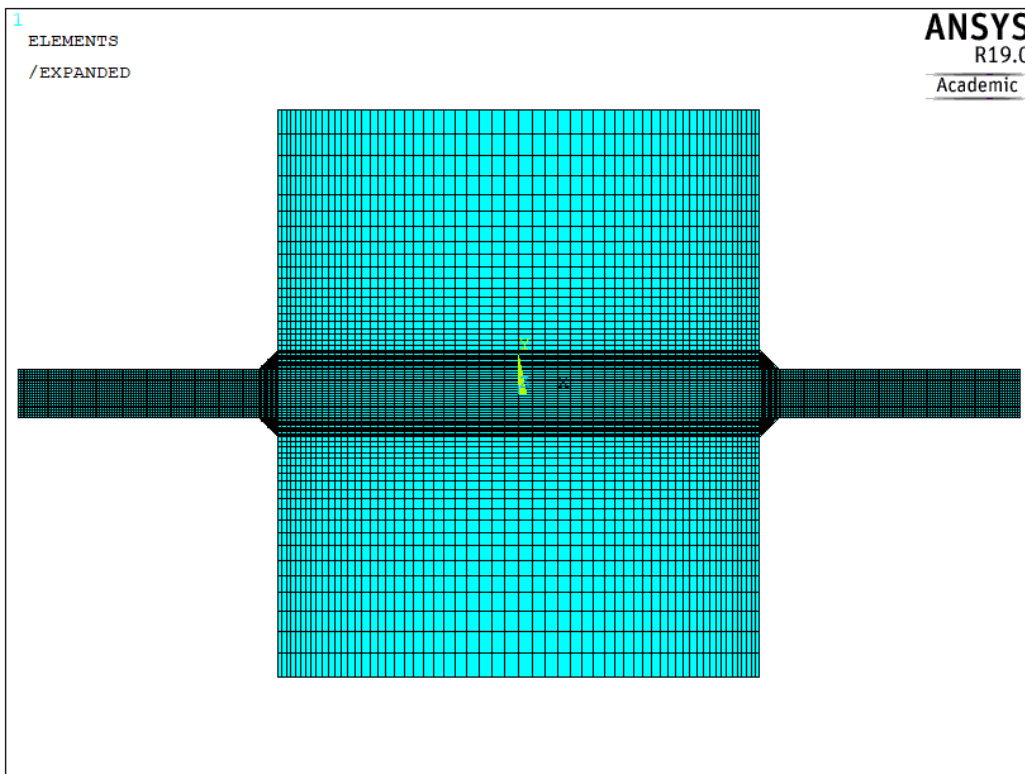


Figure 3.3: FE plane model

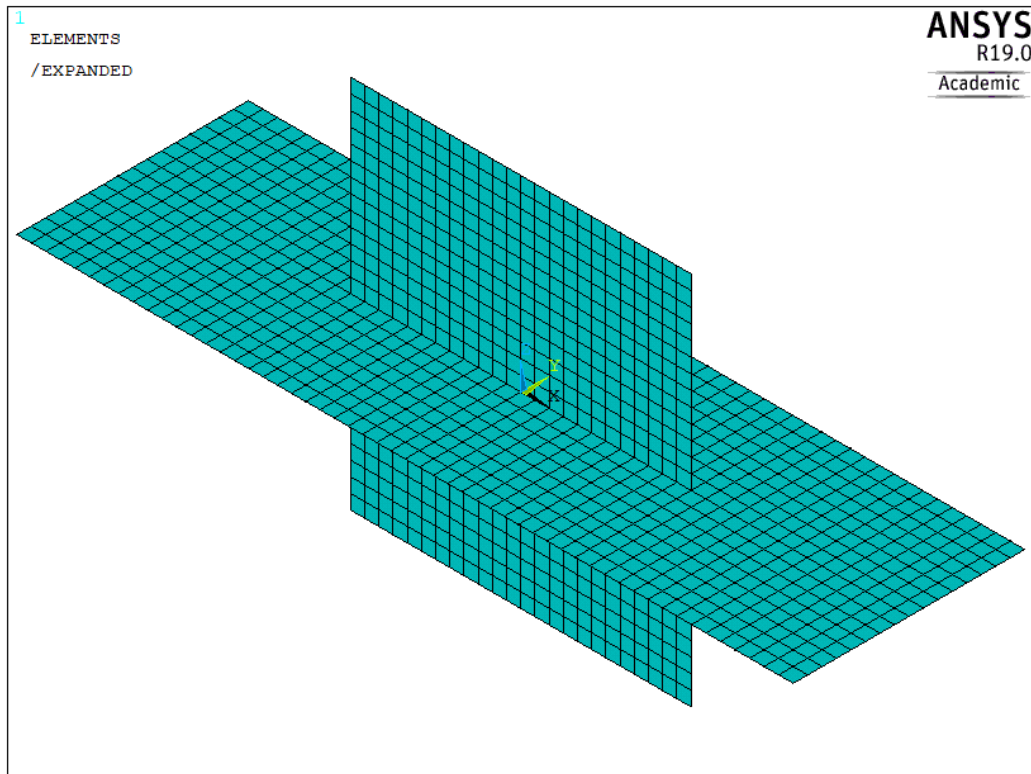


Figure 3.4: FE shell model

Comparing the weld toe stress distribution between the 3D solid element and 2D plane element with the SCF from the shell element is shown in figure 3.5. For the accuracy, two solid models are used one for the partial penetration (PP) weld and another for the full penetration (FP) weld. Exactly the same results are shown meaning using the 2D plane a.k.a. 2D solid element is appropriate for the real weld toe stress distribution of the DS longitudinal attachment.

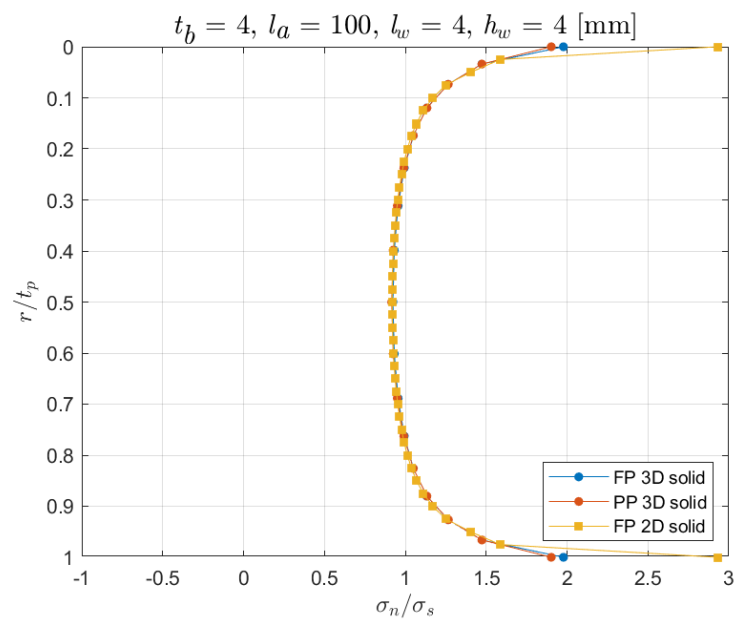


Figure 3.5: Weld toe stress distribution comparison between 2D solid(plane element) and 3D solid

3.1.1. Weld load carrying stress

Weld causes local geometry change which shifts a neutral axis. As a result bending response appears. Weld load carrying coefficient C_{bw} is defined to recognise the amount of the weld load carrying stress compared to the structural stress meaning C_{bw} is the weld load carrying proportion to the structural stress, i.e. $C_{bw} = 0.1$ equals 10% of structural stress is applied to the weld itself. Weld load carrying amount is very important because it directly affects the fatigue life of the structures. For instance, IIW recommendation categorised the fatigue life of the structures depending on the non-load carrying(NLC) and load carrying(LC) which are judged by engineers but C_{bw} shows the real amount of the weld load carrying stress. The weld load carrying stress $\sigma_s C_{bw}$ is assumed to be a linear superposition of a membrane and bending stress induced component:

$$\begin{aligned}\sigma_s C_{bw} &= \sigma_m C_{bm} + \sigma_b C_{bb} \\ &= \sigma_s \{C_{bm} - r_s(C_{bm} - C_{bb})\}\end{aligned}\quad (3.10)$$

with

$$C_{bm} = \frac{m_{bm}}{\sigma_s(1 - r_s)} \left(\frac{6}{t_b^2} \right) \quad (3.11)$$

and

$$C_{bb} = \frac{m_{bb}}{\sigma_s r_s} \left(\frac{6}{t_b^2} \right) \quad (3.12)$$

Bending moments m_{bm} and m_{bb} can be estimated by using a FE beam model. Alternatively, proposed parametric formulas can be used to get C_{bm} and C_{bb} , see Chapter 4.

The weld notch affected zone size depends on the local weld geometry and the loading. Therefore, just adjusting the weld load carrying stress in the analytic formula, Equation 3.1, does not affect the notch affected zone size but the stress gradient near the notch. Increase of C_{bw} induces higher stress near the notch namely decrease of stress gradient but less stress away from the weld notch. Following figures show the effect of C_{bw} value for the non-symmetric DS T-joint and symmetric DS longitudinal attachment. Here the symmetric means the symmetry w.r.t the half of the base plate thickness ($r/t_b = 1/2$). Three C_{bw} values are shown, i.e. 0, fitted value and higher than fitted value. The fitted value indicates the numerically fitted value of the C_{bw} to the solid FE results.

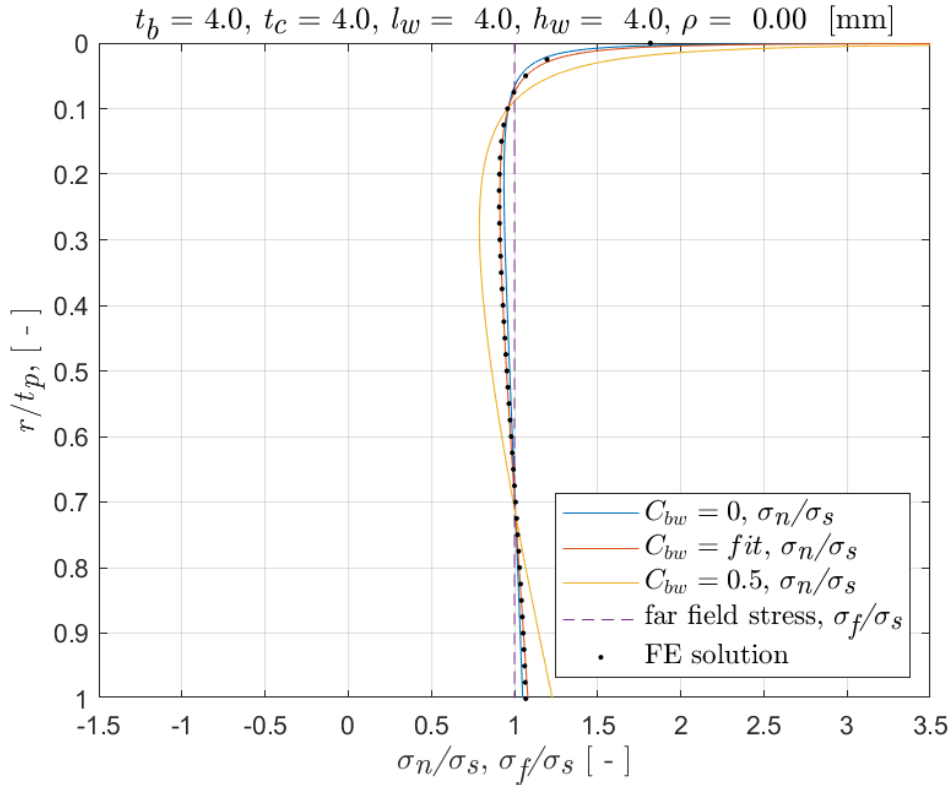
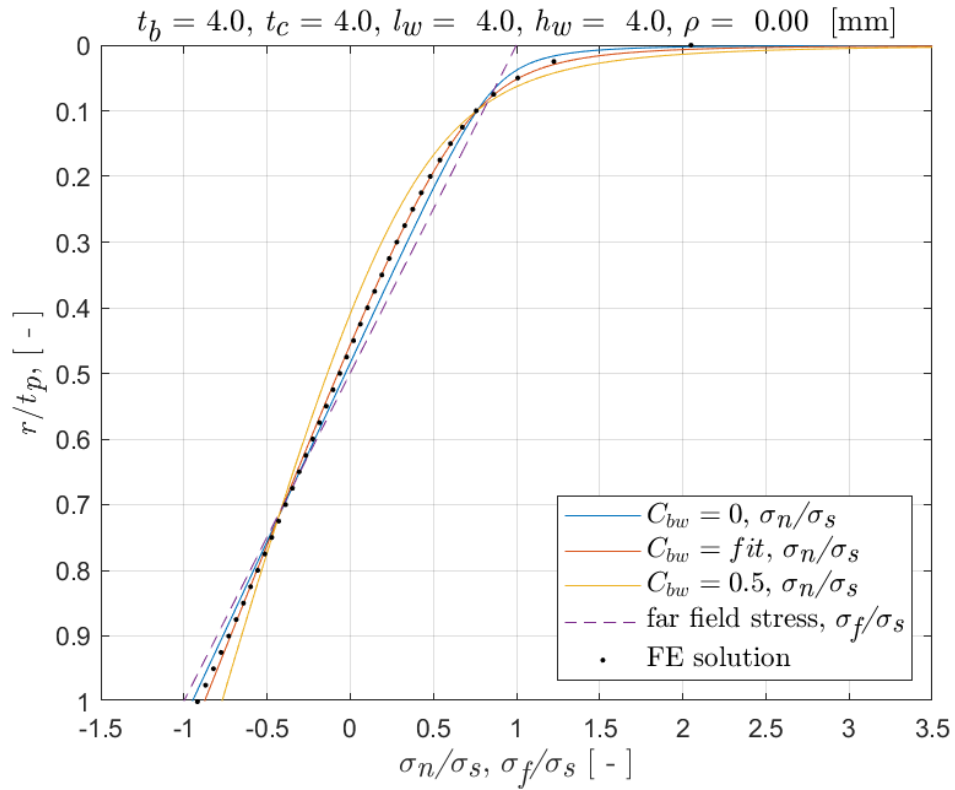
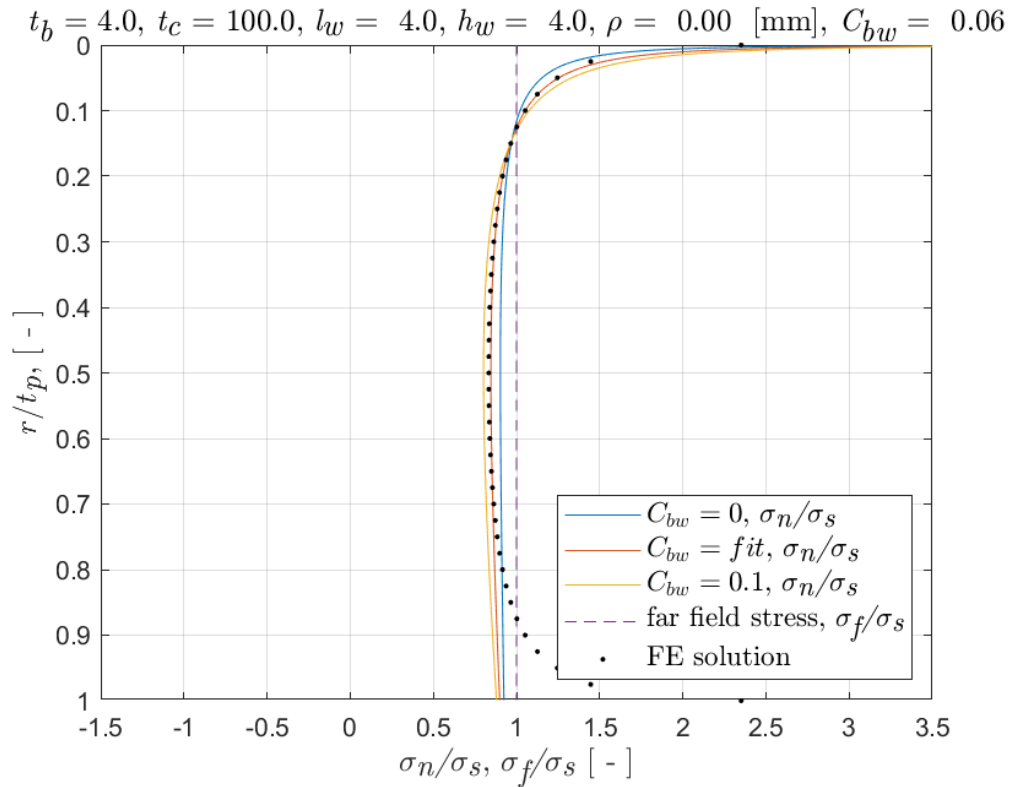


Figure 3.6: C_{bw} effect for the DS T-joint under membrane loading ($r_s = 0$)

Figure 3.7: C_{bw} effect for the DS T-joint under membrane loading ($r_s = 0$)Figure 3.8: C_{bw} effect for the DS longitudinal attachment under membrane loading ($r_s = 0$)

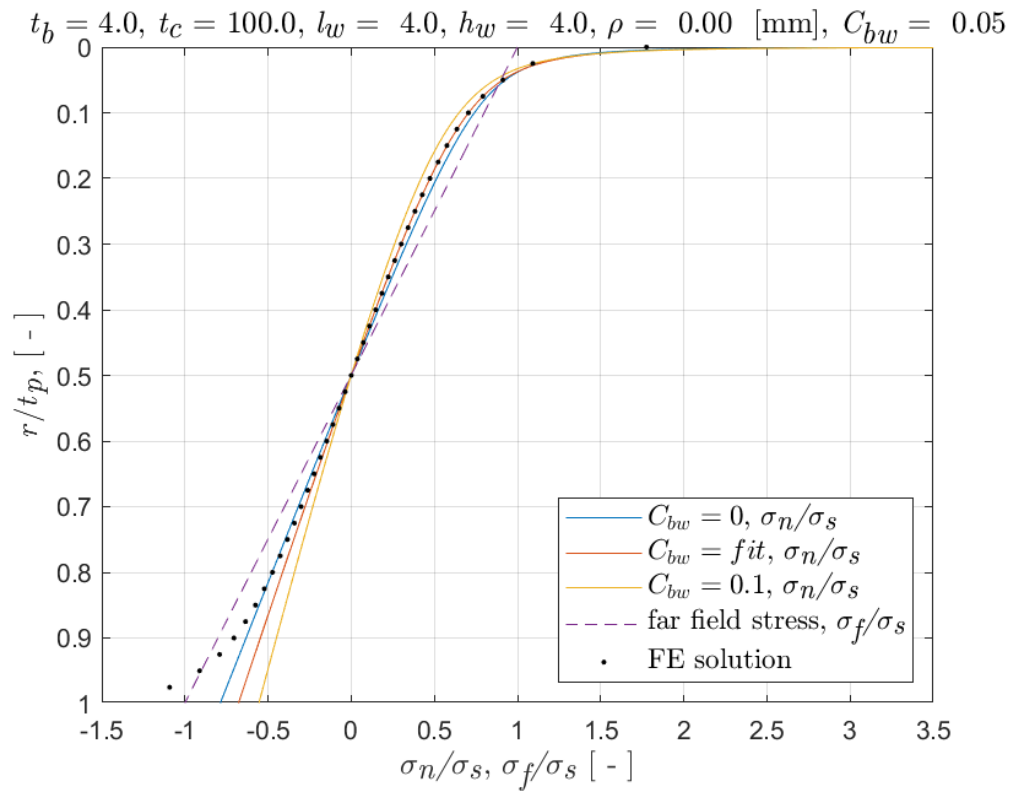


Figure 3.9: C_{bw} effect for the DS longitudinal attachment under bending loading ($r_s = 1$)

However, the symmetric bending stress distribution shows a different behaviour with changing C_{bw} . Because the symmetric bending stress distribution is determined from the symmetric membrane stress distribution by shifting and scaling for the similarity of the formulas [9]. It provides approximately good results but has a problem of the weld notch affected zone size change with the value of C_{bw} . Hence, another scaling factor which can give better stress distribution is proposed in the following section.

3.1.2. Modification in weld notch stress distribution

Den Besten's semi-analytic weld notch stress distribution for the symmetric geometry gives a good result but has a problem of the notch affected zone size change with the C_{bw} in the bending stress distribution part. Shifting and scaling of the membrane stress distribution for the symmetric geometry are used for the bending stress distribution. The original scaling factor was defined from the condition that the stress gradient at the half of the base plate thickness ($r/t_b = 1/2$) is equal to the gradient of the far field bending stress distribution. This stress gradient condition at the $r/t_b = 1/2$ is not true, see Figure 3.10. Here, a new scaling factor is proposed to improve the formula.

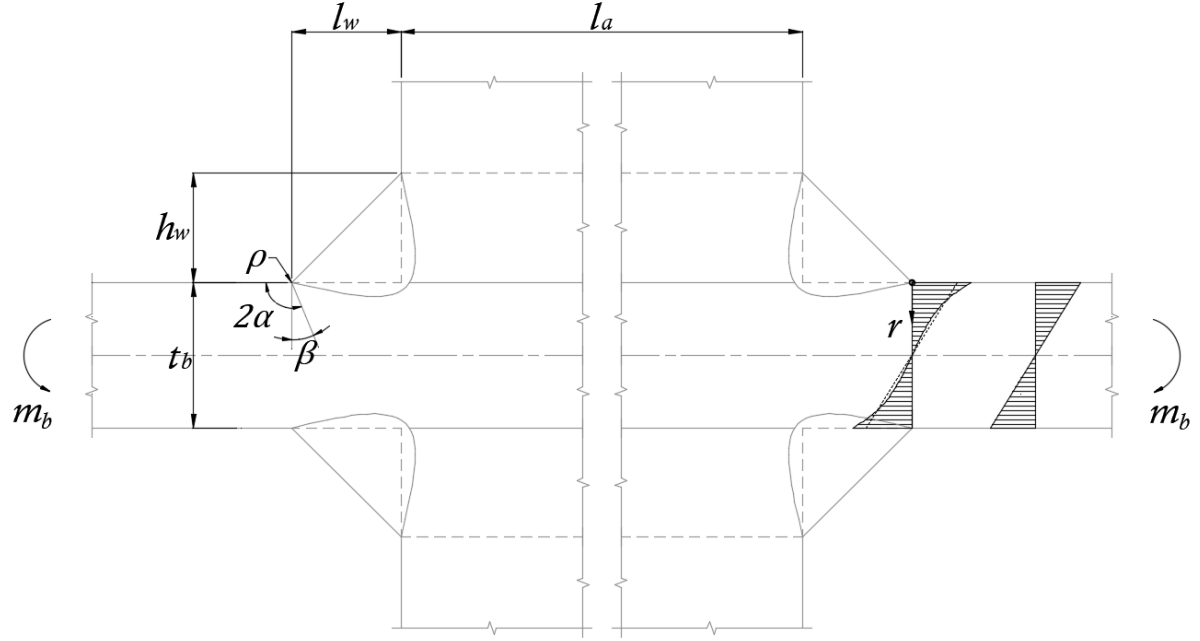


Figure 3.10: DS longitudinal attachment under bending moment. Bending stress gradient at $\left(\frac{r}{t_b} = \frac{1}{2}\right)$ is not same as far field one.

Assuming there is a scaling factor P that makes the stress distribution of the shifted membrane stress distribution to the bending stress distribution.

$$\sigma_{nb} = \sigma_s \cdot P \cdot \left[f\left(\frac{r}{t_b}\right) + \left\{1 - f\left(\frac{r}{t_b} = \frac{1}{2}\right)\right\} - 2\left(\frac{r}{t_b}\right) \right] \quad (3.13)$$

Then the scaling factor can be solved by taking force equilibrium.

$$\int_0^{\frac{1}{2}} \left\{ \sigma_{nb} \left(\frac{r}{t_b}\right) \right\} d\left(\frac{r}{t_b}\right) = \int_0^{\frac{1}{2}} \sigma_s \left\{ 1 - 2r_s \left(\frac{r}{t_b}\right) \right\} d\left(\frac{r}{t_b}\right) \quad (3.14)$$

$$P = \frac{1}{4 \left(C_{11} \mu_s + C_{22} \mu_a - \frac{1}{2} C_{bw} + \frac{1}{4} \right)} \quad (3.15)$$

with

$$C_{11} = \left(\frac{1}{2}\right)^{\lambda_s} (\lambda_s + 1) [\cos\{(\lambda_s + 1)\beta\} - \chi_s \cos\{(\lambda_s - 1)\beta\}] \quad (3.16)$$

$$C_{12} = \left(\frac{1}{2}\right)^{\lambda_a} (\lambda_a + 1) [\cos\{(\lambda_a + 1)\beta\} - \chi_s \cos\{(\lambda_a - 1)\beta\}] \quad (3.17)$$

The eigenvalues $\lambda_{\{s,a\}}$, eigenvalue coefficients $\chi_{\{s,a\}}$ and stress angle β are weld notch opening angle α dependent. The amplitude $\mu_{\{s,a\}}$ are the result of force, moment equilibrium and symmetric condition.

The obtained scaling factor P is slightly high for the correct weld notch stress distribution. Therefore, a small modification is done. The new scaling factor P is:

$$P = \left\{ \frac{1}{4 \left(C_{11}\mu_s + C_{22}\mu_a - \frac{1}{2}C_{bw} + \frac{1}{4} \right)} \right\}^{1.3} \quad (3.18)$$

Only the scaling factor is changed from $\{2f(r/t_b = 1/2) - 1\}$ to P therefore it is possible to use original form of the semi-analytic formula, Equation 3.1.

$$\sigma_n \left(\frac{r}{t_b} \right) = \sigma_s \left([1 - r_s \{1 - P\}] f \left(\frac{r}{t_b} \right) + r_s P \left[\left\{ 1 - f \left(\frac{r}{t_b} = \frac{1}{2} \right) \right\} - 2 \left(\frac{r}{t_b} \right) \right] \right) \quad (3.19)$$

with

$$P = \left\{ \frac{1}{4 \left(C_{11}\mu_s + C_{22}\mu_a - \frac{1}{2}C_{bw} + \frac{1}{4} \right)} \right\}^{1.3}$$

and

$$f \left(\frac{r}{t_b} \right) = \left(\frac{r}{t_b} \right)^{\lambda_s - 1} \mu_s \lambda_s (\lambda_s + 1) [\cos\{(\lambda_s + 1)\beta\} - \chi_s \cos\{(\lambda_s - 1)\beta\}] + \left(\frac{r}{t_b} \right)^{\lambda_a - 1} \mu_a \lambda_a (\lambda_a + 1) [\sin\{(\lambda_a + 1)\beta\} - \chi_a \sin\{(\lambda_a - 1)\beta\}] + C_{bw} \left\{ 4 \left(\frac{r}{t_b} \right) - 1 \right\} \forall \left\{ 0 \leq \left(\frac{r}{t_b} \right) \leq \frac{1}{2} \right\}$$

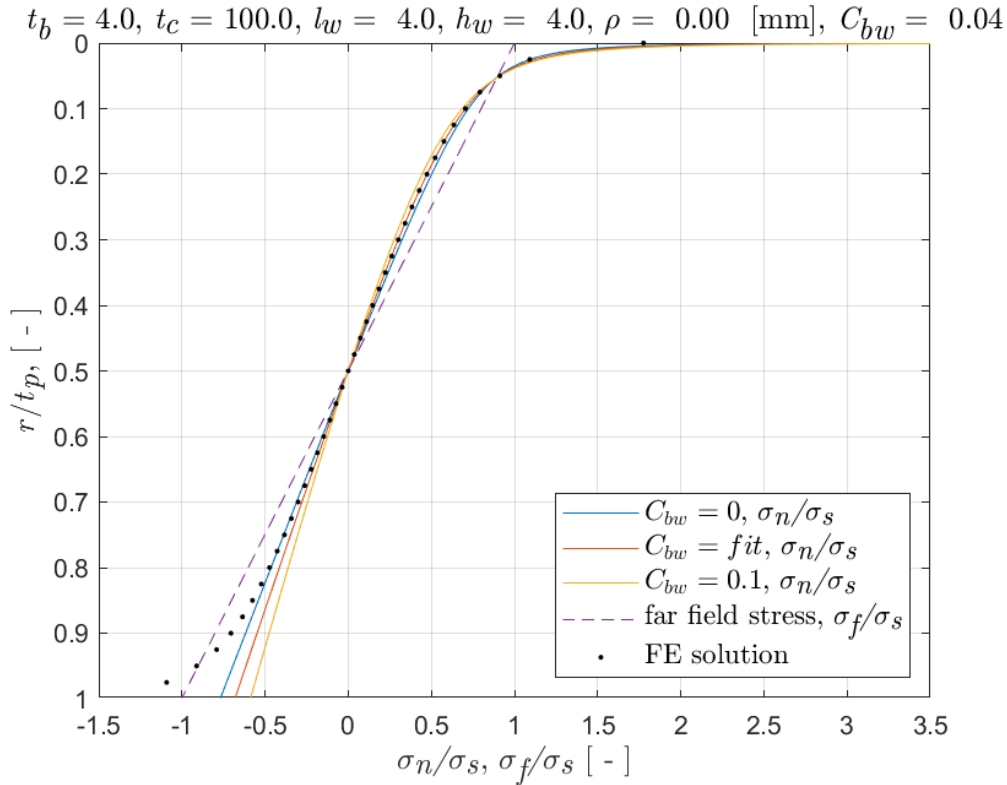


Figure 3.11: Modified weld notch stress distribution and the effect of C_{bw} ($r_s = 1$)

The scaling factor is only involved in the bending stress component. Therefore, the same membrane stress distribution can be obtained by Equation 3.19. Now the change of weld load carrying level C_{bw} only affects the stress gradient and does not affect the weld notch affected zone size.

3.2. Weld notch stress intensity

Crack growth is governed by crack driving force namely stress intensity of the crack tip. Base on the loading condition it can be varying which mode is important. However mode I opening condition is the most common and effective to the crack growing at the weld toe. Mode I stress intensity factor for the crack is:

$$K_I = (2\pi)^{1-\lambda_1} \lim_{r' \rightarrow 0^+} \{(r')^{1-\lambda_1} \sigma_{\theta\theta}(r', \theta = 0)\} \\ = \sigma_s \sqrt{\pi a} \quad (3.20)$$

Equation 3.20 is defined from the crack in an infinite plane. Therefore it does not involve the effect of global and local geometry which amplifies the stress. Taking weight functions Y_f and Y_n can involve this geometric information. Far field factor Y_f is relating to mechanical loading and crack damaged geometry effects. Notch factor Y_n incorporates the effects of weld geometry and singular notch behaviour [9].

$$K_I = \sigma_s Y_n Y_f \sqrt{\pi a} \quad (3.21)$$

The DS longitudinal attachment has a symmetric weld geometry, but it does not mean the double edge crack occurs at both weld toes symmetry to the half of plate thickness, $t_b/2$. Because of the randomness of weld quality, surface condition, etc. generally single edge crack appears because the crack always appears at the weakest location. Therefore the handbook solution far field factor Y_f for the SEC can be adopted[52]:

$$Y_f = Y_{fm} - r_s(Y_{fm} - Y_{fb}) \quad (3.22)$$

with

$$Y_{fm} \left(\frac{a}{t_b} \right) = \sqrt{\frac{2}{\pi} \tan \left(\frac{\pi}{2} \cdot \frac{a}{t_b} \right)} \cdot \frac{0.752 + 2.20 \left(\frac{a}{t_b} \right) + 0.370 \left\{ 1 - \sin \left(\frac{\pi}{2} \cdot \frac{a}{t_b} \right) \right\}^3}{\sqrt{\frac{a}{t_b} \cos \left(\frac{\pi}{2} \cdot \frac{a}{t_b} \right)}} \quad (3.23)$$

$$Y_{fb} \left(\frac{a}{t_b} \right) = \sqrt{\frac{2}{\pi} \tan \left(\frac{\pi}{2} \cdot \frac{a}{t_b} \right)} \cdot \frac{0.923 + 0.199 \left\{ 1 - \sin \left(\frac{\pi}{2} \cdot \frac{a}{t_b} \right) \right\}^4}{\sqrt{\frac{a}{t_b} \cos \left(\frac{\pi}{2} \cdot \frac{a}{t_b} \right)}} \quad (3.24)$$

The notch factor Y_n for the symmetric weld geometry can be determined by adopting the self equilibrating stress component as unit face traction [9]:

$$Y_n \left(\frac{a}{t_b} \right) = \left(\frac{2}{\pi} \right) \left(\left[1 - 2r_s \left\{ 1 - f \left(\frac{a}{t_b} = \frac{1}{2} \right) \right\} \right] f \left(\frac{a}{t_b} \right) + \right. \\ \left. r_s \left\{ 2f \left(\frac{a}{t_b} = \frac{1}{2} \right) - 1 \right\} \left[\left\{ 1 - f \left(\frac{a}{t_b} = \frac{1}{2} \right) \right\} \left(\frac{\pi}{2} \right) - \right. \right. \right. \\ \left. \left. \left. 2 \left(\frac{a}{t_b} \right) \right] + 2r_s \left(\frac{a}{t_b} \right) \right) \right) \quad (3.25)$$

with

$$f \left(\frac{a}{t_b} \right) = \left(\frac{a}{t_b} \right)^{\lambda_s - 1} \mu_s \left(\frac{\sqrt{\pi}}{2} \right) \frac{\Gamma \left(\frac{\lambda_s}{2} \right)}{\Gamma \left(\frac{\lambda_s + 1}{2} \right)} \lambda_s (\lambda_s + 1) [\cos \{ (\lambda_s + 1) \beta \} - \\ \chi_s \cos \{ (\lambda_s - 1) \beta \}] + \\ \left(\frac{a}{t_b} \right)^{\lambda_a - 1} \mu_a \left(\frac{\sqrt{\pi}}{2} \right) \frac{\Gamma \left(\frac{\lambda_a}{2} \right)}{\Gamma \left(\frac{\lambda_a + 1}{2} \right)} \lambda_a (\lambda_a + 1) [\sin \{ (\lambda_a + 1) \beta \} - \\ \chi_a \sin \{ (\lambda_a - 1) \beta \}] + \\ C_{bw} \left\{ 4 \left(\frac{a}{t_b} \right) - \frac{\pi}{2} \right\} \quad (3.26)$$

and

$$f\left(\frac{a}{t_b} = \frac{1}{2}\right) = f\left(\frac{r}{t_b} = \frac{1}{2}\right) = \frac{(\lambda_a - \lambda_s)(\lambda_s \lambda_a - 2C_{bw})}{\lambda_a(\lambda_a - 1) - \lambda_s(\lambda_s - 1)} + C_{bw} \quad (3.27)$$

It has to be noticed that the weld notch stress intensity factor from intact geometry related self equilibrating stress is not perfect but provides a good estimate because the stress intensity is relating the crack damaged geometry. Only weld load carrying stress coefficient C_{bw} is an unknown for the weld notch stress intensity factor where the others are defined from the loading condition and local geometry.

3.2.1. Modification in weld notch stress intensity

The weld notch stress intensity also has to be changed because the notch factor Y_n is defined by the self-equilibrating stress σ_{se} [9]. The change of the scaling factor in bending stress component changes the Y_n in the same perspective as the weld notch stress distribution.

$$Y_n\left(\frac{a}{t_b}\right) = \left(\frac{2}{\pi}\right) \left([1 - r_s \{1 - P\}] f\left(\frac{a}{t_b}\right) + r_s P \left[\left\{ 1 - f\left(\frac{a}{t_b} = \frac{1}{2}\right) \right\} \left(\frac{\pi}{2}\right) - 2\left(\frac{a}{t_b}\right) \right] + 2r_s \left(\frac{a}{t_b}\right) \right) \quad (3.28)$$

with

$$P = \left\{ \frac{1}{4 \left(C_{11}\mu_s + C_{22}\mu_a - \frac{1}{2}C_{bw} + \frac{1}{4} \right)} \right\}^{1.3}$$

and

$$\begin{aligned} f\left(\frac{a}{t_b}\right) = & \left(\frac{a}{t_b}\right)^{\lambda_s-1} \mu_s \left(\frac{\sqrt{\pi}}{2}\right) \frac{\Gamma\left(\frac{\lambda_s}{2}\right)}{\Gamma\left(\frac{\lambda_s+1}{2}\right)} \lambda_s(\lambda_s+1) [\cos\{(\lambda_s+1)\beta\} - \\ & \chi_s \cos\{(\lambda_s-1)\beta\}] + \\ & \left(\frac{a}{t_b}\right)^{\lambda_a-1} \mu_a \left(\frac{\sqrt{\pi}}{2}\right) \frac{\Gamma\left(\frac{\lambda_a}{2}\right)}{\Gamma\left(\frac{\lambda_a+1}{2}\right)} \lambda_a(\lambda_a+1) [\sin\{(\lambda_a+1)\beta\} - \\ & \chi_a \sin\{(\lambda_a-1)\beta\}] + \\ & C_{bw} \left\{ 4\left(\frac{a}{t_b}\right) - \frac{\pi}{2} \right\} \end{aligned} \quad (3.29)$$

Remarks

However, the original semi-analytic formula only has a small difference to the FE results at the weld notch angle h_w/l_w smaller than 1. The effect of the weld load carrying coefficient C_{bw} at such low weld notch angle is quite small. So, using the original formula is still acceptable because the modified formula is more complex and providing a small improvement.

4

Weld load carrying estimation for DS longitudinal attachment

4.1. Double weld element beam model

Originally a single weld element beam model was developed to estimate the weld load carrying coefficient C_{bw} , see Figure 4.1. There is a reason why the beam model is adopted because the FE beam model does not contain the physics of non-linear notch stress a.k.a. V-shaped notch stress which has the singularity behaviour. On the other hand, the FE solid model always provides the final stress results involving non-linear notch stress and weld load carrying stress. Also, the FE beam model is simple and easy to model with programming languages such as MATLAB.

The single weld element beam model has a limitation that unavailable to estimate the required m_{bm} and m_{bb} trends for all changing geometry dimensions [9]. To overcome this limitation, Qin et al. proposed a double weld element beam model for the DS T-joint [45]. The double weld element beam model takes two parallel weld elements which have half throat size respectively to prevent overestimated stiffness of the weld.

The geometry of the DS longitudinal attachment can be assumed as DS cruciform joint with a very thick connecting plate. From this perspective, DS longitudinal attachment beam model is modelled based on DS cruciform joint beam model designed by Qin and evaluated by Donk, see Figure 4.2 [17]. The original DS cruciform joint beam model is limited to the normal connecting plate dimension range and not valid for the very large dimension such as a long attachment length for the DS longitudinal attachment.

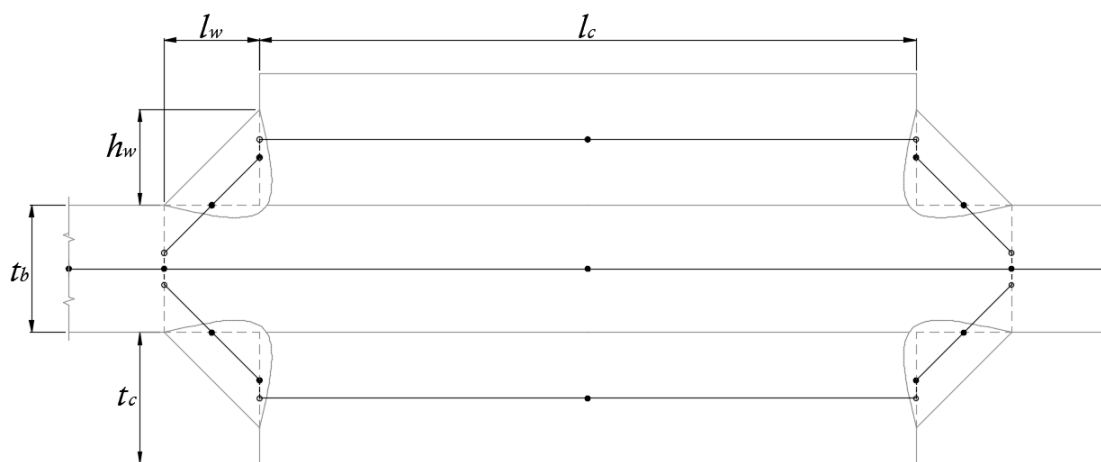


Figure 4.1: Single weld element beam model of DS cover plate [9]

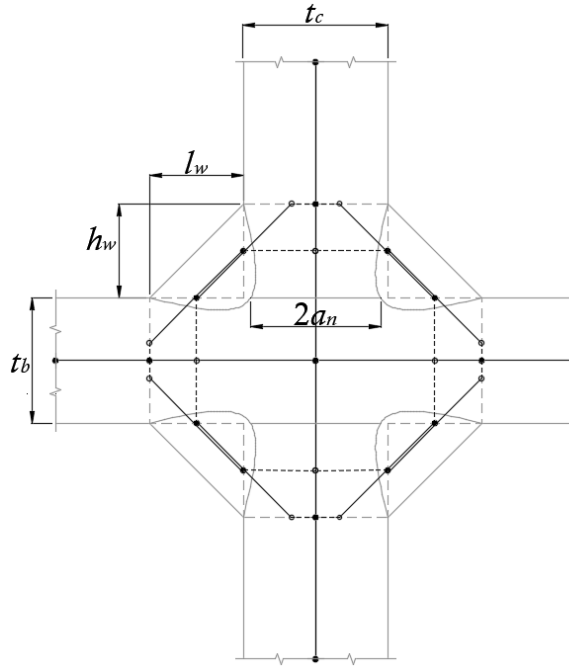
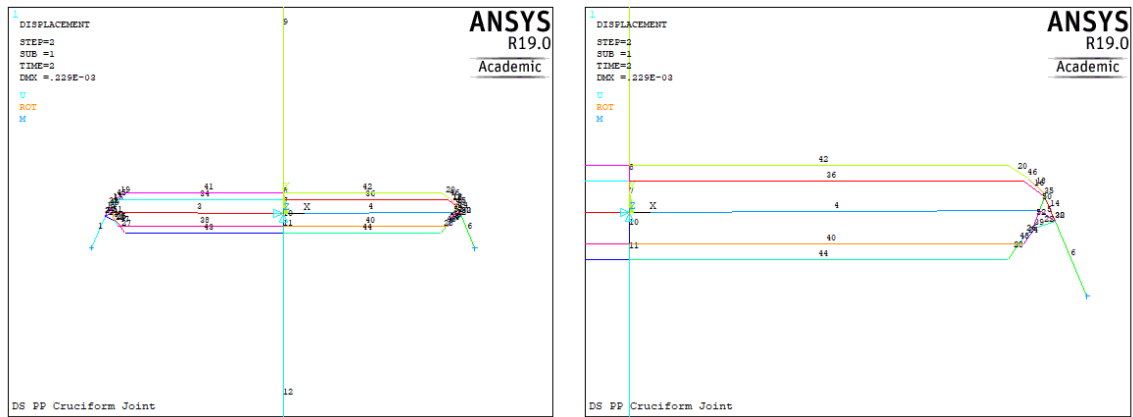


Figure 4.2: Double weld element beam model of DS cruciform joint

DS cruciform joint beam model can be obtained by taking symmetry of DS T-joint beam model, see Figure 4.2. A black solid line indicates the beam element and black dashed line indicates the rigid connection. Depending on the amount of a weld root notch size, a_n , two major limitations are observed with the large dimension of connecting plate thickness, t_c . And considering full penetration weld where the $2a_n = 0$ provides inappropriate bending deflection. Because the rigid connection is considered to connect the weld beam element to the base and connecting plate beam elements, too large dimension causes overestimated rigidity of connecting plate, see Figure 4.3.



(a) Element deformation

(b) Opposite bending deflection of element no. 4

Figure 4.3: DS cruciform joint beam model under pure bending ($r_s = 1$)

$$(t_b = 4, t_c = 100, l_w = 4, h_w = 4, a_n = 0 \text{ [mm]})$$

On the other hands, assuming $2a_n = t_c$ for partial penetration weld leads very narrow vertical beam element at the centre which connects the base plate to the connecting plate. With the small dimensions, especially small t_c , it does not matter because the weld beam elements are close to the centre. Hence there is enough rigidity to sustain a shape under membrane loading. However, if taking much larger connecting plate thickness than the standard dimension, weld beam elements cannot help the vertical beam element at the centre. Consequently, a collapse of the beam model of DS cruciform joint happens under membrane loading. This

phenomenon becomes worse with the decrease of weld notch angle h_w/l_w .

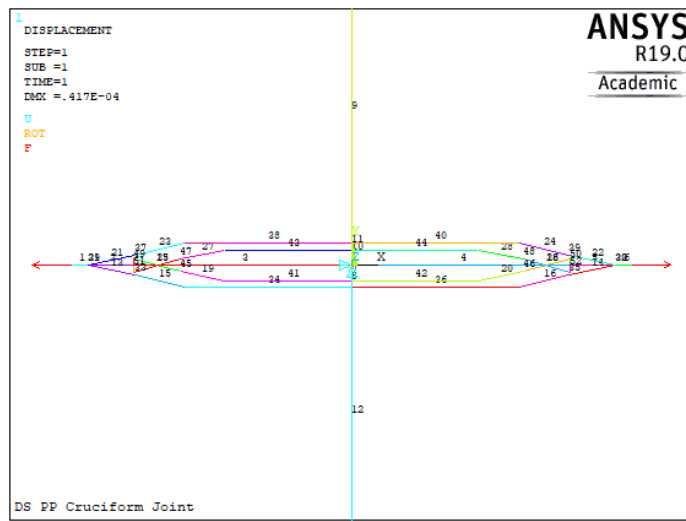


Figure 4.4: Collapse of DS cruciform joint beam model under pure membrane ($r_s = 0$)
 ($t_b = 4, t_c = 100, l_w = 4, h_w = 4, a_n = t_c/2$ [mm])

From Figure 4.4, it is easy to see the upper and lower weld elements cross each other which means the penetration of the weld beam element into the base plate. Therefore, a new double weld element beam model is proposed for the DS longitudinal attachment.

The DS longitudinal attachment beam model is designed for the large attachment size with avoiding identified problems. It is simply taking local geometry near the weld toe similarly as DS cruciform beam model and extending connecting plate thickness, the attachment length, by using more vertical beam elements.

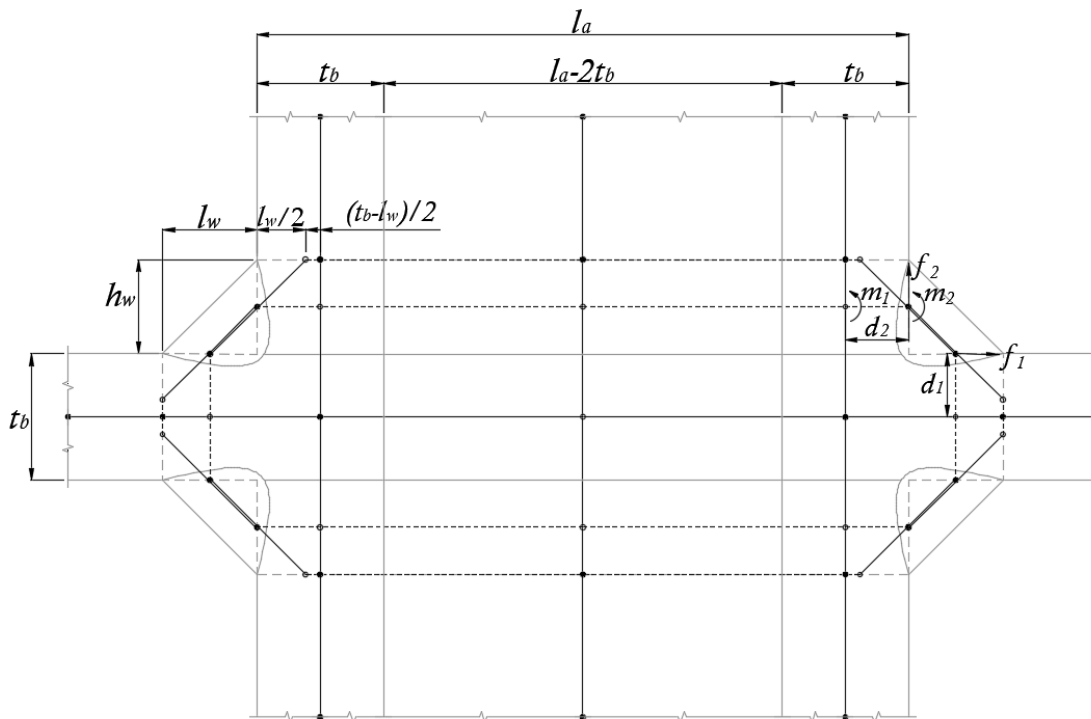
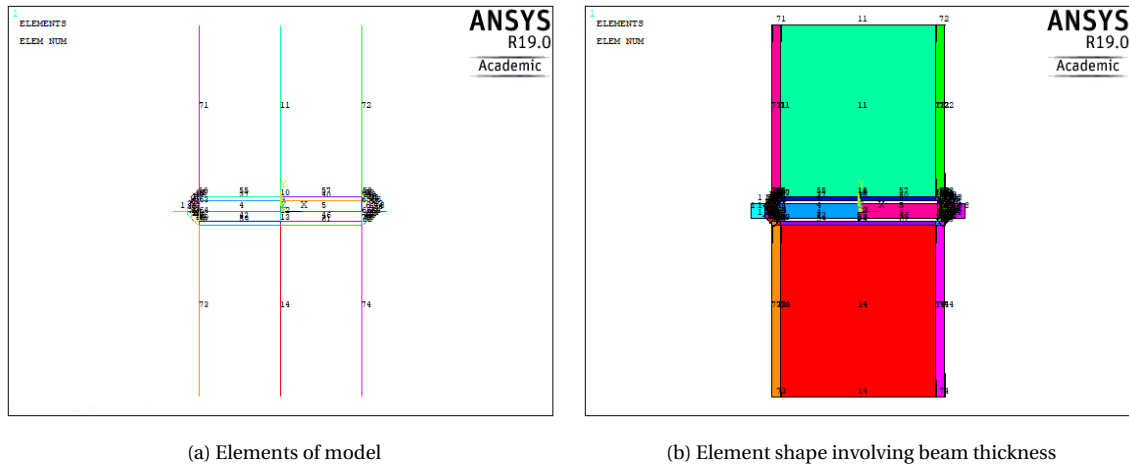


Figure 4.5: Double weld element beam model of DS longitudinal attachment



(a) Elements of model (b) Element shape involving beam thickness
 Figure 4.6: Double weld element beam model of DS longitudinal attachment

The valid 2D solid model has to be modelled as a reference to the beam model which is not possible to compare directly with the 3D solid model. It is important because the DS longitudinal attachment has different thickness orientations for the base plate and the attachments. The validity of the 2D solid model was shown in Figure 3.5. Weld toe stress distribution was compared between the 3D solid model and the 2D solid model, and the same results are obtained. Therefore the 2D solid model is possible to be adopted as a reference for the beam model as well.

The double weld element beam model is designed from the possible assumed load paths, see Figure 4.7. The amount of the weld load carrying can be estimated by evaluating the amount of the load pass through the base plate. The weld load carrying varies with local geometry parameters i.e. t_b , l_a , l_w and h_w . The result of load passes through the base plate namely base plate load, or just plate load is compared between solid and beam models with changing geometric parameters. A pure membrane and pure bending loading are applied individually.

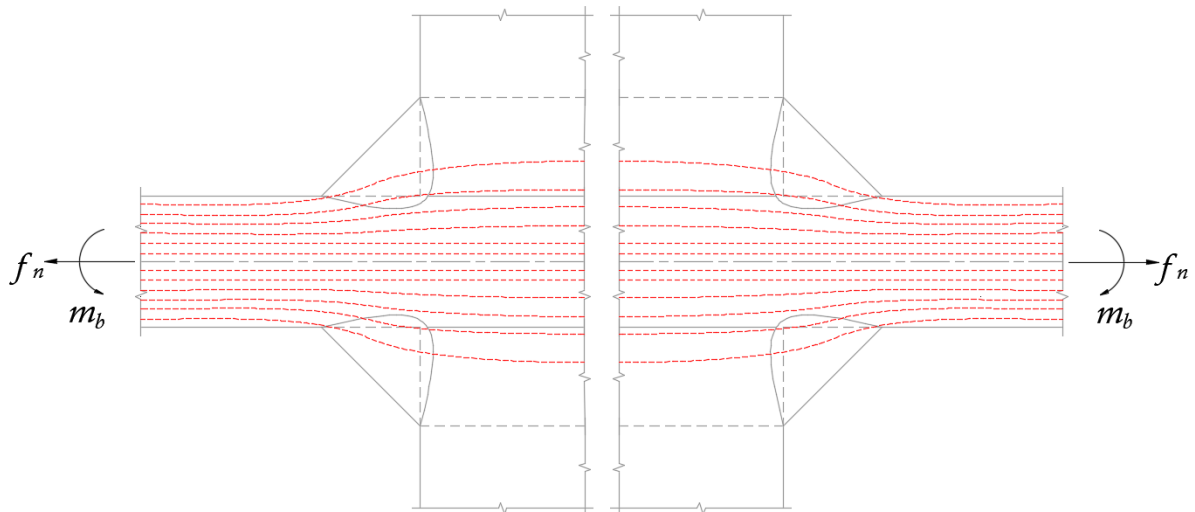


Figure 4.7: Assumed load paths of the double sided longitudinal attachment under plate loading

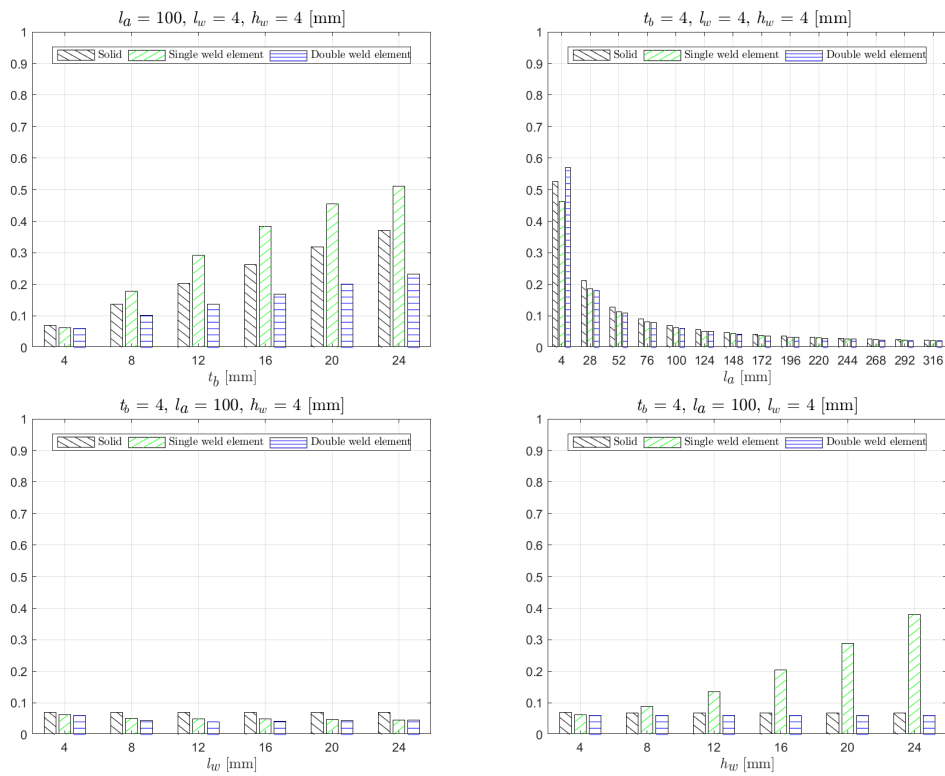


Figure 4.8: Double sided longitudinal attachment base plate load varying t_b, l_a, l_w and h_w under normal force

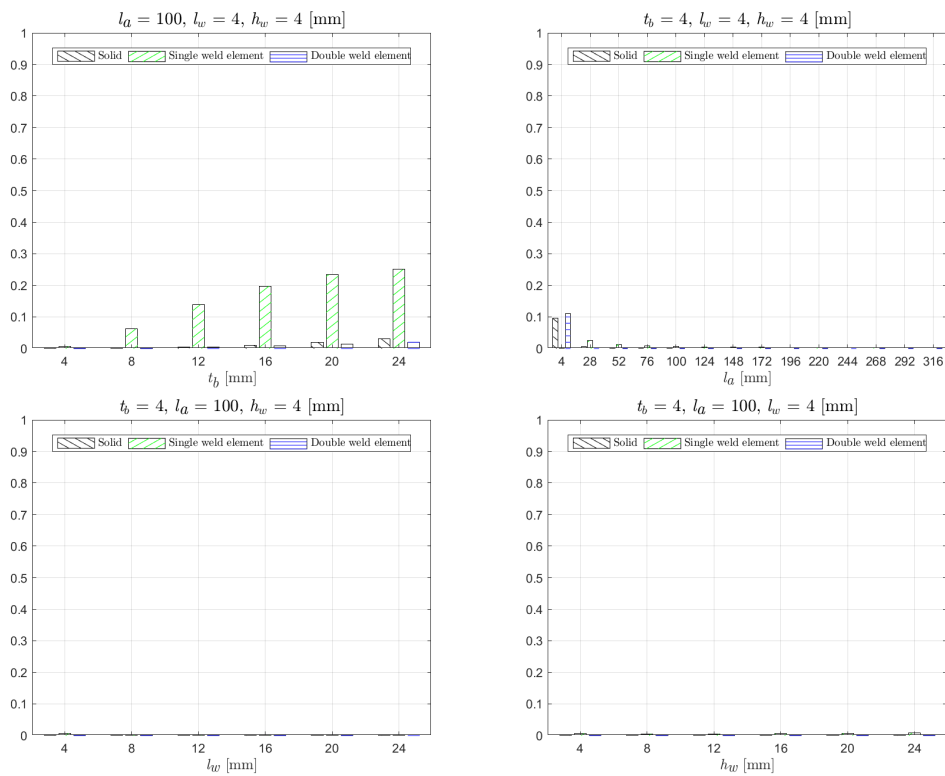


Figure 4.9: Double sided longitudinal attachment base plate load varying t_b, l_a, l_w and h_w under bending moment

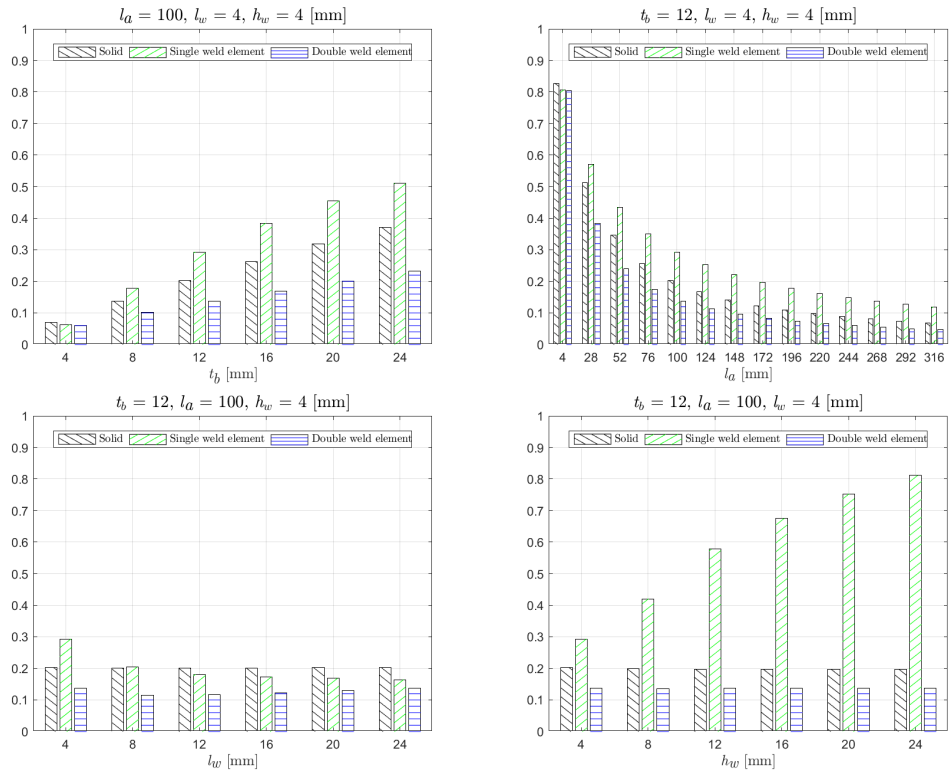


Figure 4.10: Double sided longitudinal attachment base plate load varying t_b , l_a , l_w and h_w under normal force

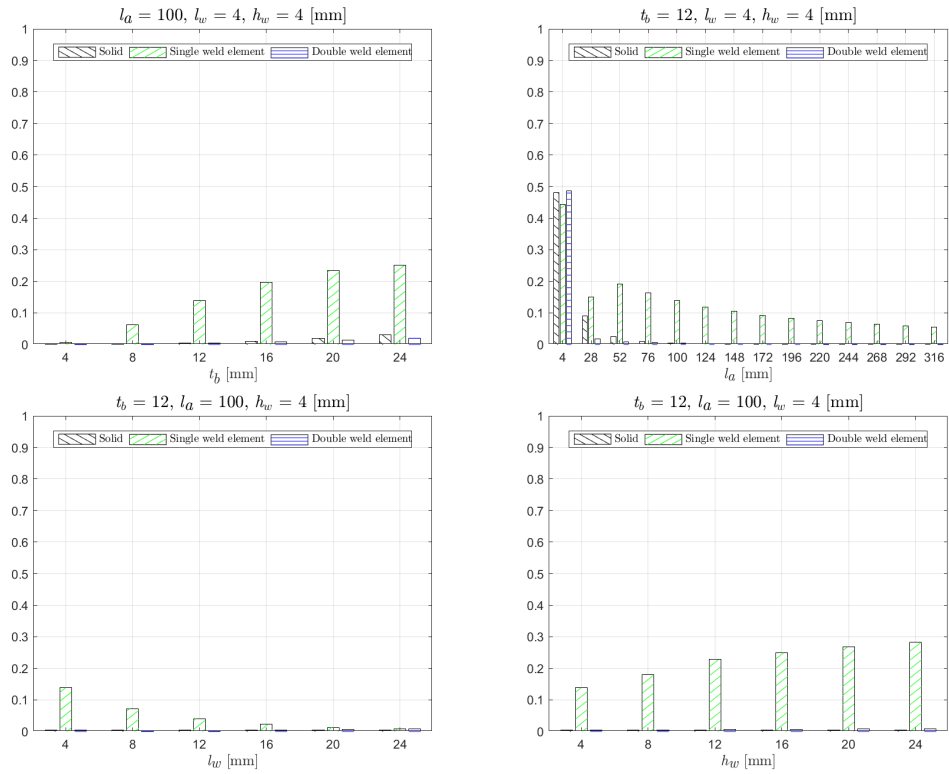


Figure 4.11: Double sided longitudinal attachment base plate load varying t_b , l_a , l_w and h_w under bending moment

Base plate load from the FE beam and solid model show similar trends with varying each geometry. Due to the additional vertical beam element at each side, the less plate load than the solid model is observed. All the weird trends of the single weld element beam model disappear with the double weld element beam model. Increasing base plate thickness, t_b , obviously leads an increase of the base plate load and increasing longitudinal attachment length, l_a , decreases the base plate load which means the higher weld load carrying level. Due to big enough attachment, weld size itself does not show a significant difference of weld load carrying level.

To get the weld load carrying stress, Equation 3.10 to 3.12, correlating the beam model nodal moments and forces to m_{bm} and m_{bb} is required. Nodes on the double weld elements are assumed as governing to get m_{bm} and m_{bb} . The concluded formulas are based on the nodal moments and nodal reaction forces multiplied with the relative nodal distances.

$$m_{bm} = \frac{1}{4.5}(m_1 - m_2) \quad (4.1)$$

$$m_{bb} = \frac{1}{8.5}(-f_1 d_1 + f_2 d_2) \quad (4.2)$$

With Equation 4.1 and 4.2, the weld load carrying coefficient C_{bw} can be determined. The result is compared with the fitted result of FE solid model. The term 'fitted' is used because the C_{bw} is determined by fitting between FE solid result of weld toe stress distribution and semi-analytic formula which gives the least discrepancy.

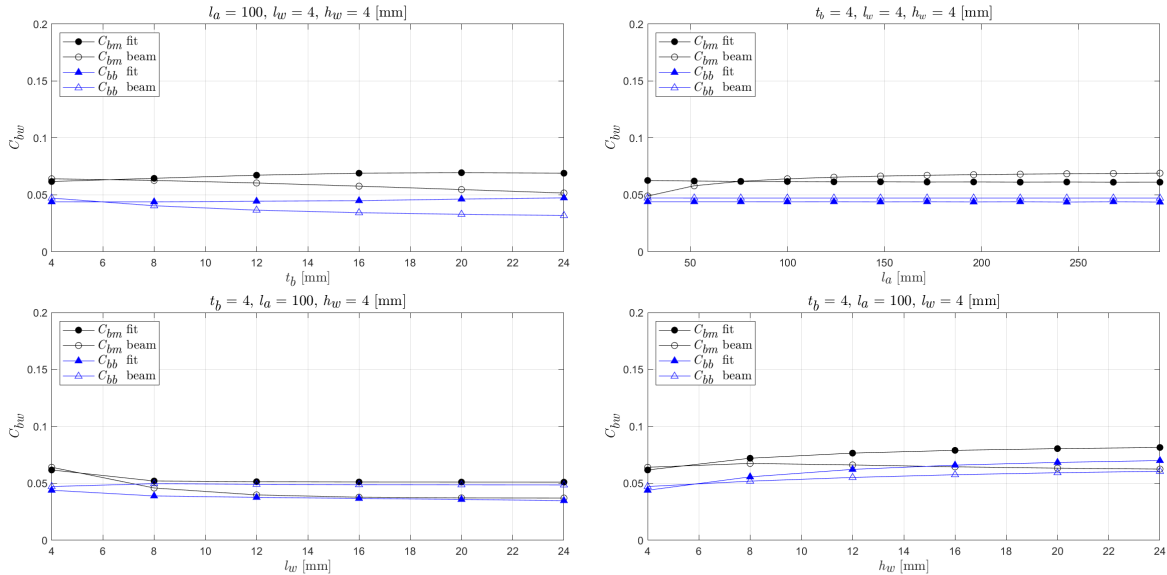


Figure 4.12: C_{bw} comparison between FE solid and double weld element beam model

C_{bm} and C_{bb} from FE beam and solid models are shown in the Figure 4.12. All the results are shown with varying each geometry. C_{bw} from FE beam model has similar trends and values compared to the FE solid results. Even extreme weld length is adopted which causes some difference in C_{bw} . The weld toe stress distributions still provide reasonable matches. In terms of increasing certain geometry, the weld length l_w is the least sensitive parameter to the C_{bw} for the weld toe stress distribution. Oppositely, weld height h_w is most sensitive parameter to the C_{bw} . It is due to the weld notch angle h_w/l_w ; a high weld notch angle induces rapid local stiffness change meaning a large shift in the local neutral axis which induces the weld notch stress where low weld notch angle induces slow local stiffness change and a small shift in the local neutral axis. However, the weld notch angle close to 45° is commonly obtained by welding in general. So it may not be a big problem for the slight mismatch at the extreme geometry.

4.1.1. Weld notch stress distribution

Equation 3.19 can directly provide the through-thickness stress distribution at the weld toe. Figure 4.13 to 4.17 show weld toe stress distribution results with several loading cases by taking C_{bw} values from Equation 4.1 and 4.2. Pure membrane ($r_s = 0$), pure bending ($r_s = 1$), membrane plus bending ($r_s = 1/3$), membrane minus bending ($r_s = -1$) are considered as following.

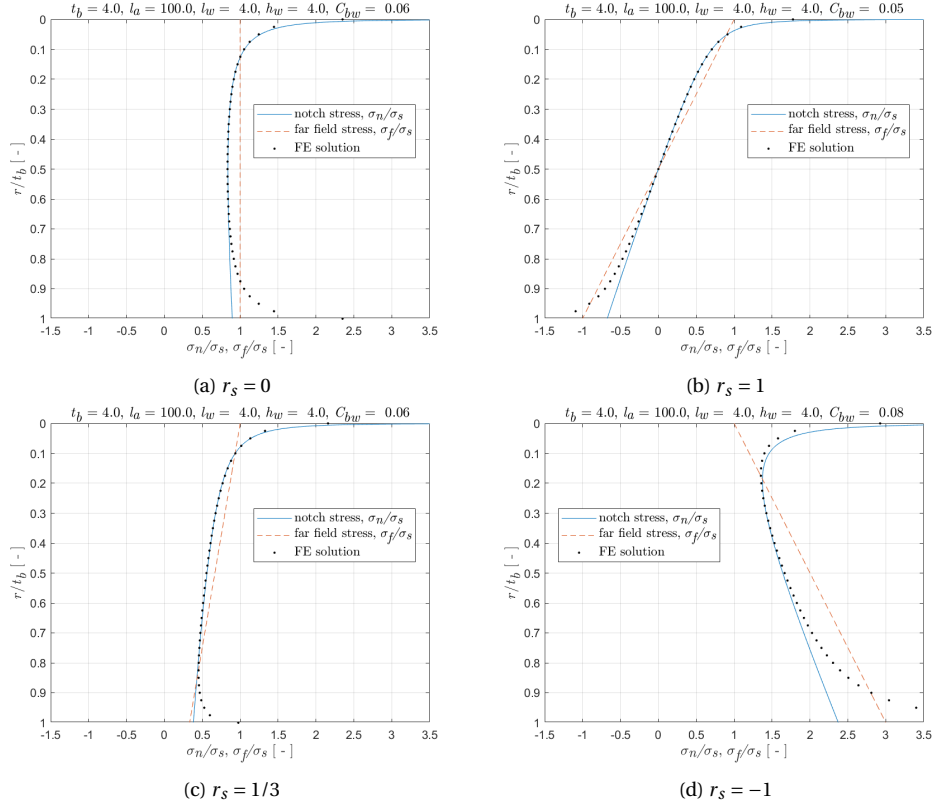


Figure 4.13: Weld toe stress distributions
($t_b = 4, l_a = 100, l_w = 4, h_w = 4$ [mm])

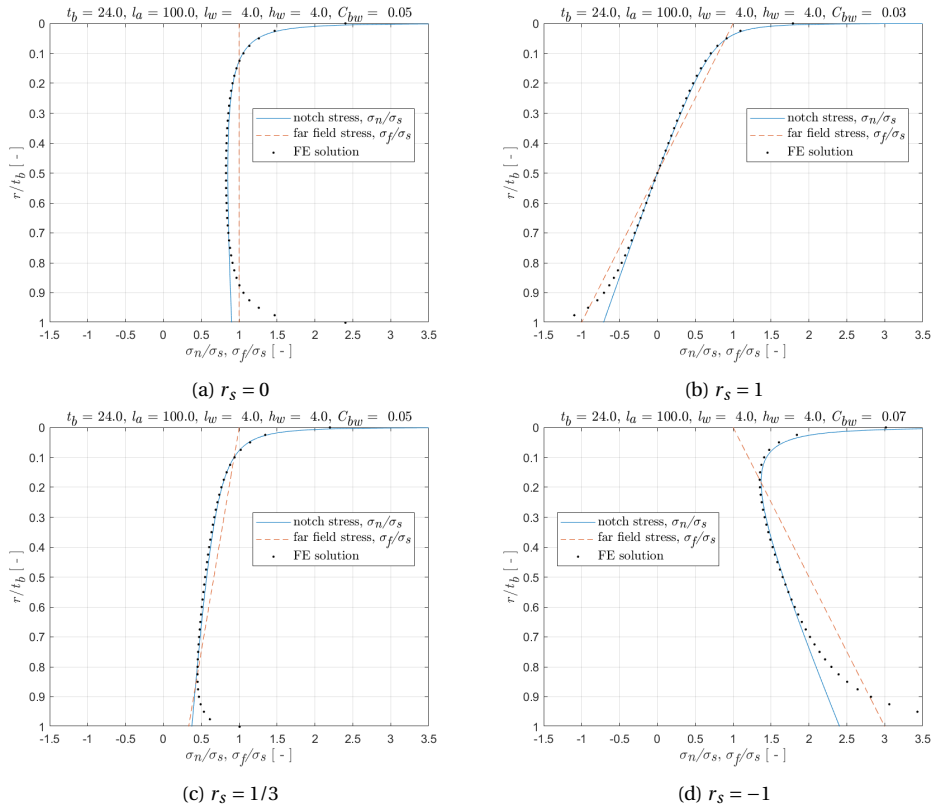


Figure 4.14: Weld toe stress distributions
 ($t_b = 24, l_a = 100, l_w = 4, h_w = 4$ [mm])

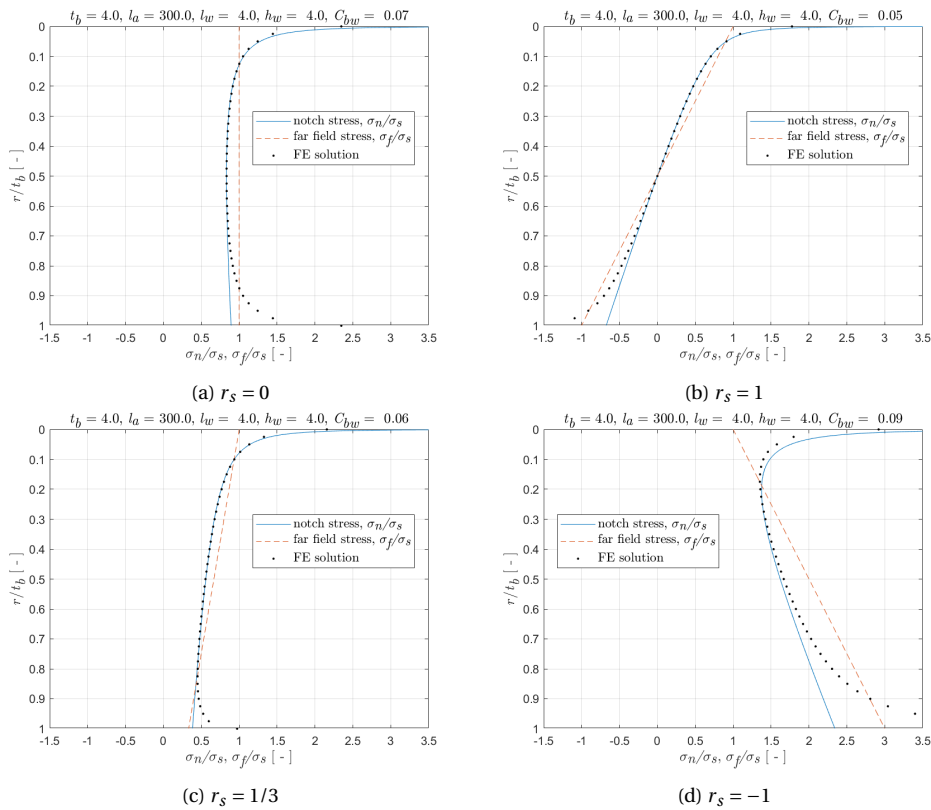


Figure 4.15: Weld toe stress distributions
 ($t_b = 4, l_a = 300, l_w = 4, h_w = 4$ [mm])

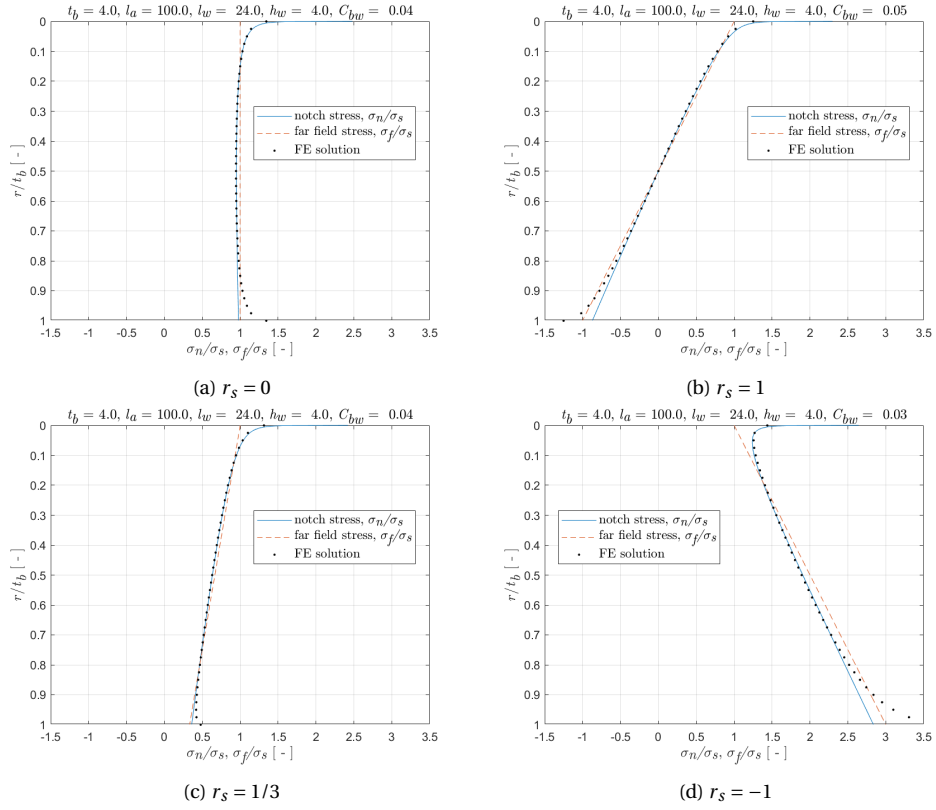


Figure 4.16: Weld toe stress distributions
($t_b = 4, l_a = 100, l_w = 24, h_w = 4$ [mm])

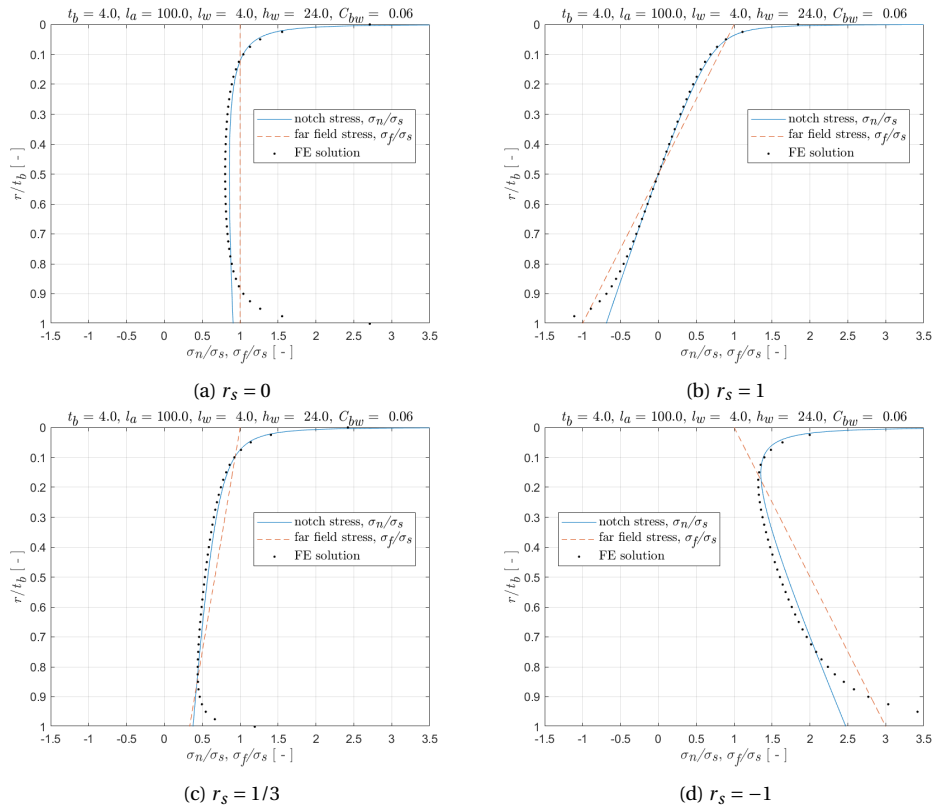


Figure 4.17: Weld toe stress distributions
($t_b = 4, l_a = 100, l_w = 4, h_w = 24$ [mm])

Results are generally acceptable with extreme dimensions. However the loading case of membrane minus bending ($r_s = -1$) shows the most discrepancies due to its sensitivity to the weld load carrying coefficient C_{bw} . Even just a small change of C_{bw} affects directly to the stress distribution of the bending stress ratio $r_s = -1$.

4.1.2. Weld notch stress intensity

Using C_{bw} from the double weld element beam model and Equation 3.21 to 3.27 provides the mode I weld notch stress intensity. The C_{bw} results can be judged by comparing with the SIF results of reference FE models. Good agreements between the semi-analytic results and the reference FE solid results are shown in the following figures.

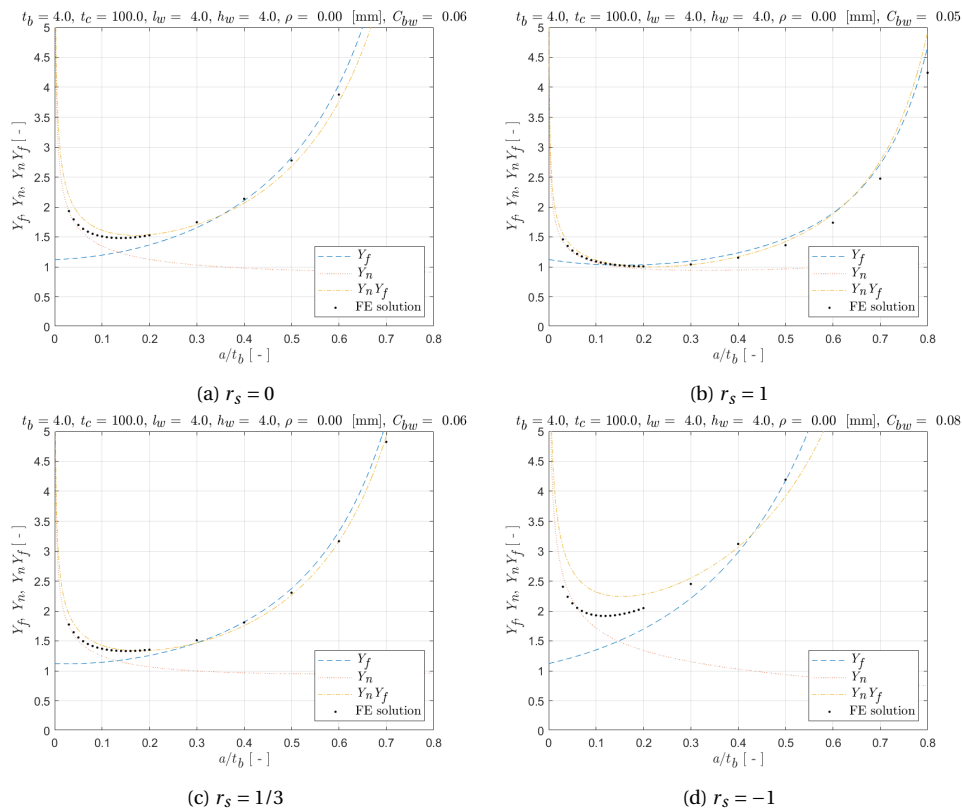


Figure 4.18: Weld notch stress intensity distributions
 ($t_b = 4$, $l_a = 100$, $l_w = 4$, $h_w = 4$ [mm])

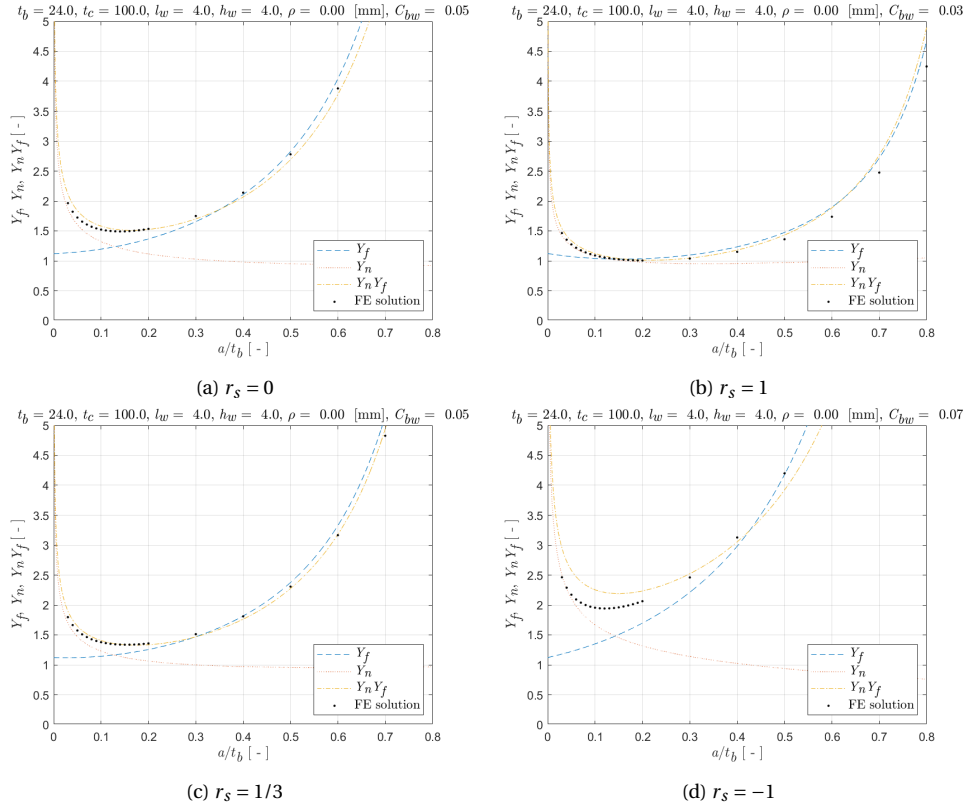


Figure 4.19: Weld notch stress intensity distributions
 ($t_b = 24$, $l_a = 100$, $l_w = 4$, $h_w = 4$ [mm])

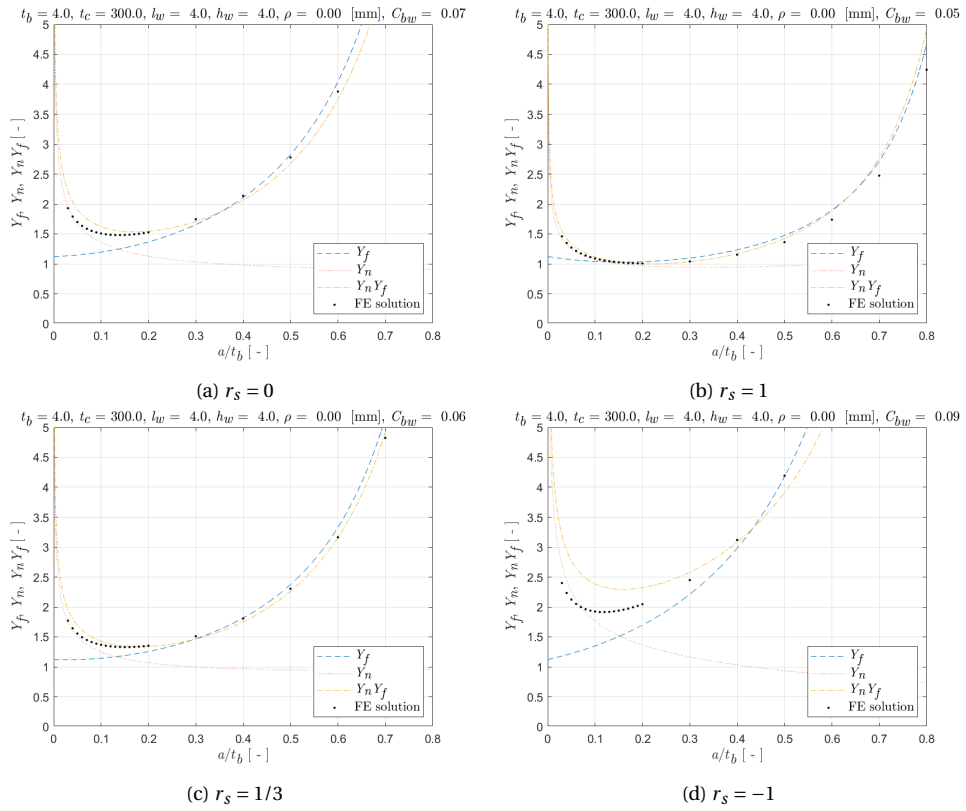


Figure 4.20: Weld notch stress intensity distributions
 ($t_b = 4$, $l_a = 300$, $l_w = 4$, $h_w = 4$ [mm])

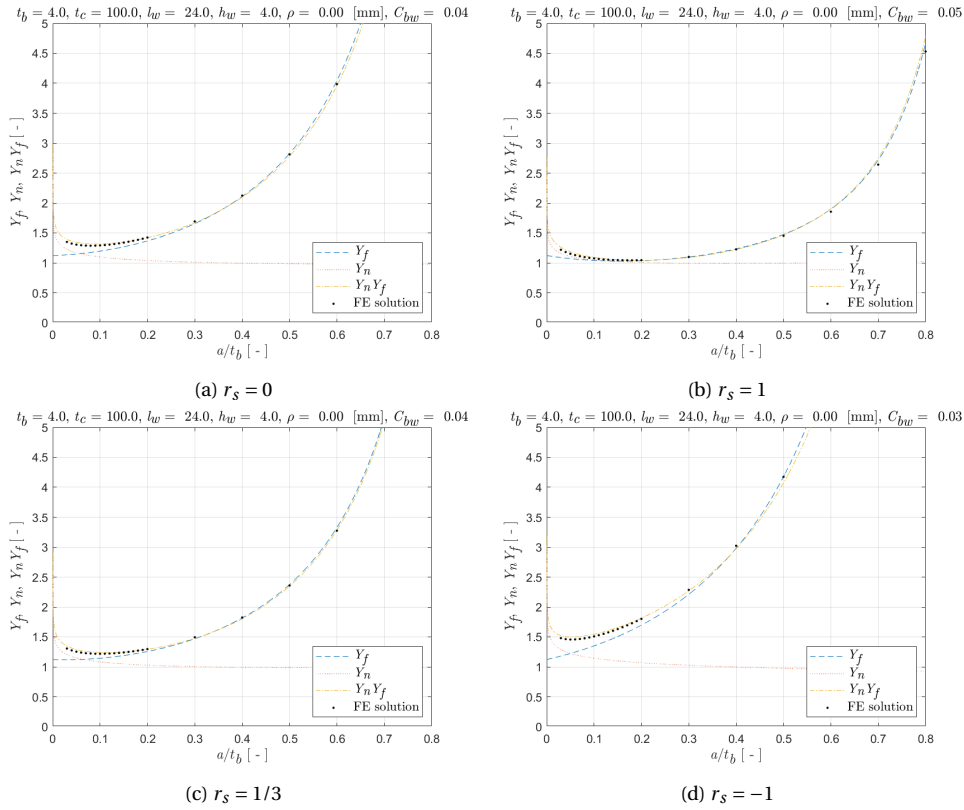


Figure 4.21: Weld notch stress intensity distributions
 ($t_b = 4$, $l_a = 100$, $l_w = 24$, $h_w = 4$ [mm])

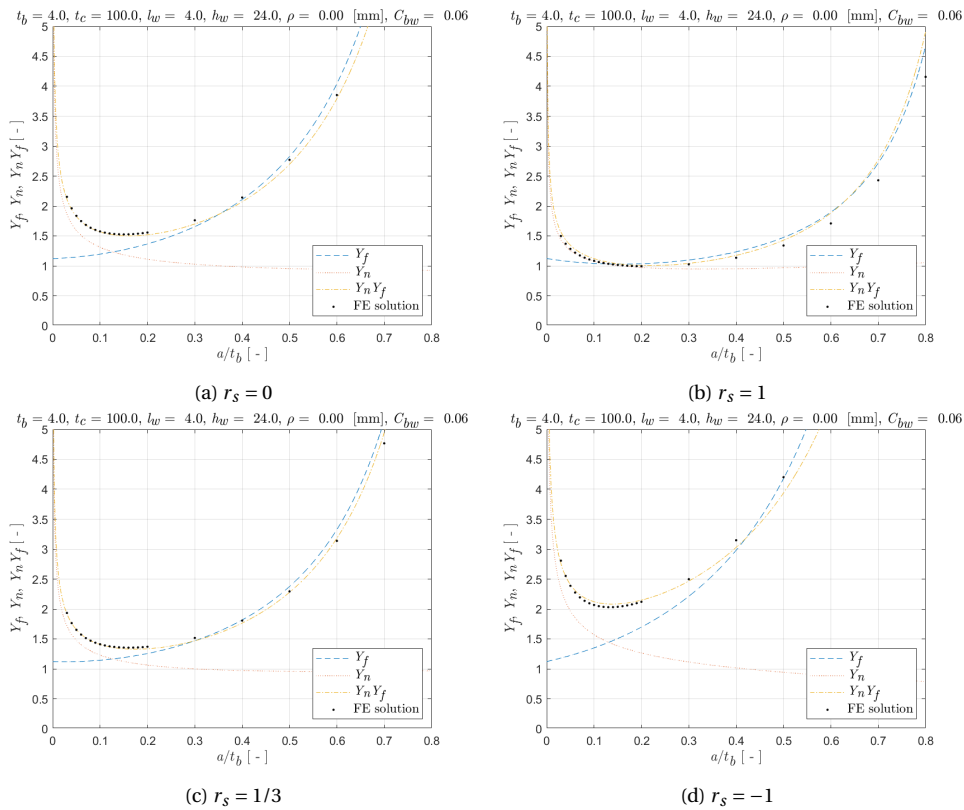


Figure 4.22: Weld notch stress intensity distributions
 ($t_b = 4$, $l_a = 100$, $l_w = 4$, $h_w = 24$ [mm])

4.2. Parametric method

Recently, Qin investigated the governing parameters for the weld load carrying coefficient of the DS T-joint [44].

- weld notch angle : h_w/l_w
- relative weld geometry size : $(0.5l_a + l_w)/t_b$

It is logical that the weld load carrying level increases with the weld notch angle h_w/l_w and converges when the weld notch angle is relatively large. At the same time, the weld load carrying level also increases with the large relative weld geometry size $(0.5l_a + l_w)/t_b$.

The similar parametric study compared to Qin has done for the welded DS longitudinal attachment. Due to relatively large weld geometry size for this configuration, only the weld notch angle h_w/l_w is a governing parameter. So the problem becomes much easier.

Parametric study is done with various geometries. The geometry range of the base plate thickness t_b , weld length l_w and weld height h_w are varying from 4 [mm] to 24 [mm] with the interval of 4 [mm]. And the attachment plate length l_a is varying from 4 [mm] to 300 [mm] with the interval of 8 [mm].

C_{bm}

Figure 4.23 shows that the membrane weld load carrying coefficient C_{bm} of the welded DS longitudinal attachment only depends on the weld notch angle h_w/l_w because of large relative weld geometry size, i.e. attachment length. Already sufficiently large relative weld geometry size does not affect the amount of the weld load carrying anymore. In the figure, the relative weld geometry size larger than 2 is considered, and it is sufficient for the longitudinal attachments. C_{bm} value converges after the relative weld size $(0.5 \cdot l_a + l_w)/h_w$ larger than around 2 in Figure 4.24. So C_{bm} is the matter of the weld notch angle. Consequently, the form of exponential formula depending on the weld notch angle h_w/l_w can be defined.

$$f_{C_{bm}} = -0.0507 \cdot e^{-0.7602 \cdot \frac{h_w}{l_w}} + 0.0797 \quad (4.3)$$

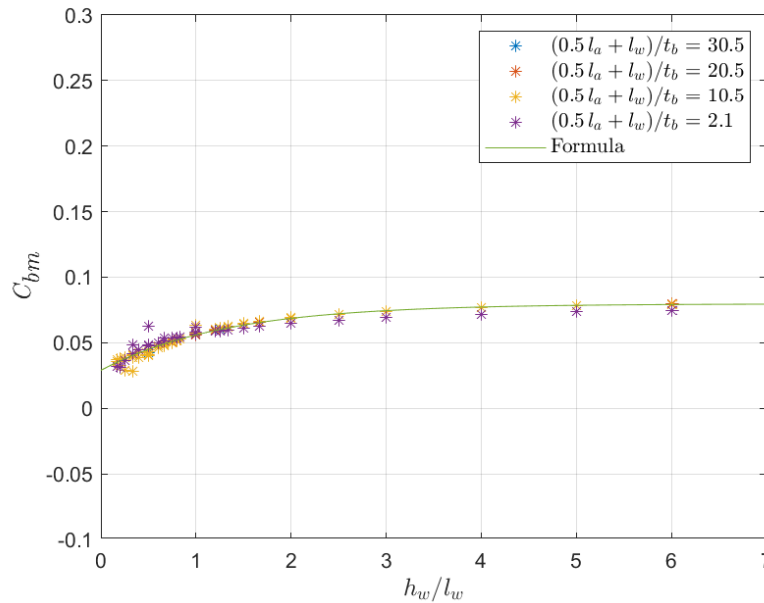


Figure 4.23: C_{bm} value with respect to the weld notch angle h_w/l_w

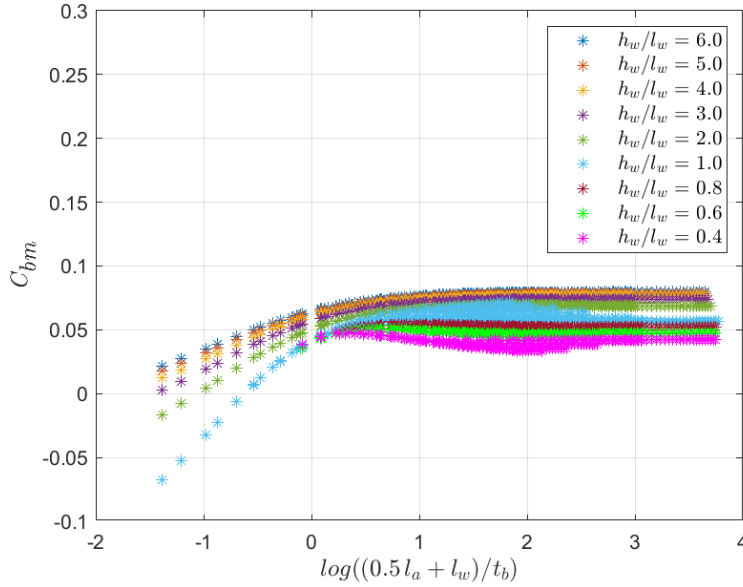


Figure 4.24: C_{bm} value with respect to the relative weld geometry size $(0.5l_a + l_w)/t_b$

C_{bb}

Bending weld load carrying coefficient C_{bb} also has similar trends as C_{bm} has, see Figure 4.25 and 4.26. And C_{bb} is even more convergent than C_{bm} . A slow increasing trend with weld notch angle h_w/l_w is shown in Figure 4.25 and convergence after the relative weld size $(0.5l_a + l_w)/t_b$ of 1 is observed in Figure 4.26. C_{bb} is also governed by the weld notch angle h_w/l_w hence similar form of the formula can be established.

$$f_{C_{bb}} = -0.0448 \cdot e^{-0.3700 \cdot \frac{h_w}{l_w}} + 0.0760 \tag{4.4}$$

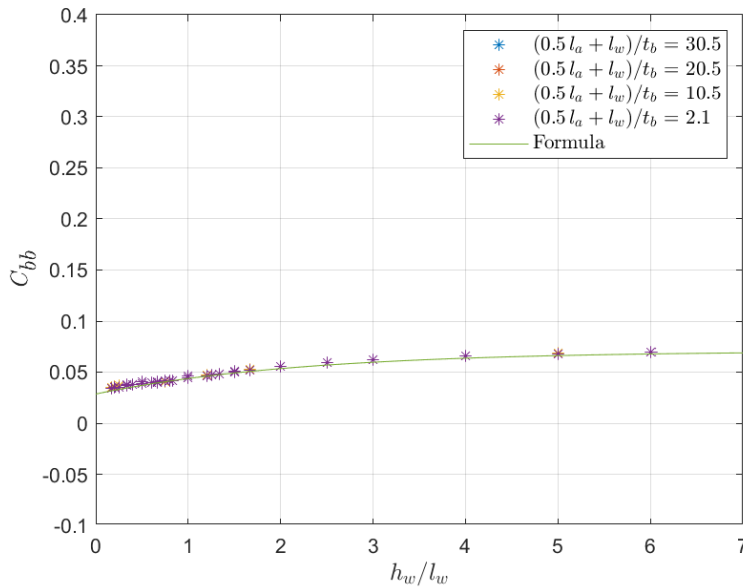


Figure 4.25: C_{bb} value with respect to the weld notch angle h_w/l_w

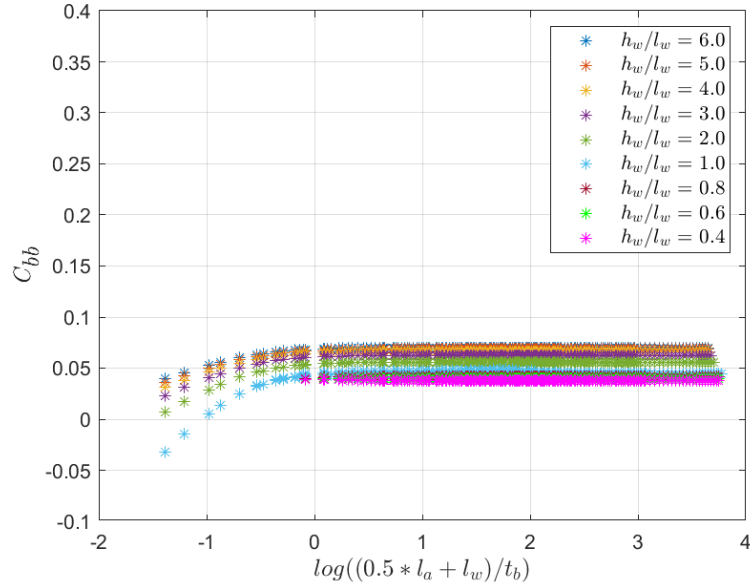


Figure 4.26: C_{bb} value with respect to the relative weld geometry size $(0.5l_a + l_w)/t_b$

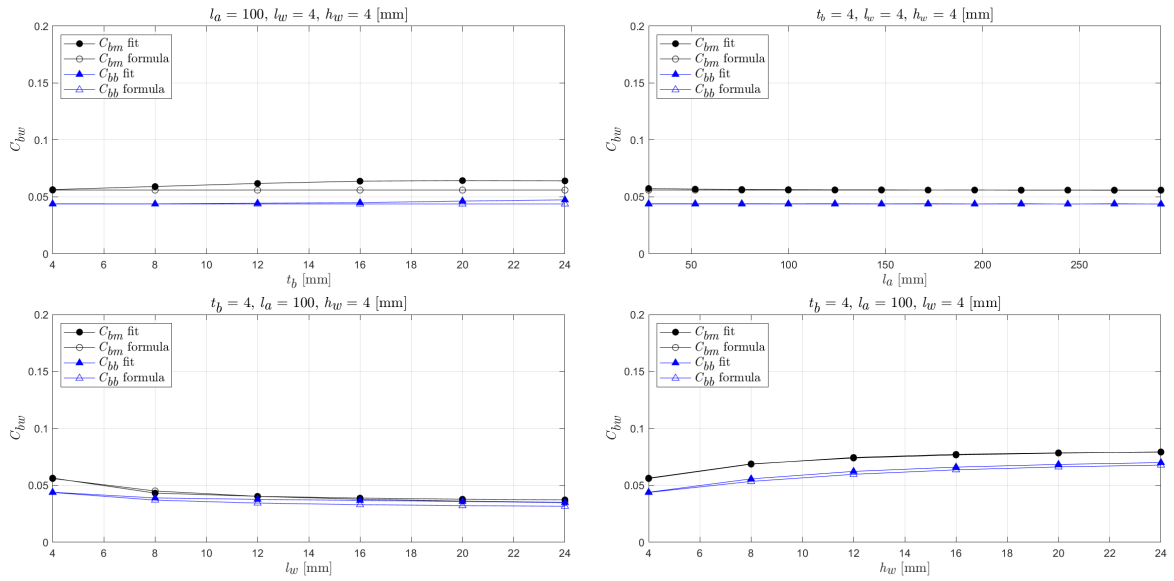


Figure 4.27: C_{bw} comparison between FE solid and parametric results

C_{bm} and C_{bb} from parametric formulas and FE solid models are shown in the Figure 4.27. All the results are shown with varying each geometry. The parametric formulas determine the accurate C_{bw} results with various geometries.

4.2.1. Weld notch stress distribution

Similar as the double weld element beam model, the weld notch stress distribution can be obtained by taking the weld load carrying coefficient C_{bw} from the parametric formulas, see Figure 4.28 to 4.32. The semi-analytic formula of the weld notch stress distribution with the weld load carrying coefficient C_{bw} from the parametric formulas provides great agreements comparing to the FE results.

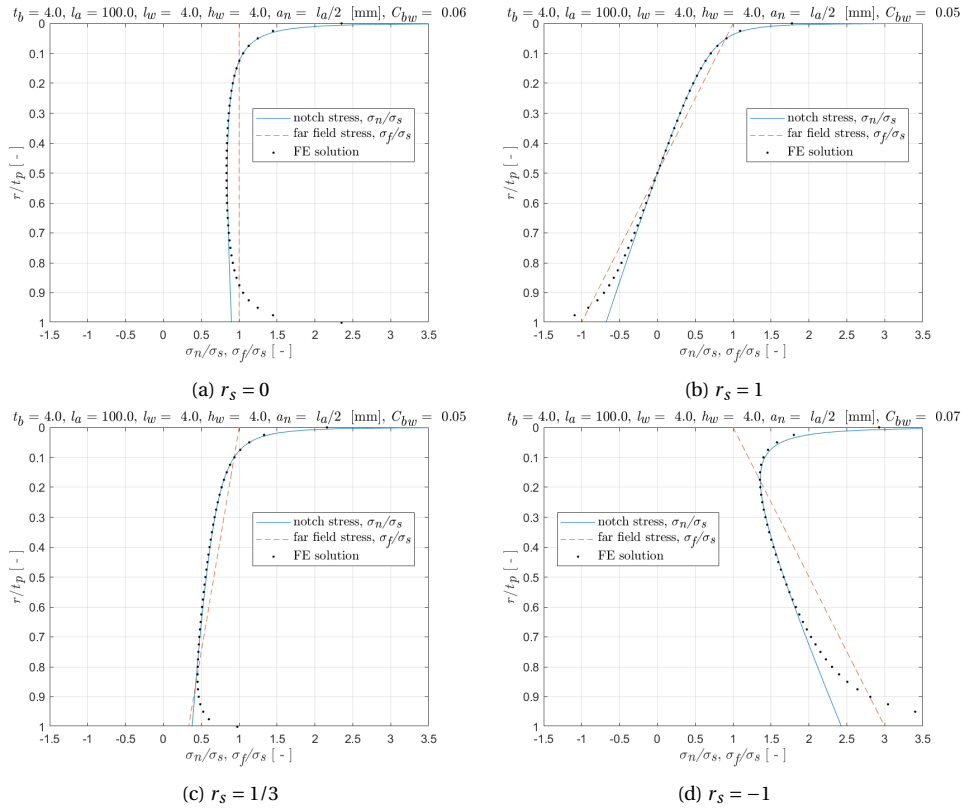


Figure 4.28: Weld toe stress distributions by taking C_{bw} from the parametric formulas ($t_b = 4$, $l_a = 100$, $l_w = 4$, $h_w = 4$ [mm])

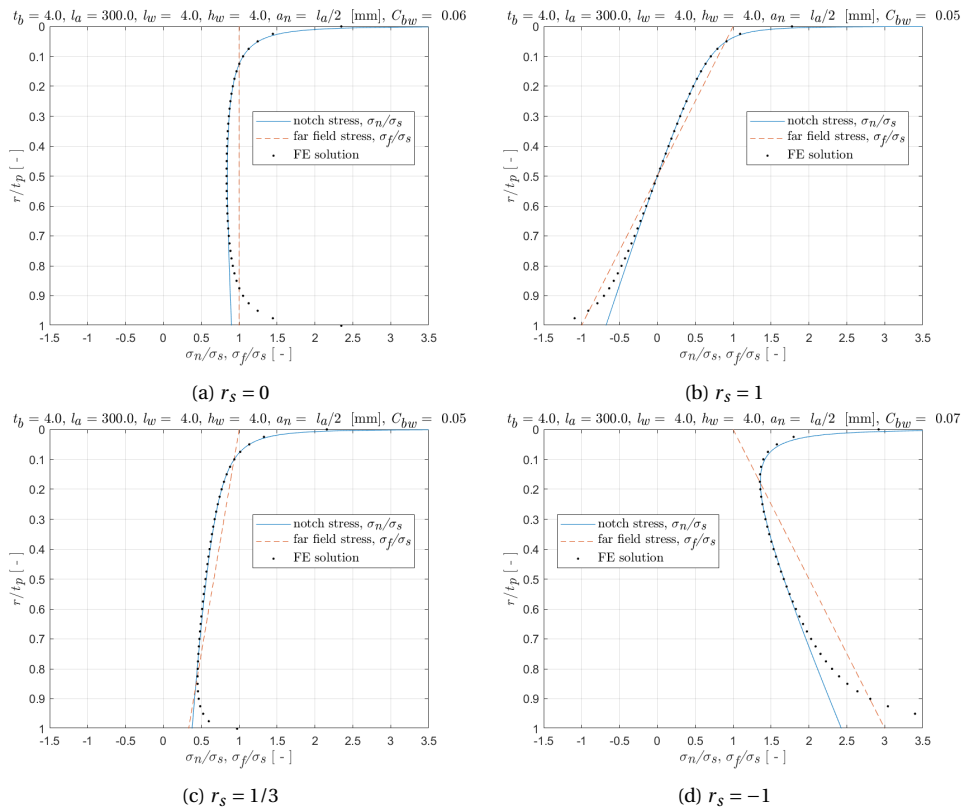


Figure 4.29: Weld toe stress distributions by taking C_{bw} from the parametric formulas ($t_b = 4$, $l_a = 300$, $l_w = 4$, $h_w = 4$ [mm])

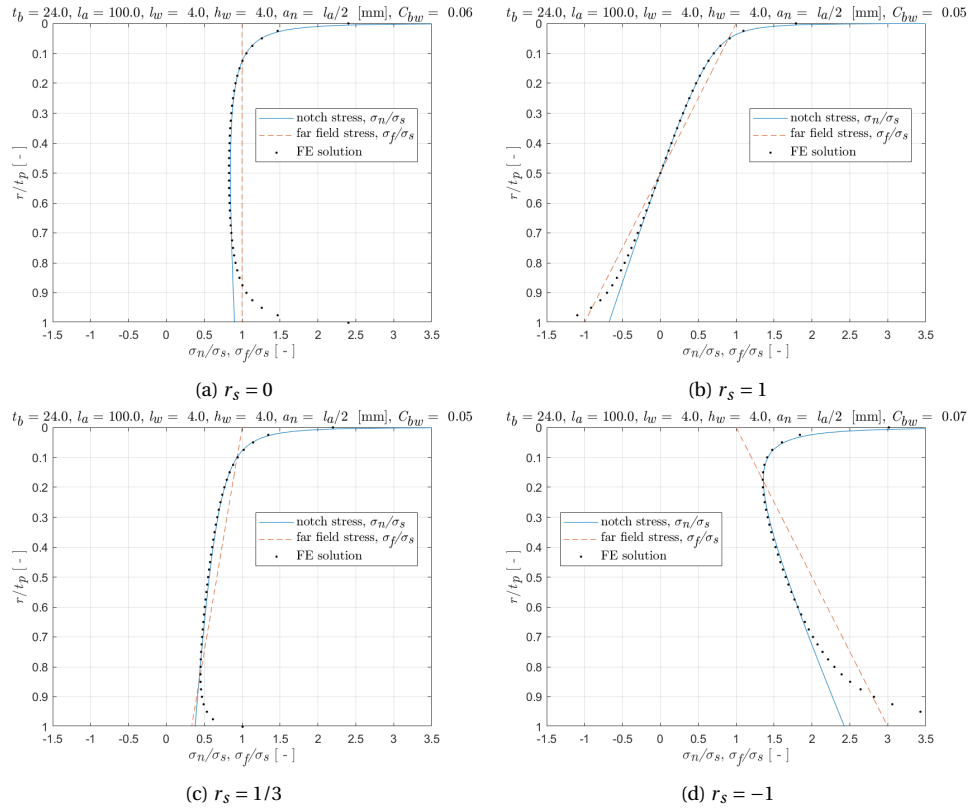


Figure 4.30: Weld toe stress distributions by taking C_{bw} from the parametric formulas ($t_b = 24, l_a = 100, l_w = 4, h_w = 4$ [mm])

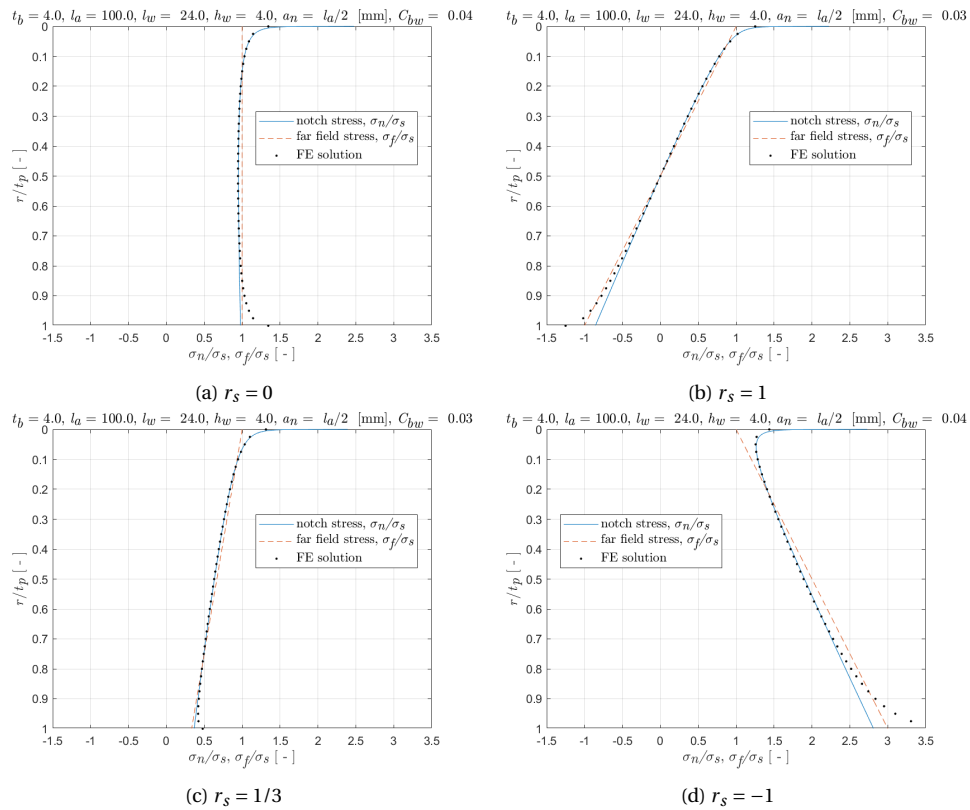


Figure 4.31: Weld toe stress distributions by taking C_{bw} from the parametric formulas ($t_b = 4, l_a = 100, l_w = 24, h_w = 4$ [mm])

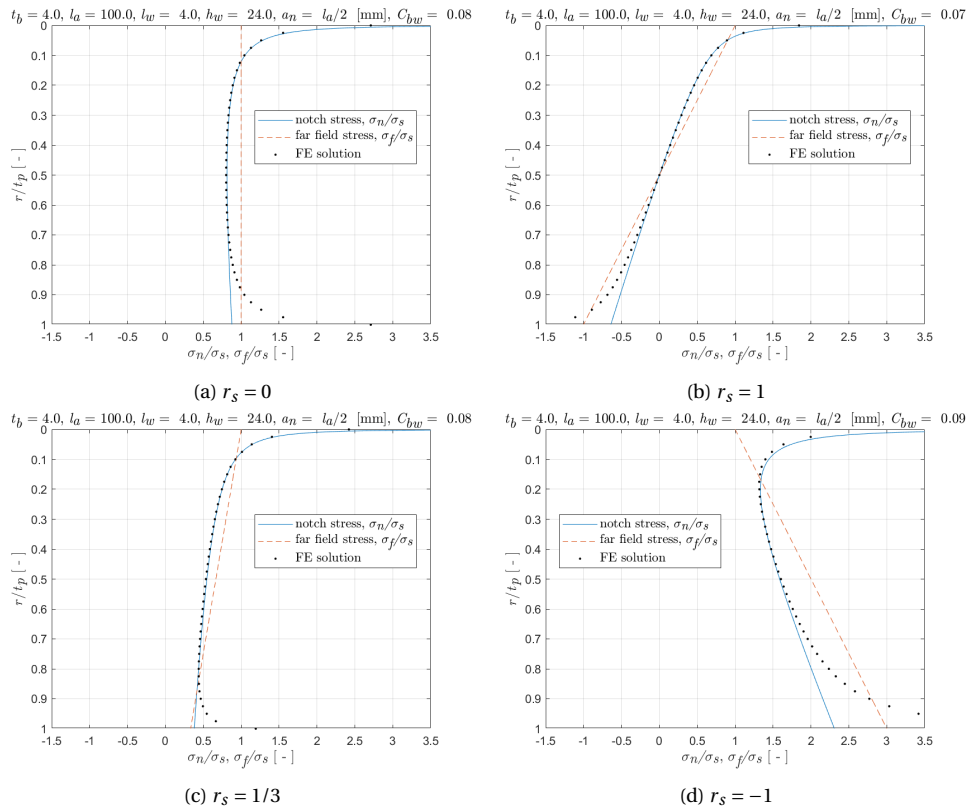


Figure 4.32: Weld toe stress distributions by taking C_{bw} from the parametric formulas ($t_b = 4, l_a = 100, l_w = 4, h_w = 24$ [mm])

4.2.2. Weld notch stress intensity

The weld notch stress intensity can be obtained by substituting the weld load carrying coefficient C_{bw} to the semi-analytic formula. Same as the double weld element beam model, the general crack type of SEC is considered. The accurate weld notch stress distributions naturally provide reliable weld notch stress intensity distributions, see Figure 4.33 to 4.37.

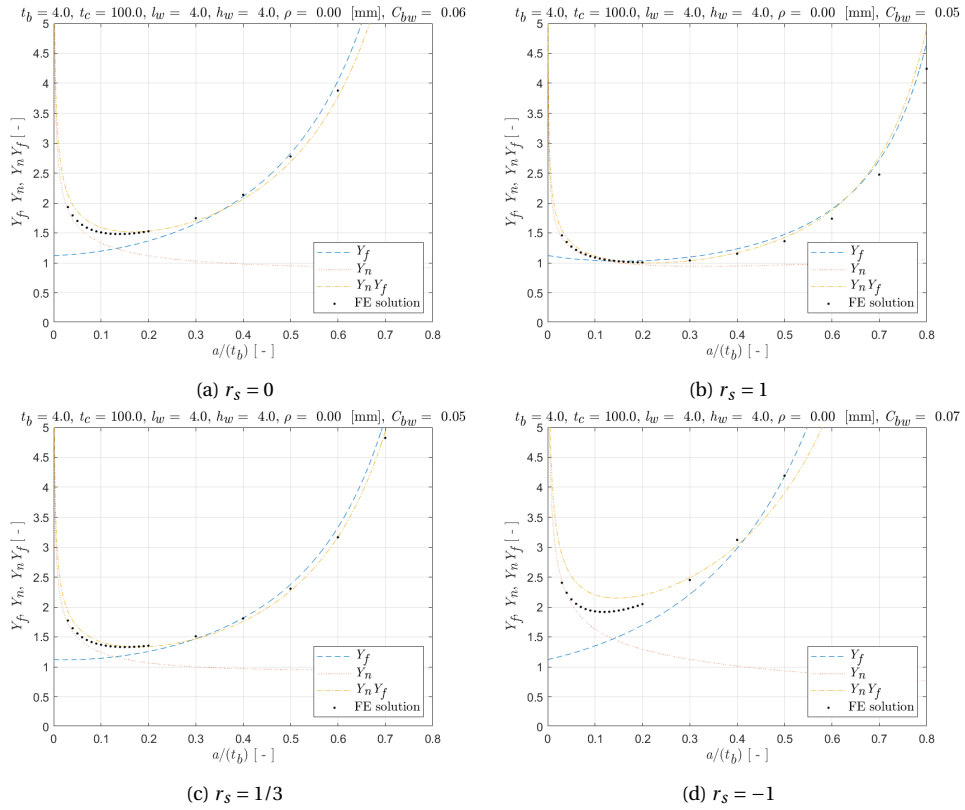


Figure 4.33: Weld notch stress intensity distributions
($t_b = 4, l_a = 100, l_w = 4, h_w = 4$ [mm])

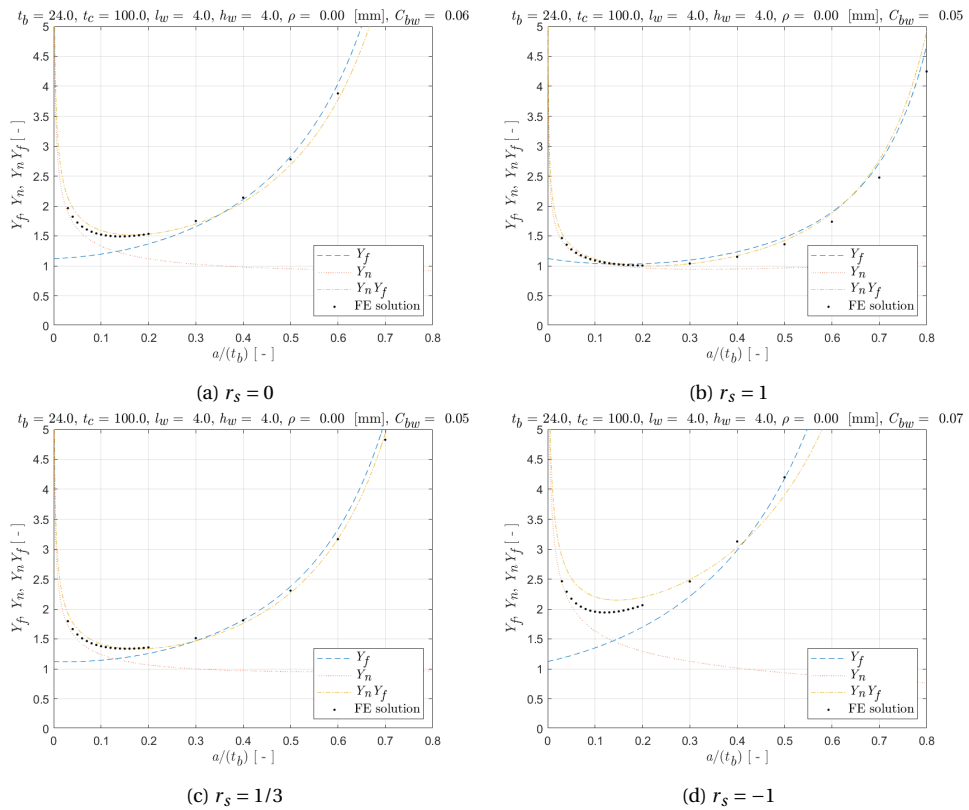


Figure 4.34: Weld notch stress intensity distributions
($t_b = 24, l_a = 100, l_w = 4, h_w = 4$ [mm])

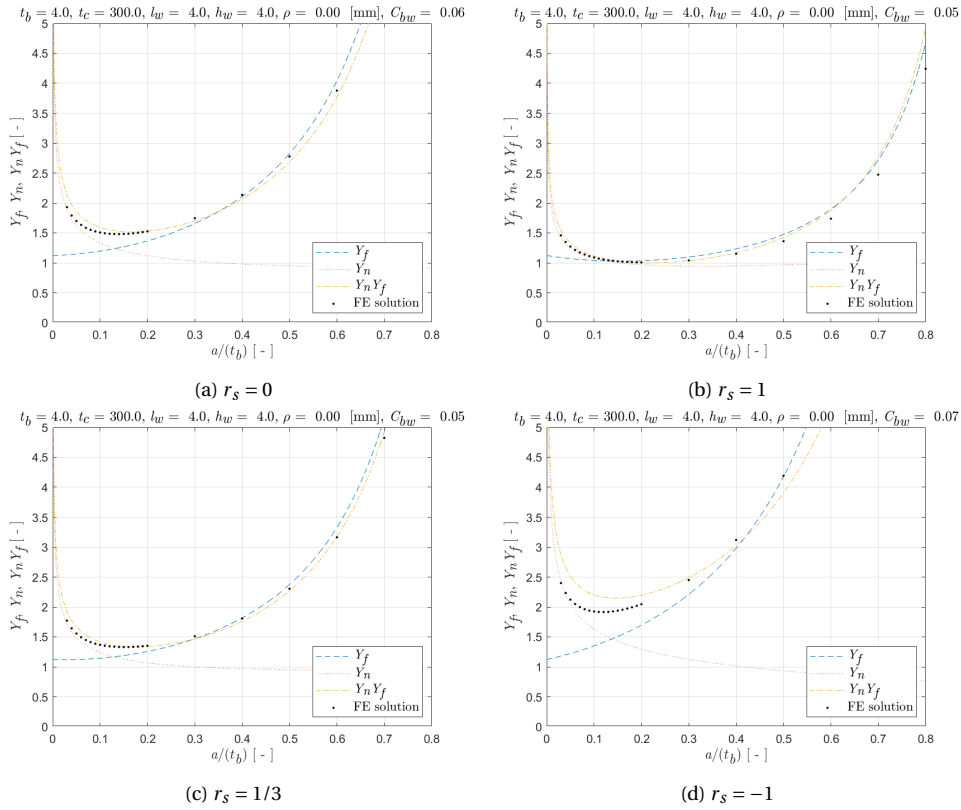


Figure 4.35: Weld notch stress intensity distributions
 $(t_b = 4, l_a = 300, l_w = 4, h_w = 4 \text{ [mm]})$

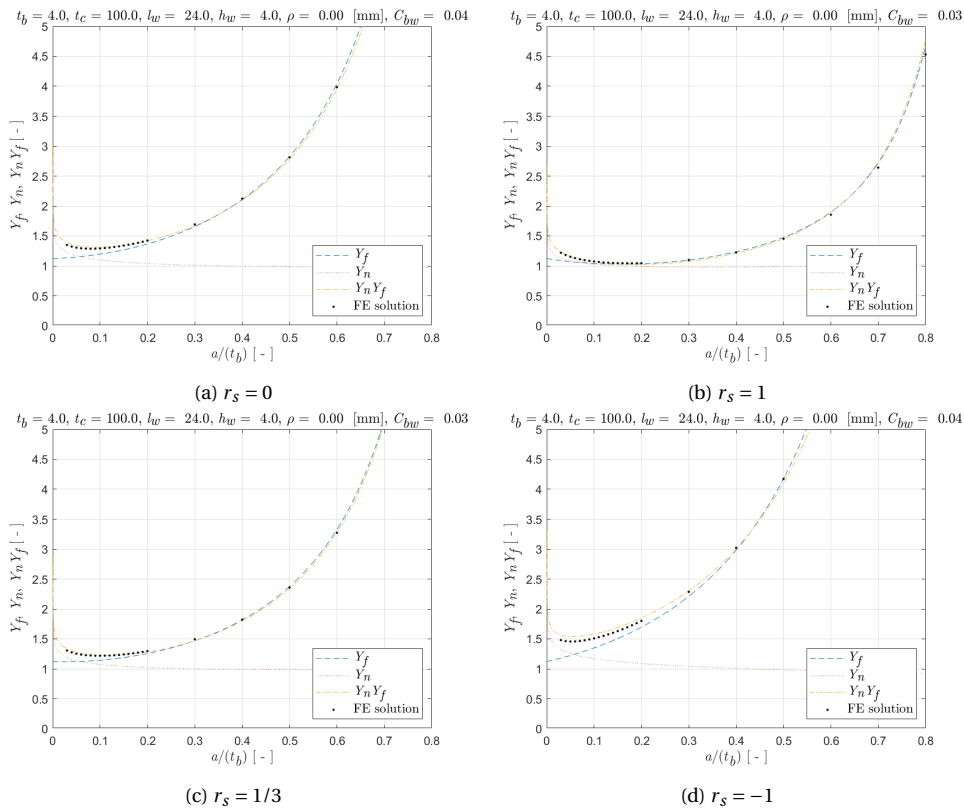


Figure 4.36: Weld notch stress intensity distributions
 $(t_b = 4, l_a = 100, l_w = 24, h_w = 4 \text{ [mm]})$

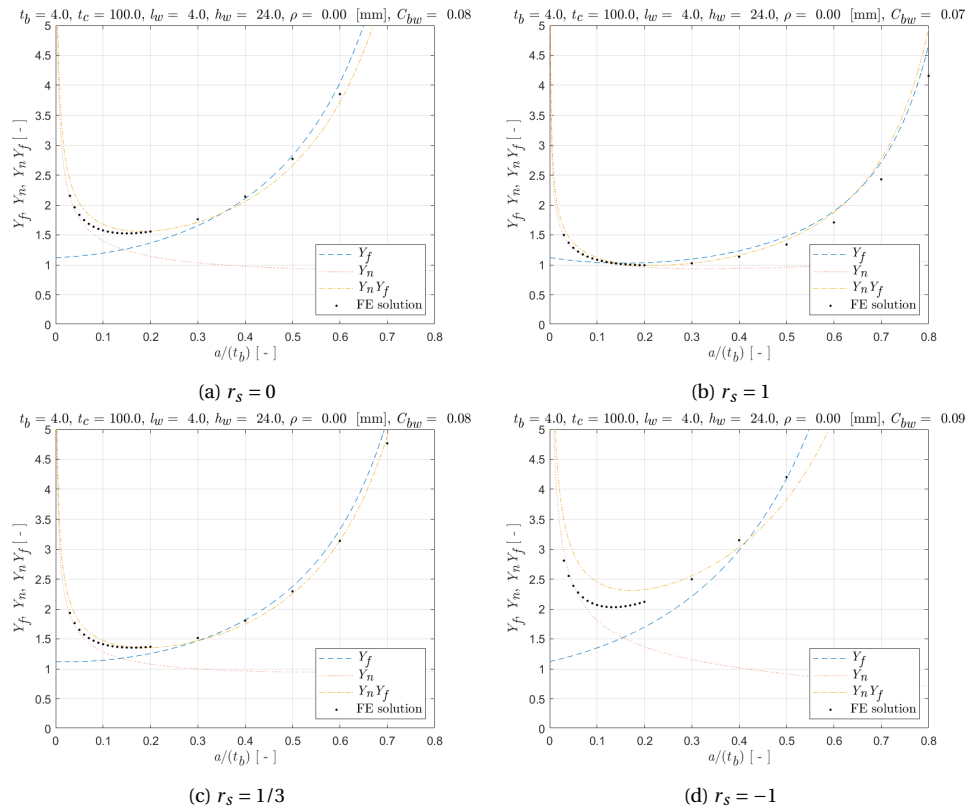


Figure 4.37: Weld notch stress intensity distributions
 $(t_b = 4, l_a = 100, l_w = 4, h_w = 24 \text{ [mm]})$

5

Fatigue resistance of DS longitudinal attachment

Several steel double sided longitudinal attachment fatigue resistance data under constant amplitude are available in literature [7, 11, 21, 23–28, 32–34, 39, 49, 53–55, 58], see Table 5.1. The dimension of base plate thickness t_b ranges from 8 to 35 [mm], the attachment length l_a from 50 to 450 [mm], the weld length l_w from 4 to 12 [mm], the weld height h_w from 4 to 12 [mm], the specimen width w from 40 to 280 [mm], the load ratio r_l from 0 to 0.7 and the yield strength σ_y from 235 to 833 [MPa].

Series	Refs.	Loading*	t_b [mm]	l_a [mm]	l_w [mm]	h_w [mm]	w [mm]	r_l [-]	σ_y [MPa]
1	Yamada, 1980	N	10	100	6	6	80	0.0	373-422
2	Shimokawa, 1985	N	30	450	12	12	280	0.1	833
3	Kawano, 1993	N	25	100	8	6	80	0.0	380
4	Marquis, 1996	N	10	150	10	6	68	0.0	328-420
5	Ohta, 2000	N	20	150	10	10	240	0.0	497-821
6	Dimitrakis, 2001	N	12.7	139.7	9.5	9.5	82.6	0.1	333
7	Kang, 2003	N	10	150	8.5	8.5	60	0.3-0.7	235
8	Huo, 2005	N	8	50	4	4	40	0.1	390
9	Maddox, 1998	N	35	230	8	8	100	0.5-0.7	385
10	Maddox, 2007	N	10	150	5	5	150	0.1	478
11	Maddox, 2011	N	30	230	8	8	100	0.5-0.7	390
12	Weich, 2008	N	16	200	4	4	60	0.1	719
13	Togasaki, 2010	N	12	110	10	10	100	0.1	514
14	Deguchi, 2012	N	16	100	8	8	80	0.0	355
15	Kim, 2013	N	10	150	8.5	8.5	80	0.1	322
16	Kim, 2018	N	10	150	8.5	8.5	80	0.1	357
17	Kainuma, 2015	N	9	120	6.0	6.0	80	0.1	282
18	Mori, 2015	N	12	110	9.5-10.7	8.8-9.6	100	0.04-0.09	456-753
19	Uchida, 2016	N	16	160	10	10	120	0.03-0.06	418

* N: Normal force

Table 5.1: Fatigue resistance data

As discussed in Section 2.4, Basquin type of single slope relation is typically adopted for the medium cycle fatigue (MCF). To estimate the parameters, intercept $\log C$, slope m and standard deviation σ , the maximum likelihood approach is performed [9, 41, 45]. The standard deviation σ and the scatter range index $T_S = S_{R10}/S_{R90}$ related to the survival probability of 10%, and 90% will be used for the performance check of the nominal stress, the structural hot spot stress and the total stress concept [9, 45, 46]. The typical value of T_S

for the fillet welded joint is 1:1.5.

5.1. Nominal stress concept

As explained in Section 2.4.1, the nominal stress concept is based on the global intact geometry. Constant amplitude (CA) fatigue resistance information is commonly obtained using small- or large-scale (beam) specimen and expressed in terms of FATigue classes or detail CATegories. The damage mechanism is assumed to be similar for all structural details, meaning the slope m is invariant [8]. The IIW has classified the FAT class for the steel longitudinal fillet welded attachment depending on the attachment length l_a , see Figure 5.1. Two FAT class of FAT71 and FAT63 are considered due to the range of the attachment length meaning the nominal stress range $\Delta\sigma_n = 71$ [MPa] and 63 [MPa] at $2 \cdot 10^6$ cycles.

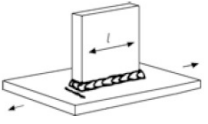
No.	Structural Detail	Description (St. = steel; Al. = aluminium)	FAT St.	FAT Al.
521		Longitudinal fillet welded gusset of length l . Fillet weld around end $l < 50$ mm $l < 150$ mm $l < 300$ mm $l > 300$ mm	80 71 63 50	28 25 20 18

Figure 5.1: IIW recommendation for the welded longitudinal attachment [20]

IIW recommends the thickness correction for the $t_b > 25$ [mm]. The various base plate thicknesses are involved in the fatigue resistance data so correcting the stress range instead of reducing the FAT class has done to keep the one FAT class [20]. So an effective nominal stress range for the $t_b > 25$ [mm] is:

$$S_{n,eff} = S_n \cdot \left(\frac{t_b}{25}\right)^{0.3} \quad \text{for } t_b > 25 \text{ [mm]} \quad (5.1)$$

The maximum likelihood approach as regression analysis for the nominal stress based fatigue test data without thickness correction provides $\sigma = 0.18$ and $T_S = 1 : 1.48$. A lognormal distribution is adopted since it provides a better fit than the HCF related extreme Weibull distribution. Approximately 160 data points are plotted without censored data. The 95 % pointwise lower and upper confidence bounds (LCB and UCB) [41] for respectively the 1 % and 99 % reliability levels are shown together.

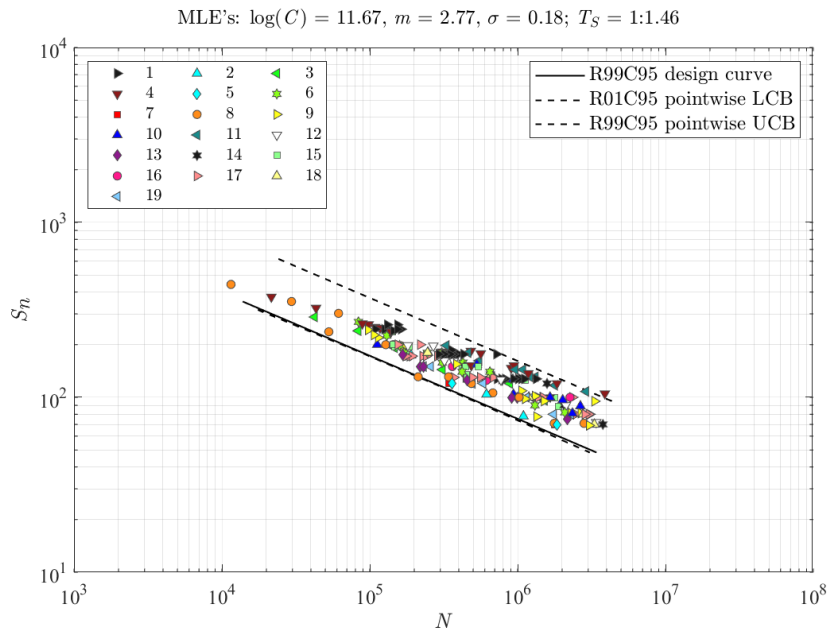


Figure 5.2: Nominal stress based fatigue resistance S-N without thickness correction

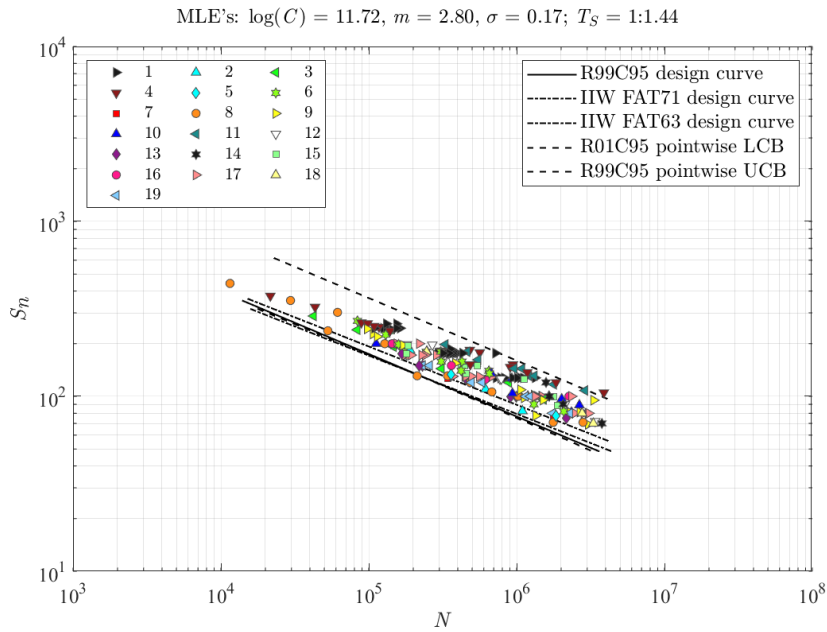


Figure 5.3: Nominal stress based fatigue resistance S-N with thickness correction

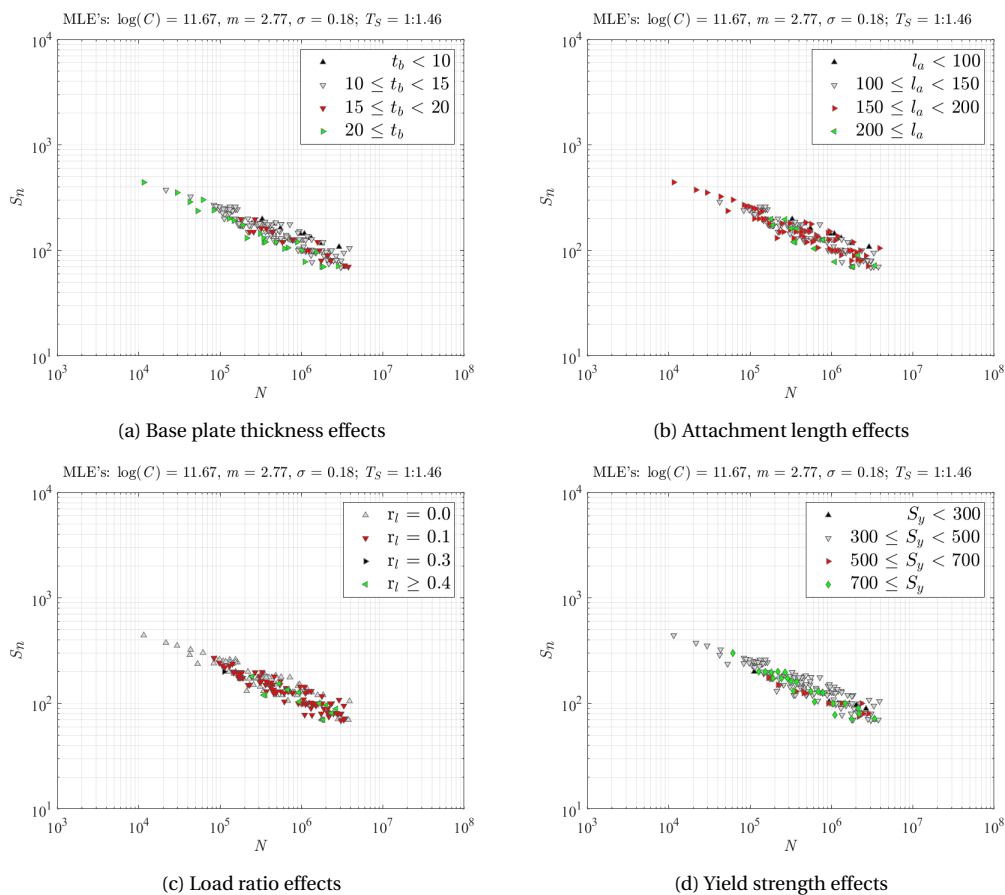


Figure 5.4: Nominal stress based fatigue resistance influence factors

The general fatigue resistance influence factors are shown with the nominal stress based S-N data without any correction. The thicker base plate thickness shows the lower fatigue resistance, and it is well-known physics that the probability of the initial defects increases due to the increased welded material volume. Also, the

increased thickness causes the increased highly stressed material near the notch due to the stress gradient change [9, 47]. The longer attachment length l_a provides the lower fatigue resistance due to the higher stress concentration at the notch. It makes clear why the IIW recommendation classified the fatigue resistance of the longitudinal attachment based on the length of attachment [20]. Generally, the higher load ratio meaning higher mean stress provides the shorter fatigue resistance as well [47]. However, it is not clearly shown in the above figure. Similarly, the yield strength does not explicitly affect the fatigue resistance.

5.2. Structural hot spot stress concept

The structural hot spot stress concept is also based on intact geometry. However, the structural hot spot stress contains the stress concentration due to the local geometry change. The number of classification based on structural details decreases compared to the nominal stress concept. Two FAT classes are determined based on the amount of the weld load carrying. FAT90 for the non-load carrying (NLC) and FAT 100 for the load carrying (LC) fillet weld. Distinguishing NLC and LC is based on engineering judgment. The IIW has recommended the FAT100 for the steel longitudinal fillet ends meaning the structural hot spot stress range $\Delta\sigma_s = 100$ [MPa] at $2 \cdot 10^6$ cycles. However, the FAT90 is also considered here due to the large attachment may induce the load carrying fillet weld.

To get the precise structural hot spot stress, the through-thickness linearization method invented by Dong [14] is adopted with the 8 nodes solid element. The structural hot spot based fatigue resistance is given as follows.

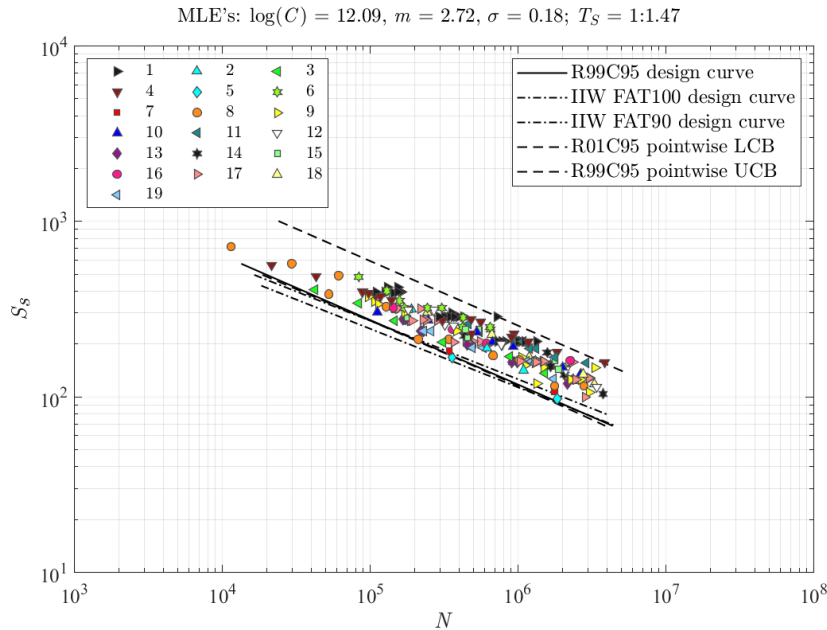


Figure 5.5: Structural hot spot stress based fatigue resistance S-N

No improvement is observed with the structural hot spot stress concept. The same standard deviation σ of 0.18 and the similar scatter range index T_S of 1.47.

In the Section 4.2, it was shown that the weld load carrying coefficient is the function of the weld notch angle $C_{bw} = f(h_w/l_w)$ and the V-shaped notch stress is also a function of the opening angle and base plate thickness. Consequently, the self equilibrating stress component which governs the peak stress and stress gradient is the function of the weld notch angle and the base plate thickness, see Equation 3.1. The stress concentration effect does not consider the size effect which affects the peak stress and the stress gradient near the weld notch. Therefore, almost no improvement is observed, and it is more clear to check the fatigue resistance influence factors, see Figure 5.6. The base plate thickness effect dominates the fatigue resistance rather than the attachment length and others. It is evident because another important factor attachment length effect is already involved in the structural hot spot stress, see Figure 5.7. So the attachment length is already in-

incorporated. Other influence factors, load ratio and yield strength, do not affect the fatigue resistance of DS longitudinal attachment explicitly.

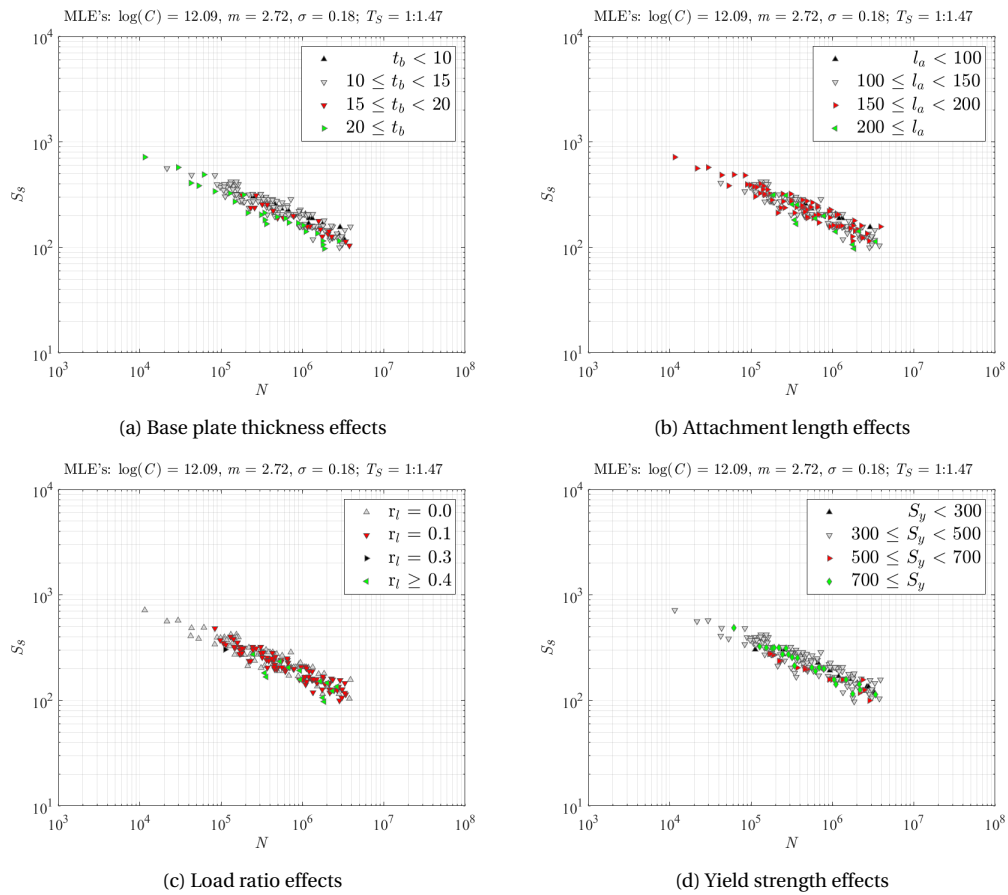


Figure 5.6: Structural hot spot stress based fatigue resistance influence factors

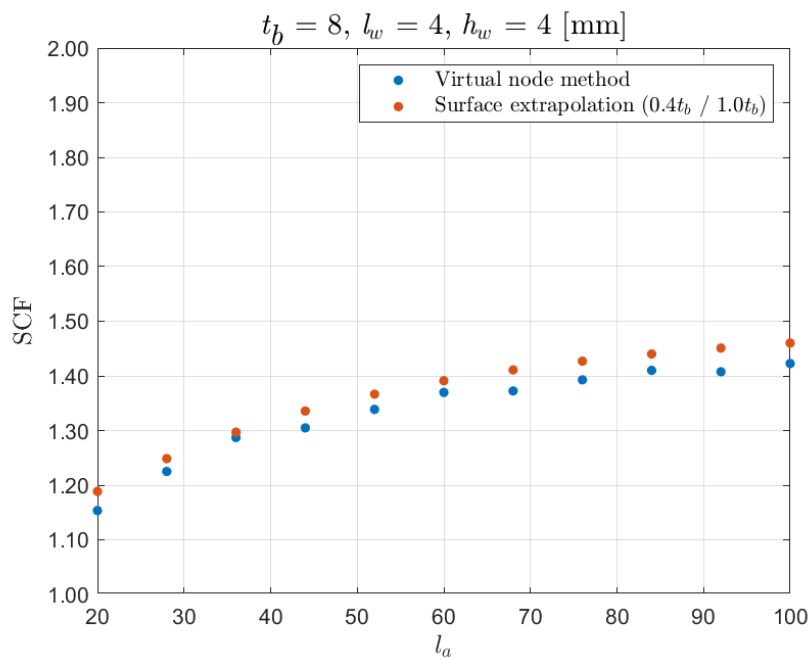


Figure 5.7: Relation between attachment length l_a and SCF at weld toe

5.3. Total stress concept

The total stress parameter S_T is developed from the two-stage crack growth model involving notch affected micro crack growth and far field affected macro crack growth considering the SIF as the crack driving force. The notch factor Y_n involves the weld load carrying stress coefficient C_{bw} which can be defined by the double weld element beam model or parametric formula. The brief description of the total stress concept was in Section 2.4.4. Again the total stress parameter S_T is shown as below:

$$S_T = \frac{\Delta\sigma_s}{(1-r_l)^{1-\gamma} \cdot I_N^{\frac{1}{m}} \cdot t_b^{\frac{2-m}{2m}}} \quad (5.2)$$

with

$$I_N = \int_{\frac{a_i}{t_b}}^{\frac{a_f}{t_b}} \frac{1}{\left\{Y_n\left(\frac{a}{t_b}\right)\right\}^n \cdot \left\{Y_f\left(\frac{a}{t_b}\right)\right\}^m \cdot \left(\frac{a}{t_b}\right)^{\frac{m}{2}}} d\left(\frac{a}{t_b}\right) \quad (5.3)$$

Notch crack growth integral I_N requires an initial crack length and final crack length. And the result of integration is much more sensitive to the initial crack length a_i rather than the final crack length a_f [3]. The realistic initial crack length ratio a_i/t_b of 10^{-3} is adopted same as Dong [16]. Naturally the final crack length a_f of the base plate thickness t_b is considered i.e. $a_f/t_b = 1$ because of the through-thickness crack behavior.

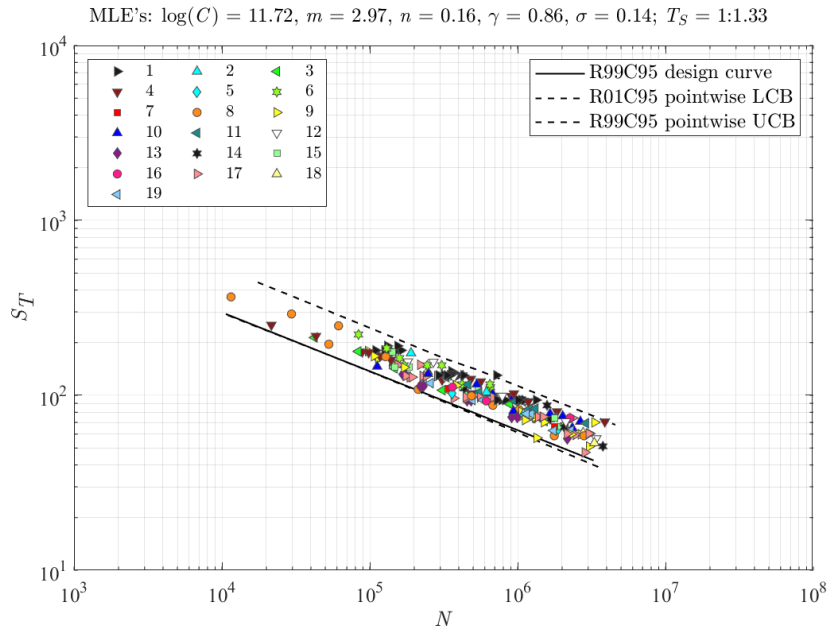


Figure 5.8: Total stress based fatigue resistance S-N

Maximum likelihood estimation with various initial crack lengths a_i is shown in Table 5.2. Results show that the bigger initial crack length is more likely. However, too large initial crack length such as $a_i/t_b \geq 0.1$ is not realistic that is already out of the notch affected region for the intact as-welded joints [15]. Most of the parameters are not sensitive to the a_i except the fatigue resistance constant C and the elastoplasticity coefficient n .

a_i/t_b	$\log(C)$	m	n	γ	σ	T_σ	\mathcal{L}
$1 \cdot 10^{-1}$	13.22	2.97	1.41	0.86	0.14	1:1.33	58.5230
$5 \cdot 10^{-2}$	12.86	2.97	0.76	0.86	0.14	1:1.33	58.5401
$1 \cdot 10^{-2}$	12.31	2.97	0.33	0.86	0.14	1:1.33	58.5832
$5 \cdot 10^{-3}$	12.12	2.97	0.25	0.86	0.14	1:1.33	58.5982
$1 \cdot 10^{-3}$	11.72	2.97	0.16	0.86	0.14	1:1.33	58.6227
$5 \cdot 10^{-4}$	11.56	2.97	0.13	0.86	0.14	1:1.33	58.6297
$1 \cdot 10^{-4}$	11.20	2.97	0.09	0.86	0.14	1:1.33	58.6405
$5 \cdot 10^{-5}$	11.05	2.97	0.08	0.86	0.14	1:1.33	58.6435
$1 \cdot 10^{-5}$	10.71	2.97	0.06	0.86	0.14	1:1.33	58.6484
$5 \cdot 10^{-6}$	10.56	2.97	0.06	0.86	0.14	1:1.33	58.6498

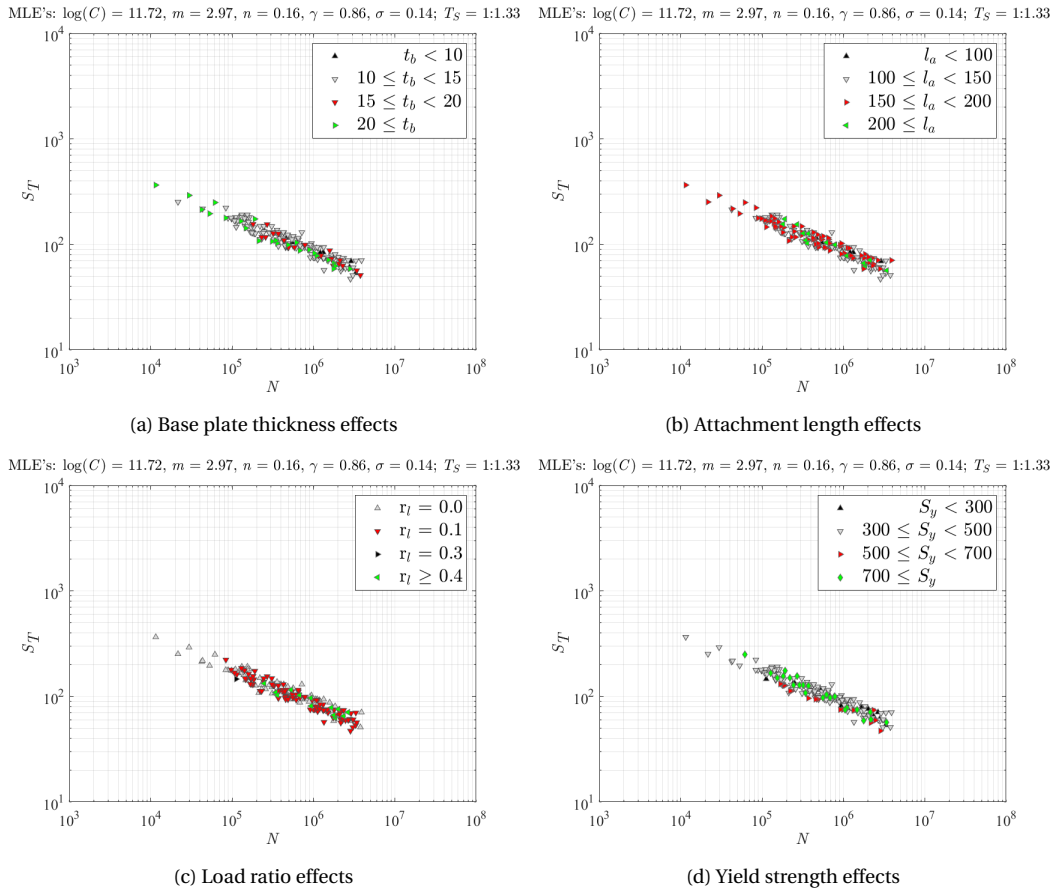
Table 5.2: Likelihood and scatter range index for varying initial crack length a_i/t_b 

Figure 5.9: Total stress based fatigue resistance influence factors

In Figure 5.9, the fatigue resistance influence factors t_b and r_l are incorporated because the size effect and mean stress effect are explicitly considered by using scaling parameter $t_b^{2-m/2m}$ and the effective structural stress range $\Delta\sigma_s/(1-r_l)^{1-\gamma}$ receptively. Also, the considered through thickness stress distribution with the weld load carrying coefficient C_{bw} contributes the size effect as well. The attachment length l_a is also incorporated because the total stress parameter S_T is based on the structural stress which contains the attachment length effect.

	σ	T_S	T_N^*
Nominal stress	0.18	1:1.46	1:2.85
Hot spot stress	0.18	1:1.47	1:2.85
Total stress	0.14	1:1.33	1:2.33

$$* T_N = T_S^m$$

Table 5.3: Comparison between the nominal, structural hot spot and total stress concept

The total stress concept provides a significant improvement where the standard deviation decreases to 0.14, and the scatter range index becomes 1:1.33. Decrease of the standard deviation σ indicates more accurate fatigue life estimation. Decrease of the scatter range index T_S , and T_N indicates the increase of the quality of the fatigue life estimation.

6

Fatigue testing of single sided butt joints using a Hexapod

The aim of this section is to propose a working design for full scale riser specimen containing single sided butt joint to be tested in the Hexapod test setup at TU Delft. Two design options have been investigated. FE analysis is performed to evaluate local and global geometry stresses.

6.1. Riser response and critical failure location

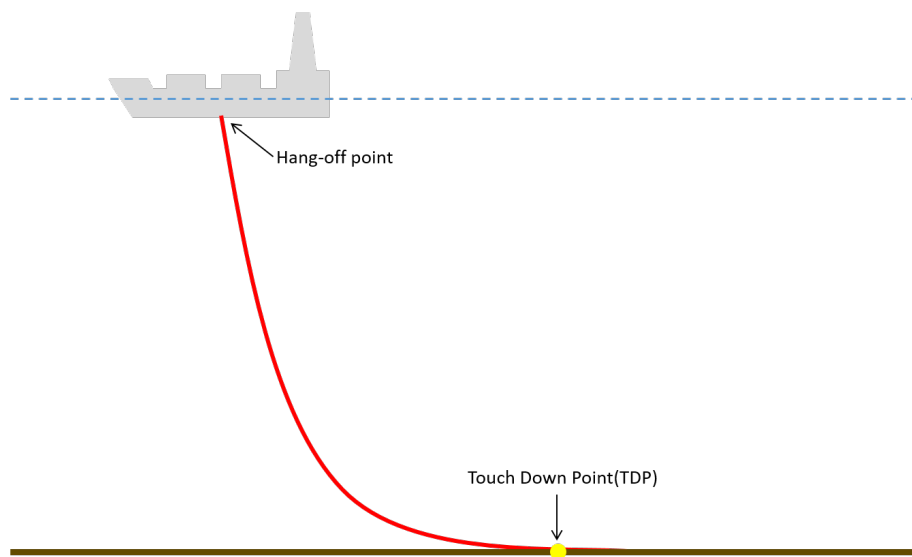


Figure 6.1: Schematic for typical free hanging SCR

The free hanging configuration is the simplest configuration for the riser system. It is also the cheapest to install because of minimal subsea infrastructure, and relatively easy to install. However, the free hanging configuration is exposed to severe loading due to vessel motions. The riser is simply lifted off and lowered down on the seabed by the vessel motion. This cyclic loading due to vessel motions is a trigger for the fatigue failure of the welded joint at the touch down point (TDP) location, detailed in Figure 6.1. The full scale specimen with single sided girth welded butt joint will be tested by simulating the critical loading and response at the touch down point. Details of the welded geometry are shown in Figure 6.2. For most of the practical purposes, the weld reinforcement is grinded and fatigue failure is observed at the weld root location. The SCR is fabricated by welding together seamless pipe segments produced from high strength steel (X65-X70). Figure 6.1 shows a schematic for a typical free hanging steel catenary riser (SCR) configuration.

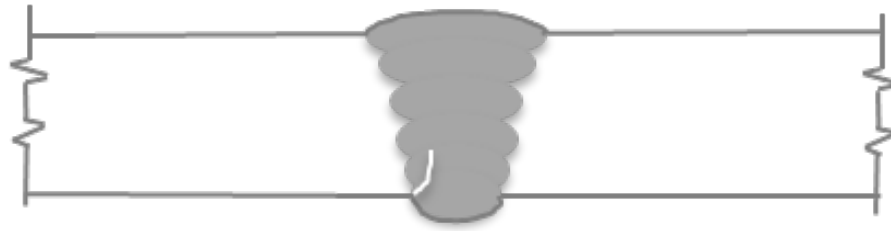


Figure 6.2: Single sided girth weld with weld root crack

6.2. Loading Condition

To represent real physics, proper loading condition of the specimen has to be determined for the experiment. From the simulation with OrcaFlex 10.0a, desired response level of the TDP riser FSS is determined in SCReen preliminary report [40]. The major loading condition for fatigue failure is Mode I cyclic bending due to vessel motion. Although dynamic loading is an uni-axial, the static loading condition is multi-axial due to combined global tension, bending and internal pressure. These multi-axial static loading condition will act as a mean value of fatigue loading. The external pressure is not considered because the net pressure direction is outward from the centre of the riser. Desired response level at the middle girth weld location is shown in Table.

Normal stress, σ_n [MPa]	Bending stress, σ_b [MPa]	Internal pressure, p_i [MPa]
43.5	150	20

Table 6.1: Desired static response level

6.3. Full scale fatigue testing rig

The experiment is conducted with a unique test machine Hexapod at TUDelft, Figure 6.3. It is capable of applying dynamic loading and displacement in 6 Degrees of Freedom. For fatigue testing, the full scale specimen must be fixed in the Hexapod using a bolted connection.

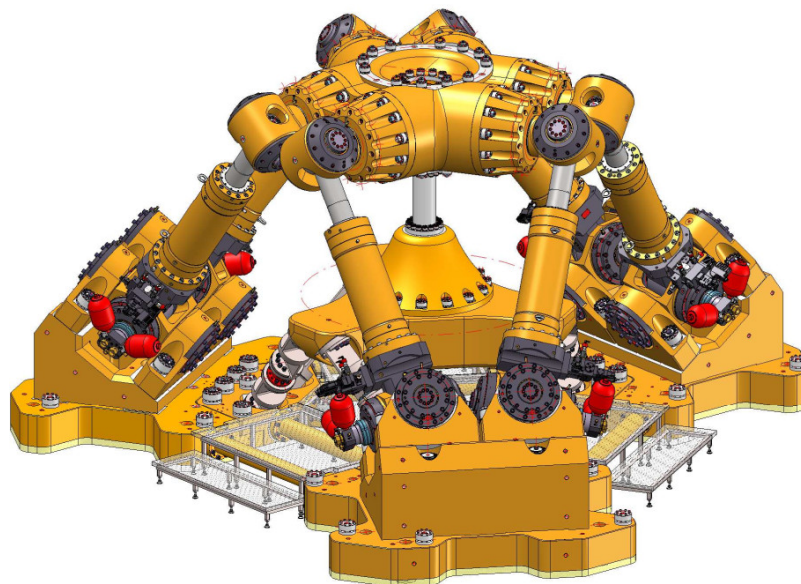


Figure 6.3: Fatigue test rig - Hexapod (TU Delft)

6.4. Specimen Design

The main aim of the specimen design is to propose an intermediate connection such that the riser pipe can be bolted to the Hexapod. The design criteria is that the riser weld to be tested must remain the fatigue sensitive

location in the specimen.

Size [in.]	Outside Diameter [in.]	Outside Diameter [mm]	Wall Thickness [in.]	Wall Thickness [mm]
8	8.625	219.1	0.812	20.62

Table 6.2: 8" pipe dimension [2]

Grade	Yield Strength, Min. [MPa]	Yield Strength, Max. [MPa]	Ultimate Tensile Strength, Min. [MPa]	Ultimate Tensile Strength, Min. [MPa]
X65	448	600	531	758

Table 6.3: X65 steel grade specification [2]

6.4.1. Specimen Design - Option 1

A riser pipe segment with weld will be provided by companies associated with SCReen project. To attach this riser pipe segment with the Hexapod, the first option proposed here is welding flanges with holes at the pipe ends. This seems to be a very simple and economical option. However, this option must be checked to fulfil the design criteria. Detailed geometry is shown in Figure 6.4 and 6.5.

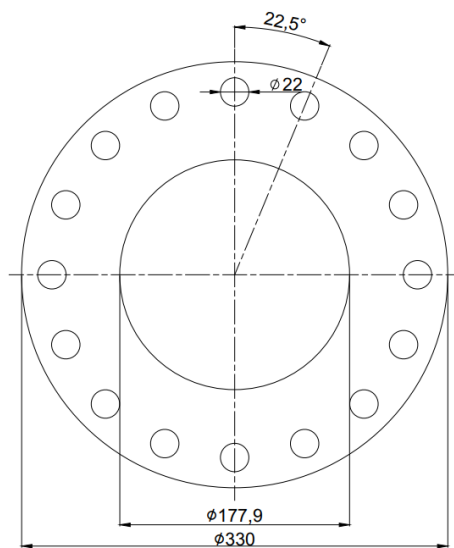


Figure 6.4: Top view of specimen

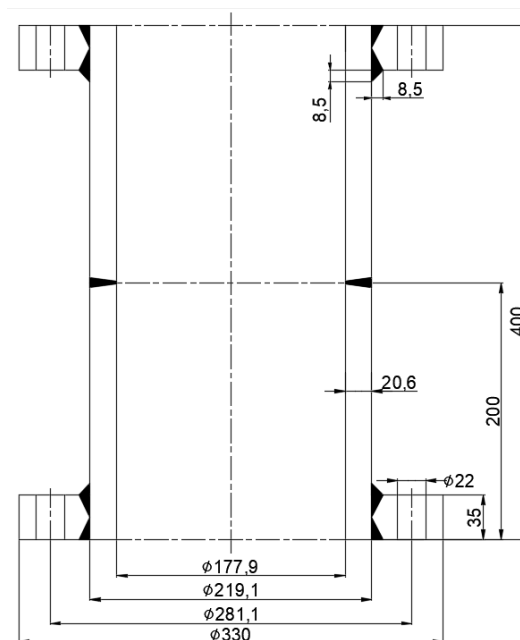


Figure 6.5: Specimen geometry

FE model

Only half of the specimen is modelled due to its symmetric geometry and computational efficiency. In the FE model, the platform is included. The platform is a component to represent the test machine that transfers the load to specimen. And also it helps the accuracy of analysis by considering the contact mechanism between specimen and test machine. The FE model is shown in Figure 6.6.

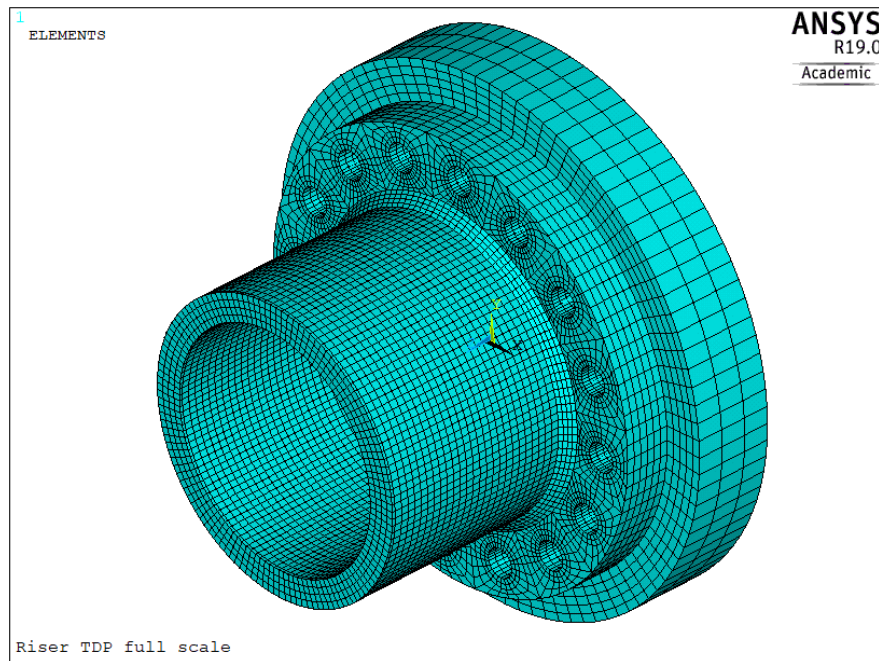


Figure 6.6: FE model of riser specimen with platform

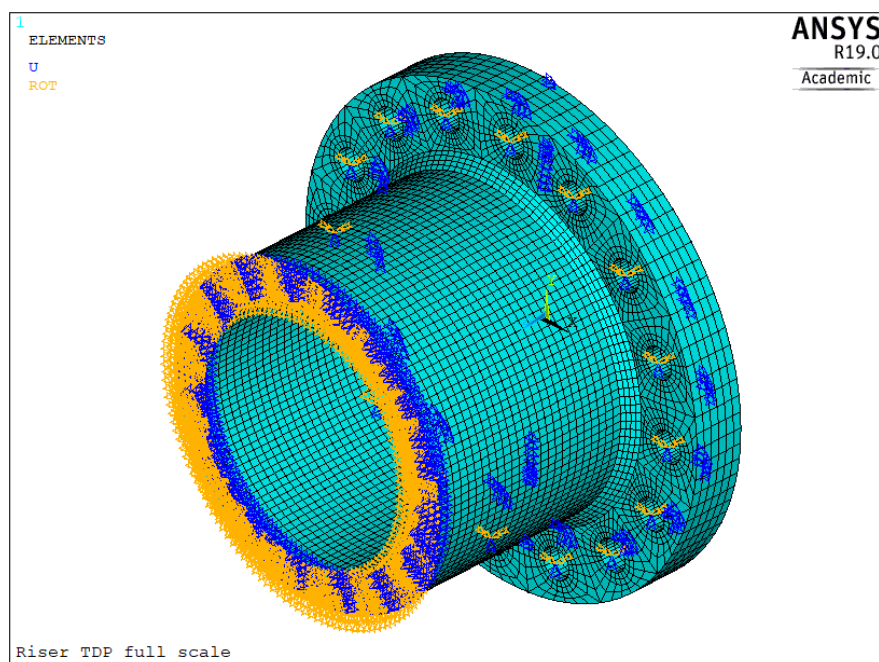


Figure 6.7: FE model of riser specimen without platform including boundary conditions (Blue: displacement constraint, Orange: rotation constraint)

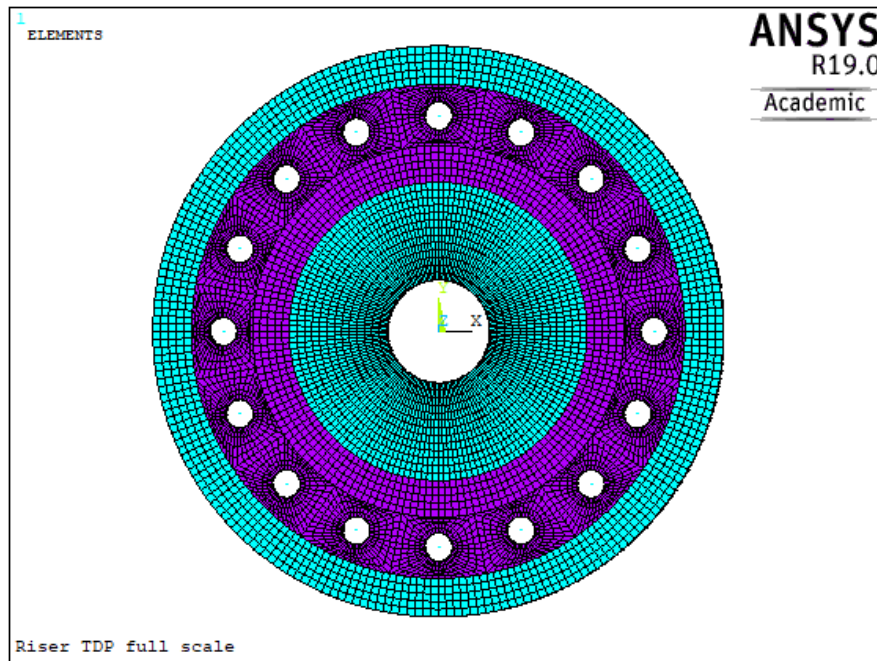


Figure 6.8: Contact elements at the platform surface

The separation allowed contact modelling is done at the surface of the flange and platform. Connecting Bolts are modelled with the beam elements and rigid sections.

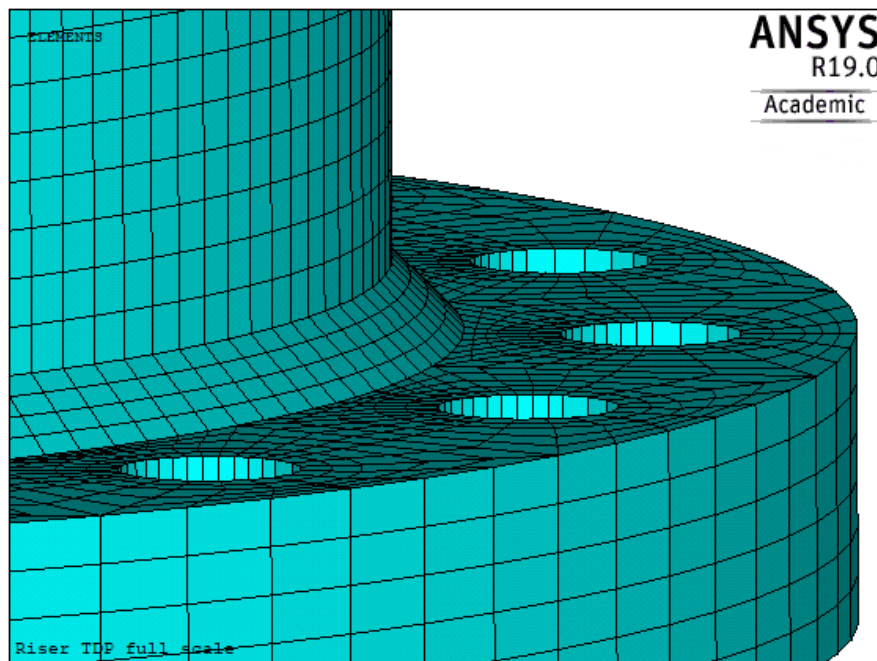


Figure 6.9: Flange-pipe connection

Response

Only bending loading condition is considered in here which is major mode I fatigue load. Axial normal force and internal pressure are rather constant hence only induce the mean stress. Bending load is applied from test machine same as the platform in FE model and transferred to the specimen through bolts. Bolts are modelled with the beam elements. The bolt heads and nuts are modelled by rigid section. The target bending response is when the bending stress at the weld root equals 150[MPa]. The master node is taken to apply the bending moment to the surface of the platform.

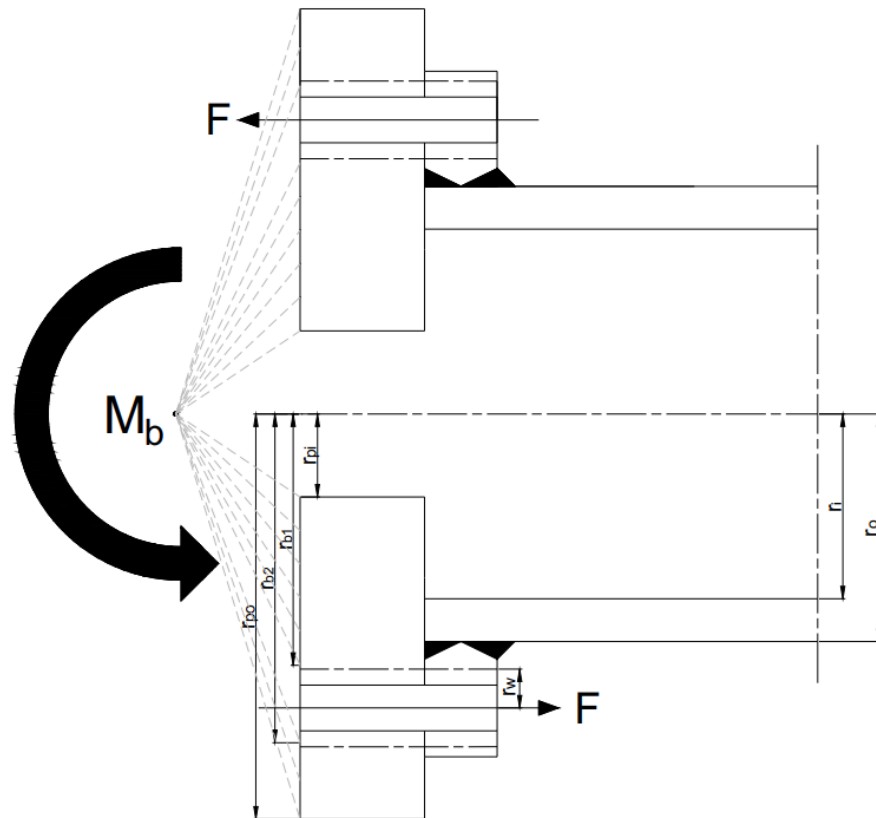


Figure 6.10: Schematic plot for the bending loading

From simple beam bending theory, stress distribution through the thickness should be a below formula.

$$\sigma_b = \frac{M_b \cdot y}{I_x} \quad (6.1)$$

From the above simple formula, required bending moment can be calculated as 107.85[kNm]. Because of nonlinearity at the contact surface between specimen and test machine, a response could have some difference with the analytical solution, but it is acceptable.

Bending stress response of FEM is shown below.

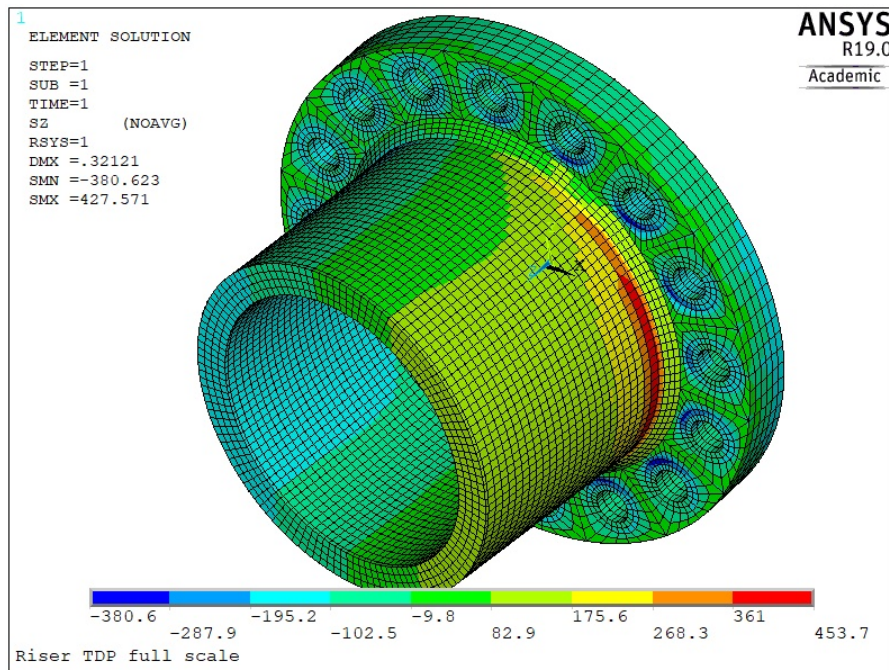


Figure 6.11: Bending stress distribution under pure bending

And the cross section of the specimen in FE result is following.

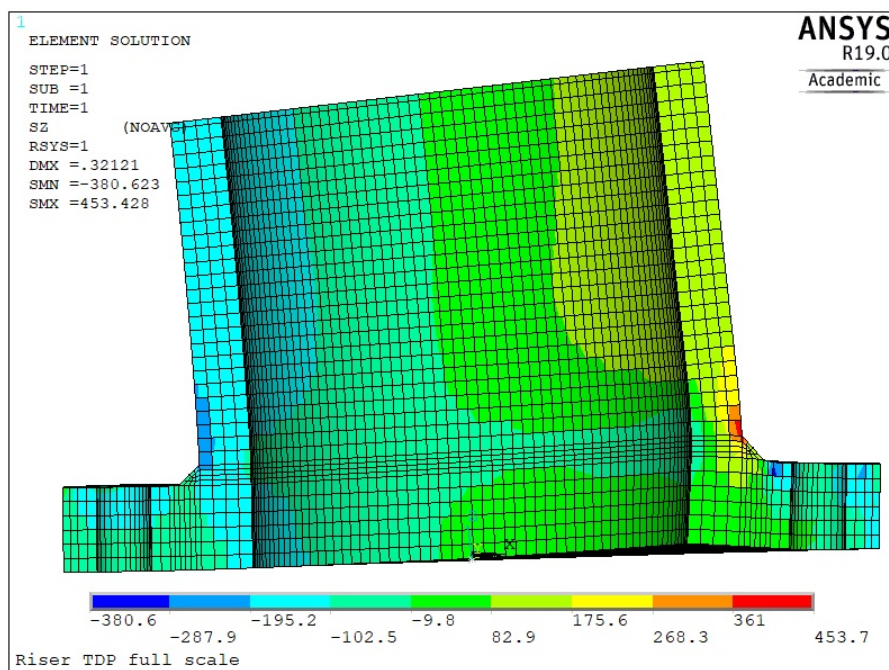


Figure 6.12: Cross sectional bending stress distribution

Local geometry change at the flange-pipe connection causes normal stress varying in the pipe wall. Therefore enough distance is required for girth weld location from the flange-pipe connection. But for the cost and testing frequency, a short specimen is recommended. Therefore the optimum length of the specimen is checked by comparing FEM bending stress results with different lengths.

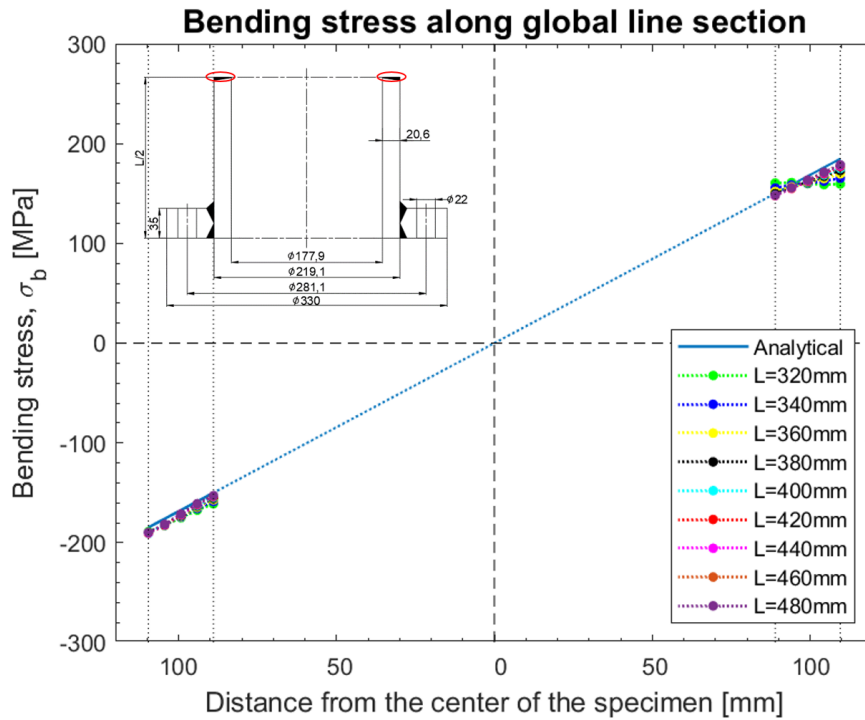


Figure 6.13: Bending stress at the middle cross section with various total length of specimens

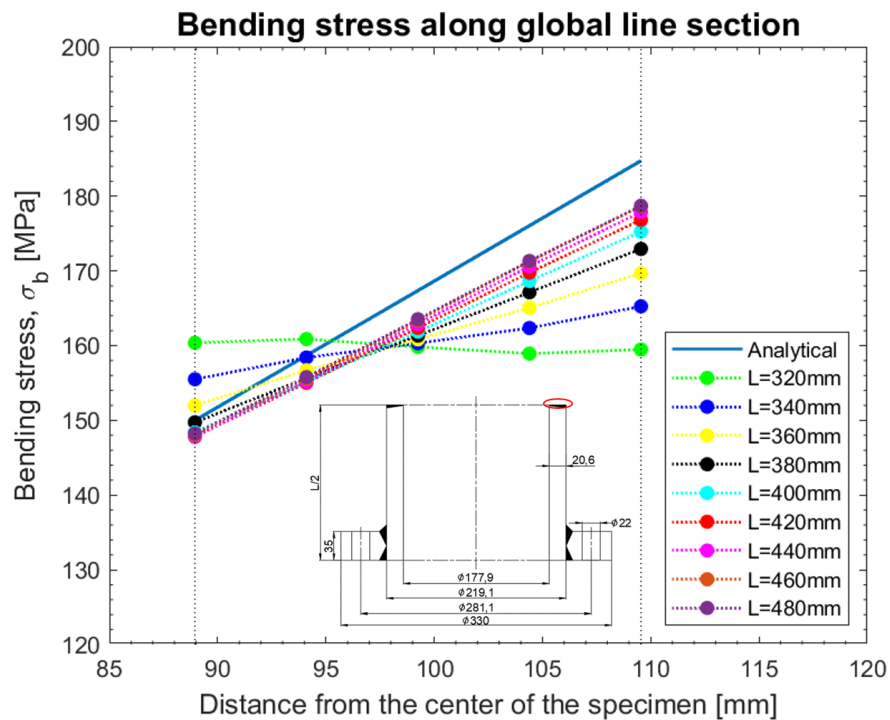


Figure 6.14: Zoomed plot of Figure 6.13

Apart from the value shown in Figure 6.14, stress gradient in through-thickness direction is important. From the total length of 400 [mm] which is around double of the outer diameter, stress gradient does not change much and shows similar to an analytical result. So total specimen length of 400 [mm] is adopted for the analysis. Therefore, the total weight of the full specimen is roughly 63.7[kg] including the flange.

Fatigue resistance

In the specimen geometry, the fillet weld toe at flange-pipe connection is obviously critical. Thus the fatigue resistance comparison is required with girth weld root. Even though the girth weld is not considered in the FE model, considering the worst scenario would be helpful for real case. The hot spot stress S-N curves for girth weld from DNV and load carrying single side T-joint from IIW recommendation are adapted to compare the fatigue resistances between girth weld at the middle of the specimen and flange-pipe connection.

S-N curve comparison From the DNVGL-RP-C203 [12] and IIW recommendation [20], girth weld with small misalignment is the FAT class of 80 and load carrying T-joint is FAT class of 90 with different slopes at HCF region. Both S-N curves are based on as-welded and hot-spot stress, see Figure 6.15

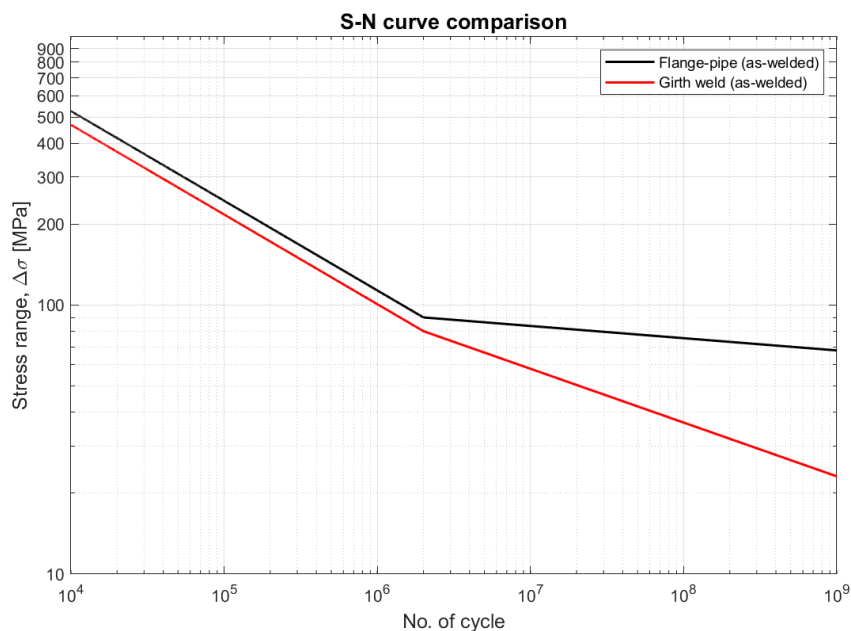


Figure 6.15: S-N curves of girth weld and T-joint based on hot-spot stress

From the FE analysis, structural stress of 151.6[MPa] at the weld root location and 412.7[MPa] at the weld toe of flange-pipe connection fillet weld are obtained. Taking the structural stress of weld root as reference stress then SCF at the weld toe of flange-pipe connection becomes 2.75. It means stress range is also amplified factor of SCF in the S-N curve. For the sake of comparison between two S-N curves, factored S-N curve by SCF is performed for flange-pipe connection, see Figure 6.16.

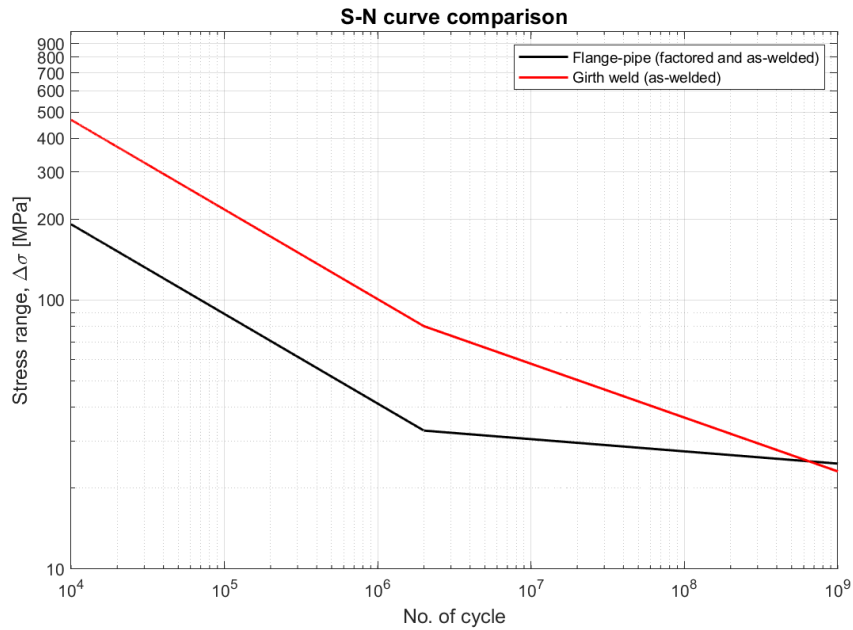


Figure 6.16: Factored S-N curve by SCF

Now the flange-pipe connection is weaker than the girth weld in most of the lifetime of the specimen. And this is an unpleasant situation for the fatigue test of girth weld. Even though post weld improvement is considered such as grinding effect is not enough, see Figure 6.17. For the hot-spot stress based S-N curve of load carrying fillet weld, grinding improves FAT class to 112 [20].

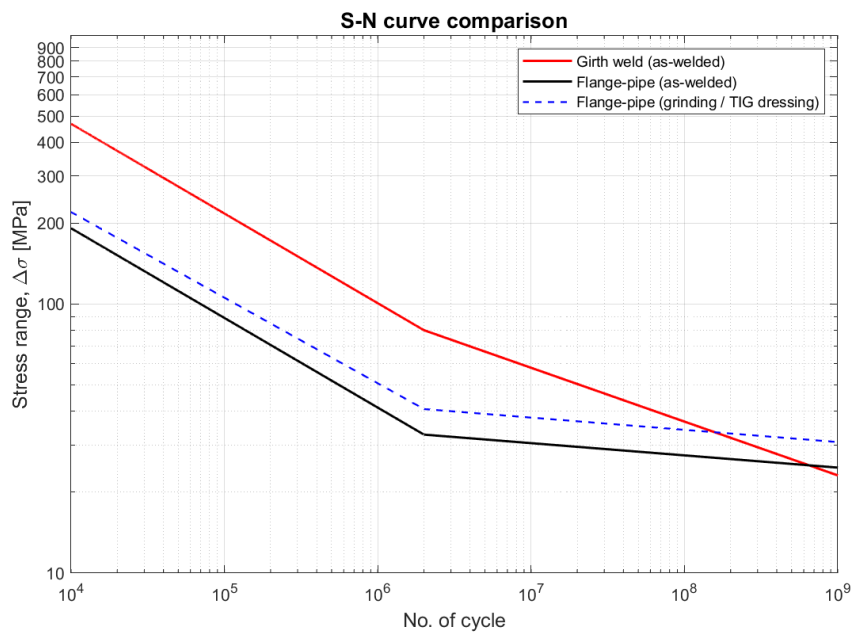


Figure 6.17: Factored and grinding considered S-N curve

Smaller SCF is required to get the fatigue critical location at the girth weld. For fatigue failure to occur at the girth weld location, the required SCF at the flange-pipe weld connection has been evaluated.

$$\text{As-welded : } \frac{90}{SCF_{req}} > 80 \rightarrow SCF_{req} < 1.125 \tag{6.2}$$

$$\text{Grinding : } \frac{112}{SCF_{req}} > 80 \rightarrow SCF_{req} < 1.4 \tag{6.3}$$

Geometric modification

Part of the real riser pipe is provided by companies. Therefore, there is a limitation to modify the specimen geometry. To reduce stress at the structural component, increasing thickness is the easiest way. However, increasing wall thickness is not possible; hence varying flange thickness is tried. Additionally, changing specimen length shows different stress at the middle in Figure 6.13 and 6.14. Hence varying specimen length is also tried and best geometric values will be selected regarding flange thickness and specimen length.

Flange thickness Changing flange thickness reduces bending response at the flange-pipe connection. Therefore, stress concentration can be reduced. However, flange thickness also affects the stress distribution at the middle of the specimen for that reason the length of the specimen should be modified together, see Figure 6.18 and 6.19

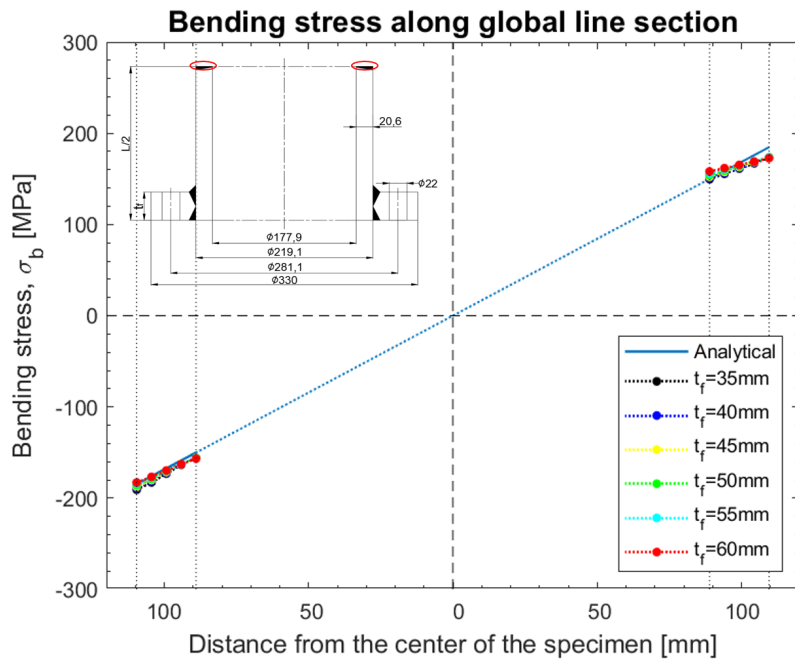


Figure 6.18: Bending stress at the middle cross section with various flange thickness under fixed length of specimen

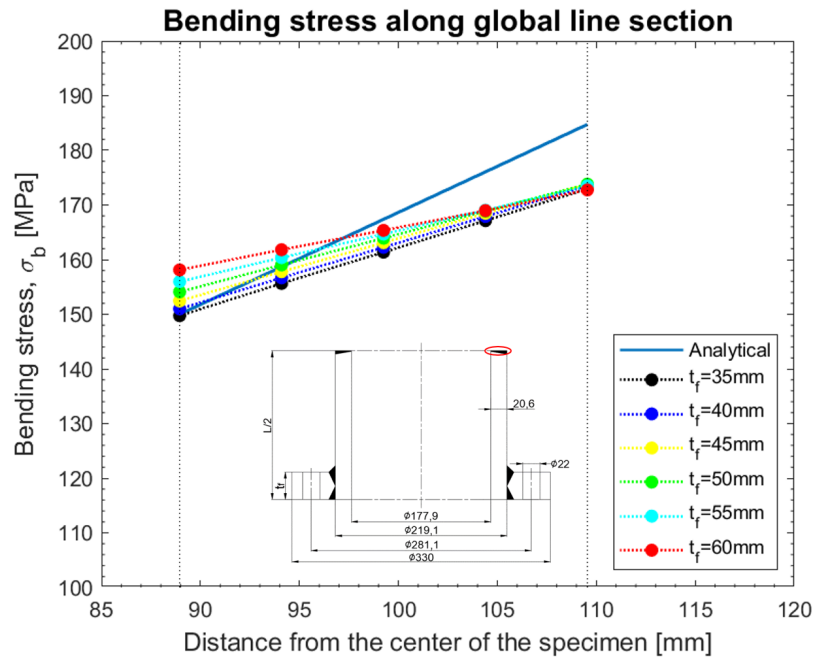


Figure 6.19: Zoomed plot of Figure 6.18

From Figure 6.18 and 6.19, bending stress distribution change is observed with increasing flange thickness. For thicker flanges, the flange-pipe weld connections move closer to the centre weld and effectively the notch stress at the flange-pipe weld affects the stress distribution at the centre weld.

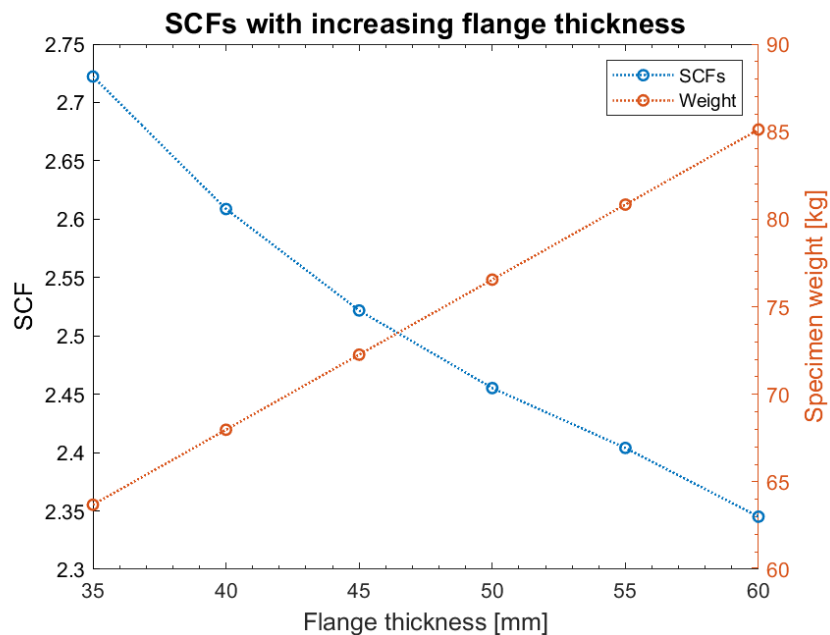


Figure 6.20: SCFs with various flange thicknesses

Increasing flange thickness can reduce the stress concentration but naturally the weight increases, see Figure 6.20. Since it is difficult to handle and install heavier specimens in the laboratory, the weight of the specimen must also be kept to the minimum possible.

Specimen length Figure 6.13 and 6.14 show that increasing specimen length causes less bending stress change due to the flange. Consequently, at least some amount of the specimen length is necessary to get rid of the effect of the flange.

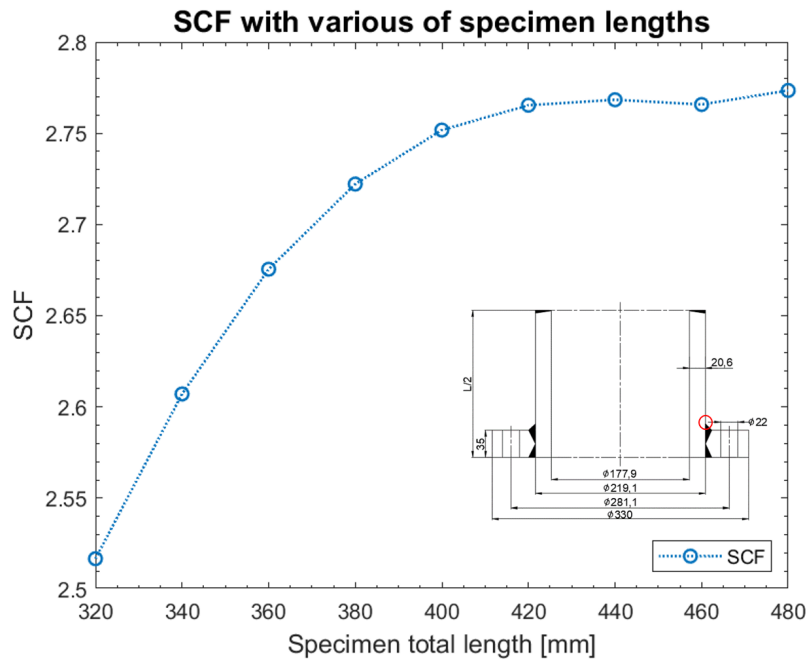


Figure 6.21: SCFs with various specimen lengths

Since the total length of 400 [mm] around double of the diameter, convergent SCFs are observed in Figure 6.21. Meaning, at least the distance of 165 [mm] between the top of the flange and the middle of the specimen is required to avoid stress change due to the flange at the middle girth weld location.

From the Equation 6.3 in Section 6.4.1, SCF smaller than 1.4 is required for even grinding considered situation. But SCF is still far higher than the required design criterion. Other various post weld improvement methods will be discussed to clarify the availability of the first specimen design option.

Post weld improvement methods

There are many post weld improvement techniques however these can be categorized into two main groups: *Residual stress method* and *Weld geometry improvement method*, see Figure 6.22.

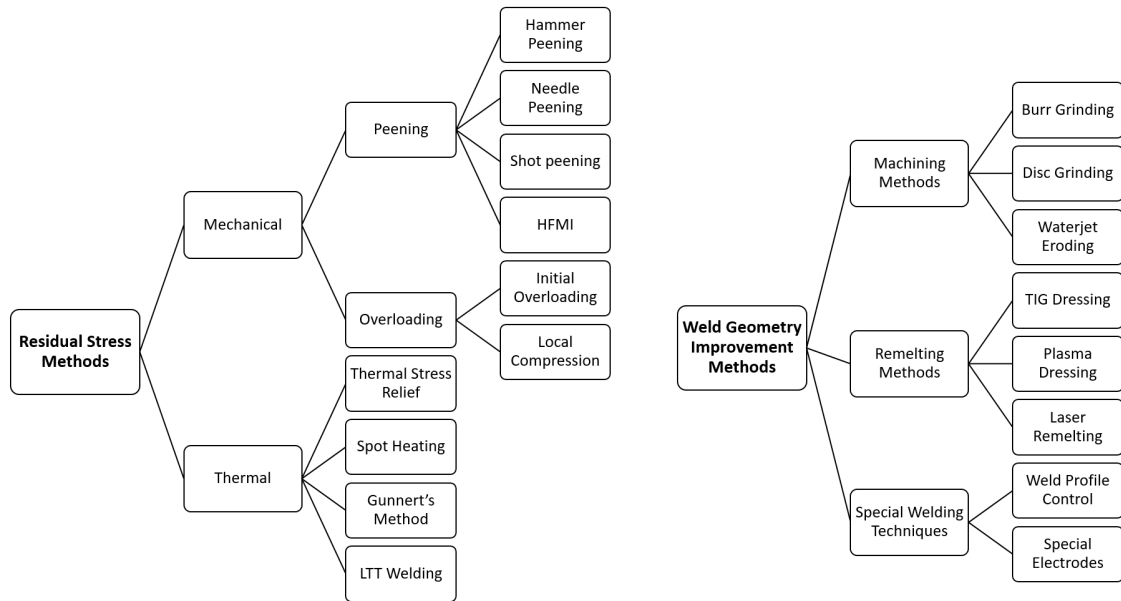


Figure 6.22: Overview of different weld improvement techniques [35]

Residual stress method aims to reduce tensile residual stress due to weld by inducing compressive residual stress with mechanical or thermal way. Weld geometry improvement method aims to improve weld surface quality to reduce stress concentration. IIW recommendation covers some post weld methods such as hammer, needle peening and grinding but still many methods are not covered yet. Therefore post weld methods already have enough reliability from international codes especially IIW recommendation is considered here.

Weld geometry improvement methods

Grinding Grinding removes weld toe imperfections at weld toe and reduces the stress concentration. It can be performed with burr and disc. For the steel, FAT class with structural hot-spot stress can be improved to 112 for load carrying fillet welds by IIW recommendation. It was shown in Section 6.4.1.

Material	Load-carrying fillet welds	Non-load-carrying fillet welds and butt welds
Mild steel, $f_y < 355$ MPa	112	125
Higher strength steel, $f_y \geq 355$ MPa	112	125
Aluminium alloys	45	50

Table 6.4: FAT classes for use with structural hot-spot stress at joints improved by grinding [20]

TIG dressing Tungsten Inert Gas (TIG) dressing remelts weld toe to remove the weld toe imperfections and make smooth transition similar for reducing stress concentration. TIG dressing has the same improvement in fatigue resistance as grinding. FAT class with structural hot-spot stress of steel will increase until 112 for load carrying fillet welds.

Material	Load-carrying fillet welds	Non-load-carrying fillet welds and butt welds
Mild steel, $f_y < 355$ MPa	112	125
Higher strength steel, $f_y > 355$ MPa	112	125
Aluminium alloys	45	50

Table 6.5: FAT classes for use with structural hot-spot stress at joints improved by TIG dressing [20]

Residual stress methods

Residual stress method induces beneficial compressive stress by causing plastic deformation at the weld toe. Stress ratio is an important variable to assess fatigue resistance with this method because it is related to the residual stress. Consequently, there is no benefit when the stress ratio is high which means high mean stress compared to stress range.

Hammer and needle peening Hammer and needle peening induce compressive stress by plastic deformation. The effect depends on yield stress and stress ratio.

Material	Load-carrying fillet welds	Non-load-carrying fillet welds
Mild steel, $f_y < 355$ MPa	112	125
Higher strength steel, $f_y \geq 355$ MPa	125	140
Aluminium alloys	50	56

Table 6.6: FAT classes for use with structural hot-spot stress at joints improved by hammer peening [20]

Material	Load-carrying fillet welds	Non-load-carrying fillet welds
Mild steel, $f_y < 355$ MPa	112	125
Higher strength steel, $f_y > 355$ MPa	125	140
Aluminium alloys	50	56

Table 6.7: FAT classes for use with structural hot-spot stress at joints improved by needle peening [20]

Both peening methods depend on applied stress ratio $R = r_l = \sigma_{min}/\sigma_{max}$. Detailed stress ratio effect is following [20] :

- if, $R < 0$: The S-N resistance curve is used with full stress range $\Delta\sigma$
- $0 < R \leq 0.4$: The S-N resistance curve is used with the maximum stress σ_{max}
- $0.4 < R$: Then there is no benefit

HFMI High Frequency Mechanical Impact(HFMI) is the method to induce beneficial compressive stress at the weld toe by cylindrical indenters with high frequency(about 90[Hz]). Table 6.8 shows how much fatigue resistance improvement occurs by HFMI.

f_y (MPa)	Load-carrying fillet welds		Non-load carrying fillet welds	
	FAT	$K_{S,min}$	FAT	$K_{S,min}$
	As-welded, $m = 3$			
All f_y	90	–	100	–
	Improved by HFMI, $m = 5$			
<355	140	–	160	–
355–550	160	–	180	–
550–750	180	–	200	1.15
750–950	200	1.15	225	1.25
>950	225	1.25	250	1.40

Table 6.8: FAT classes for use with structural hot-spot stress at joints improved by HFMI [35]

A load carrying fillet welds part in Table 6.8 is graphically shown in the following Figure 6.23 as a function of yield stress.

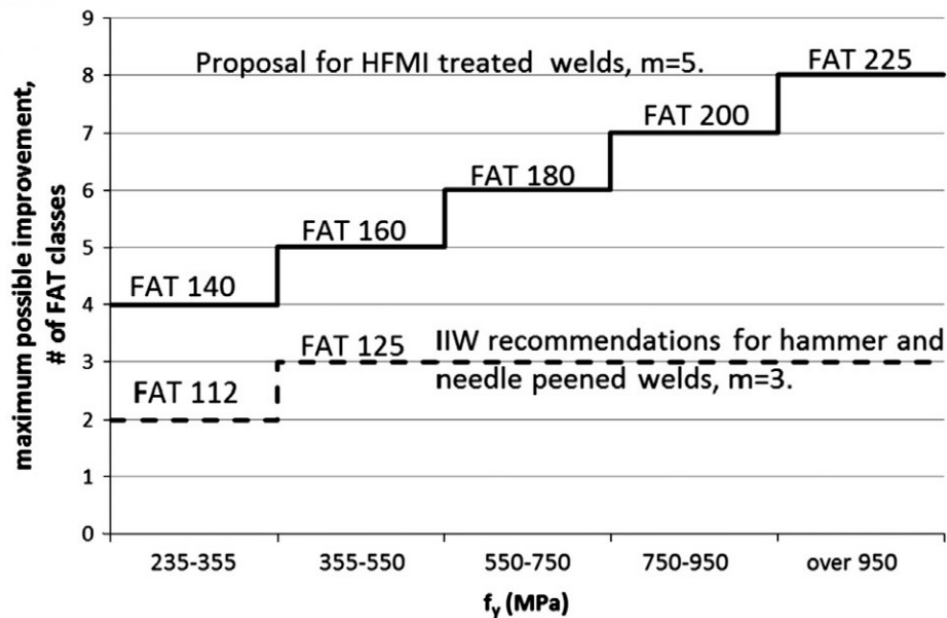


Figure 6.23: Proposed FAT values by HFMI for structural hot-spot stress approach as a function of f_y for load carrying fillet welds [59]

HFMI is also the residual stress method therefore stress ratio effect exists [35].

- if,
- $R < 0.15$: No reduction due to stress ratio
 - $0.15 < R \leq 0.28$: One FAT classes reduction
 - $0.28 < R \leq 0.4$: Two FAT classes reduction
 - $0.4 < R \leq 0.52$: Three FAT classes reduction
 - $0.52 < R$: No data available. The degree of improvement must be confirmed by testing.

Applying post weld improvements

In the previous section, increasing the flange thickness was discussed, and it was limited due to the specimen weight. Therefore the same S-N curve in Figure 6.16 is adopted. FAT class improvement by TIG dressing is the same as the grinding, and it is already performed in Figure 6.17. It is clear that weld geometry improvement methods are not enough.

Both hammer and needle peening have the same amount of improvement. Moreover, both methods have some limitation with stress ratio to deal with full stress range. Figure 6.24 considers $R < 0$ which the full benefit of improvement is taken into account. If stress ratio is larger than 0, then the improvement effect decreases as referred in Section 6.4.1.

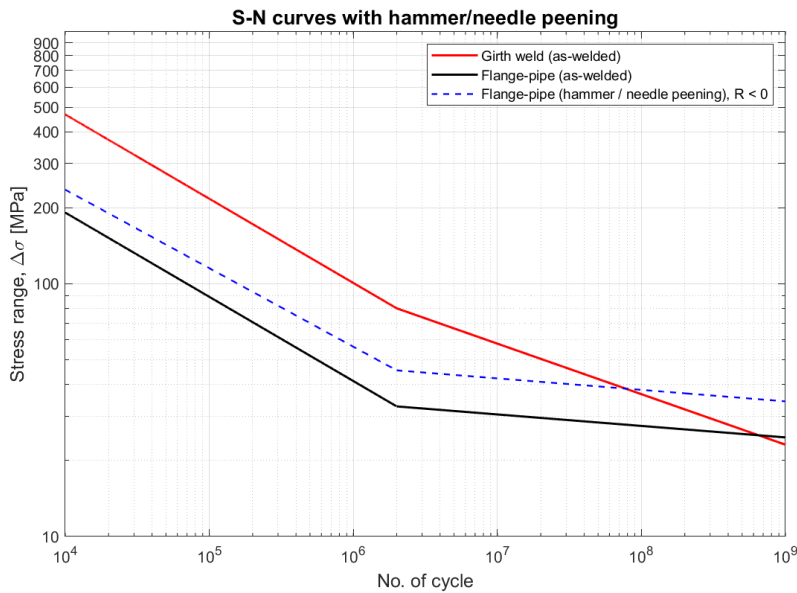


Figure 6.24: Modified S-N curve with hammer/needle peening

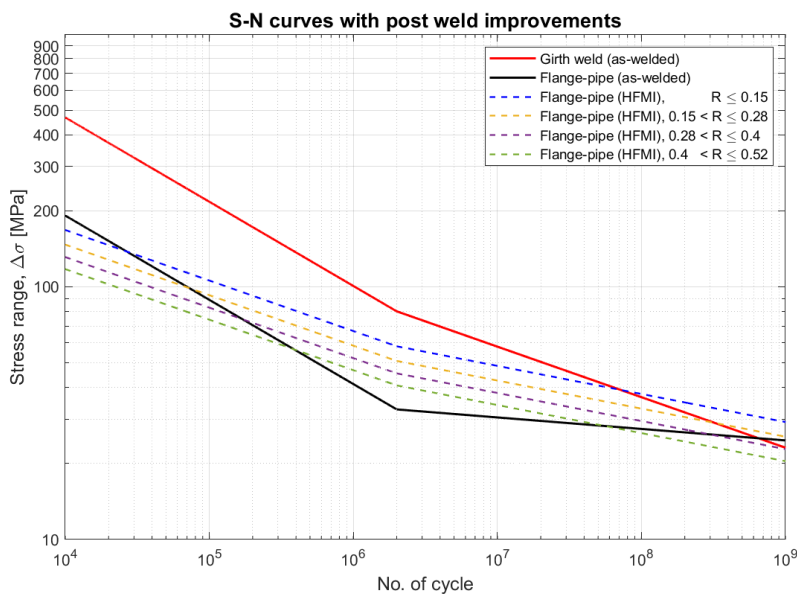


Figure 6.25: Modified S-N curve with HFMI for various stress ratios

In Figure 6.25, modified S-N curves by HFMI with various stress ratios are given. All the discussed improvement methods fail to provide a safe design for the flange-pipe weld connection. The first design option for the specimen does not satisfy the design criteria and is therefore unacceptable.

6.4.2. Specimen Design - Option 2

A second option is composed of a machined flange-pipe component and a pipe component connected by the girth weld. To assure better fatigue resistance at the flange-pipe connecting girth weld, machining of weld reinforcement at both sides, weld toe and root, is required.

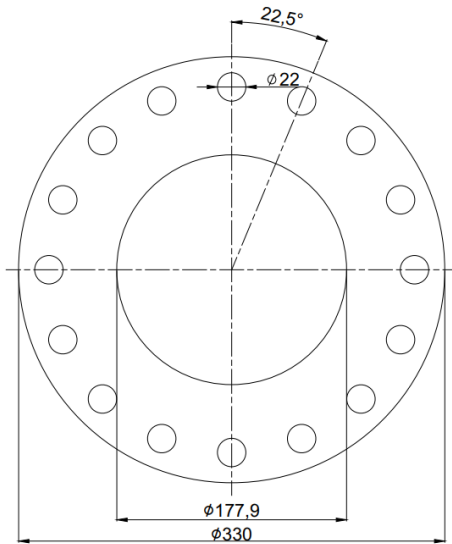


Figure 6.26: Top view of specimen

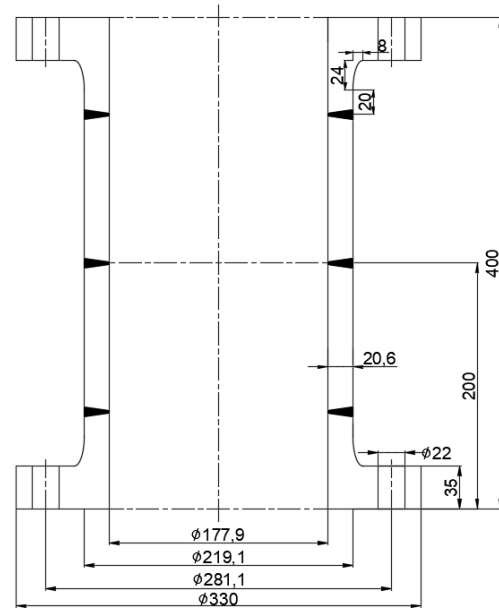


Figure 6.27: Specimen geometry

FE model

Same principles, i.e. contact mechanism, bolt modelling and loading condition are taken as previous FE analysis, see Section 6.4.1. The only difference is the local geometry of the connection part. Instead of straight fillet weld geometry, elliptical machined geometry is adopted.

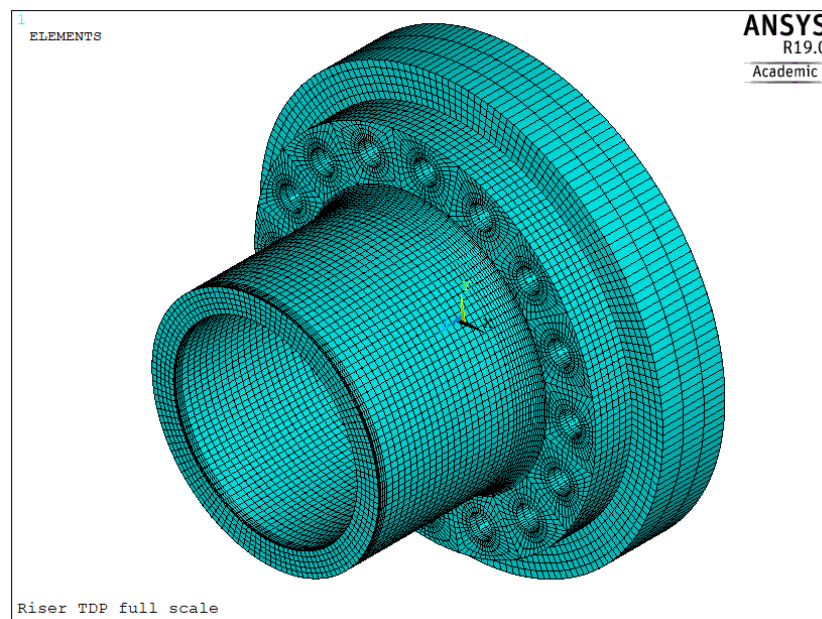


Figure 6.28: FE model of riser specimen with platform

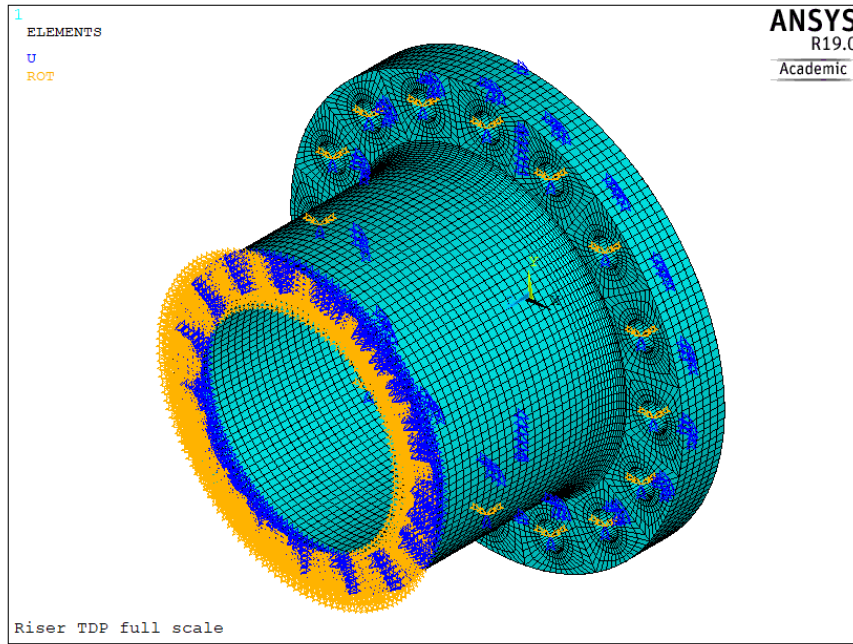


Figure 6.29: FE model of riser specimen without platform including boundary conditions (Blue: displacement constraint, Orange: rotation constraint)

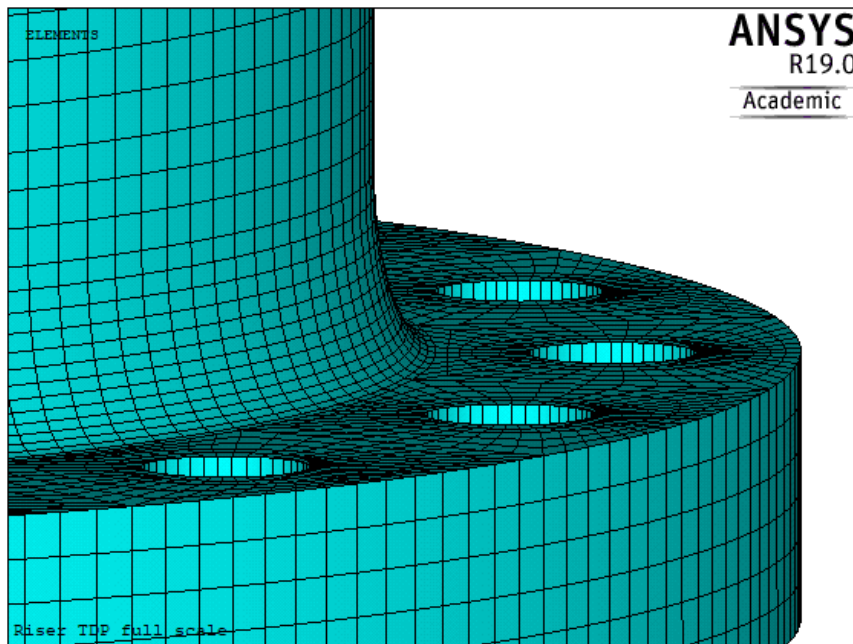


Figure 6.30: Machined flange-pipe transition location

Response

Same as the previous design, only bending loading condition is considered in here which is a major mode I fatigue loading condition. The target bending response is the 150[MPa] at the weld root of the middle girth weld. This design also needs sufficient specimen length due to the flange. However, a local geometry change at the connection is small. Thus the same length is taken as previous analysis, see Figure 6.33 and 6.34. Bending stress response of FEA is shown as below.

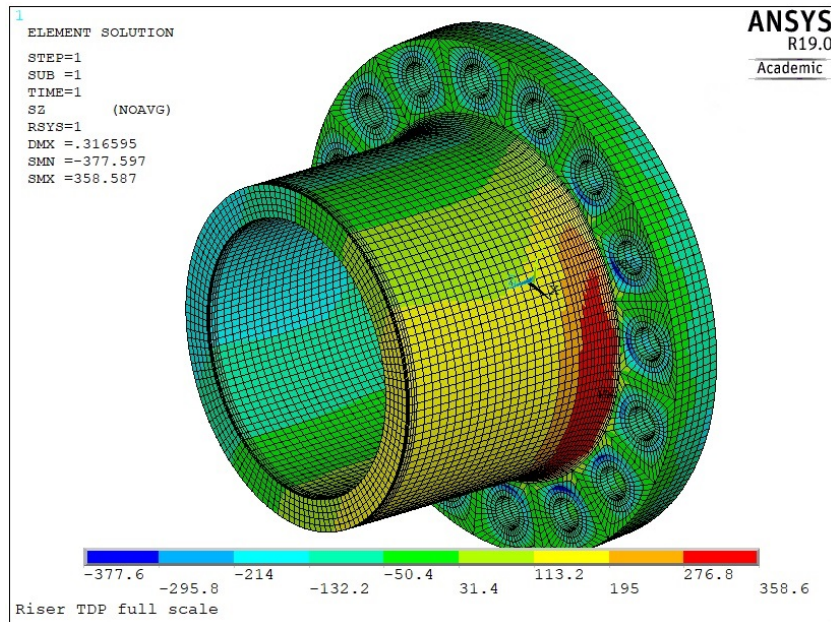


Figure 6.31: Bending stress distribution under pure bending

And a cross section of the specimen in FE result is following.

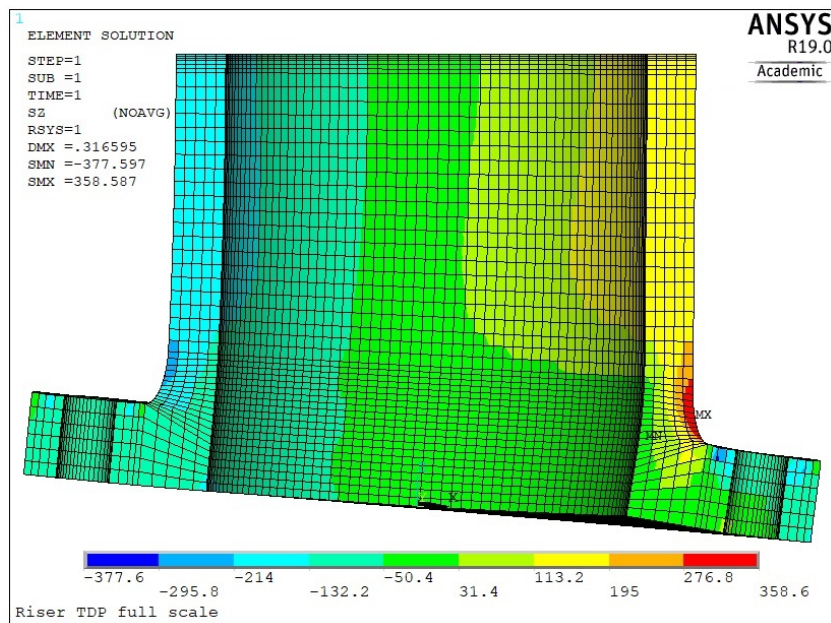


Figure 6.32: Cross sectional bending stress distribution under pure bending

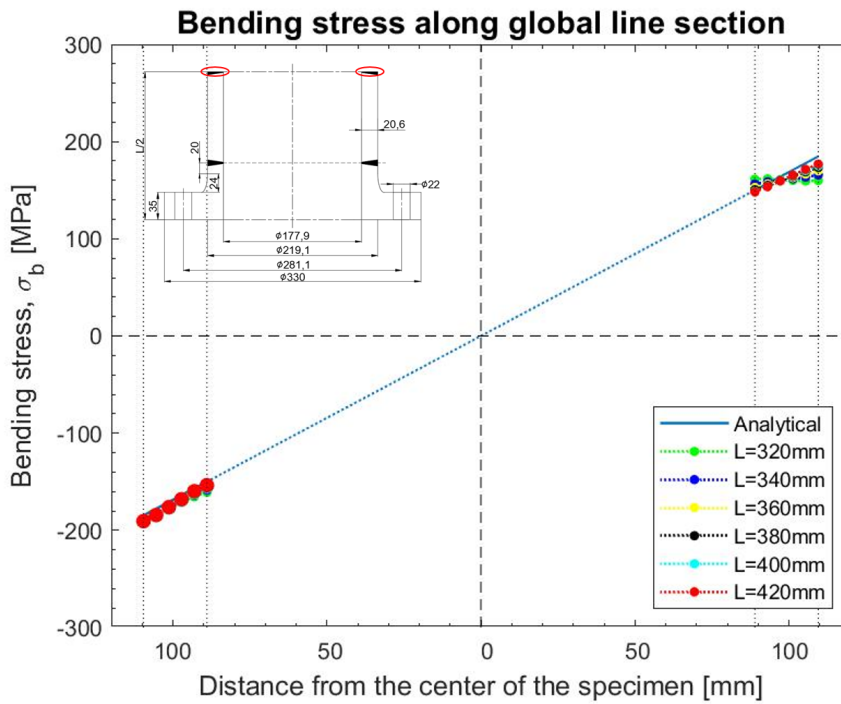


Figure 6.33: Bending stress at the middle cross section with various total length of specimens

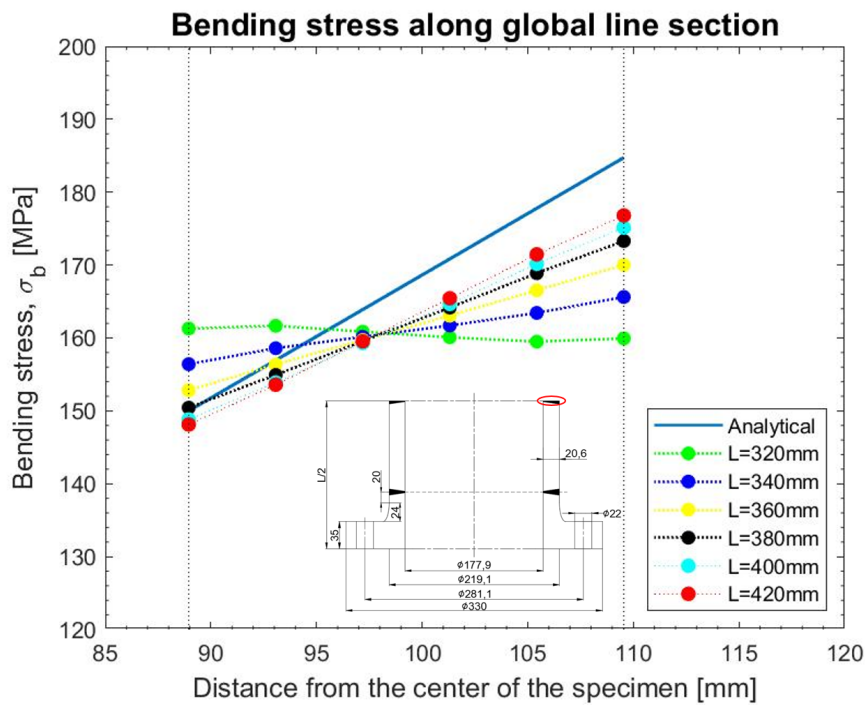


Figure 6.34: Zoomed plot of Figure 6.33

Nearly the same behaviour is observed compared to the first design option. Hence the same total specimen length as previous 400 [mm] is adopted for the analysis. The total weight of the full specimen is roughly 64.3[kg] including the flange. Finding a proper location of the first girth weld at the flange-pipe connection is essential to assure better fatigue resistance than the middle girth weld. A gap distance value from the end of the machined curvature to the first girth weld location is evaluated.

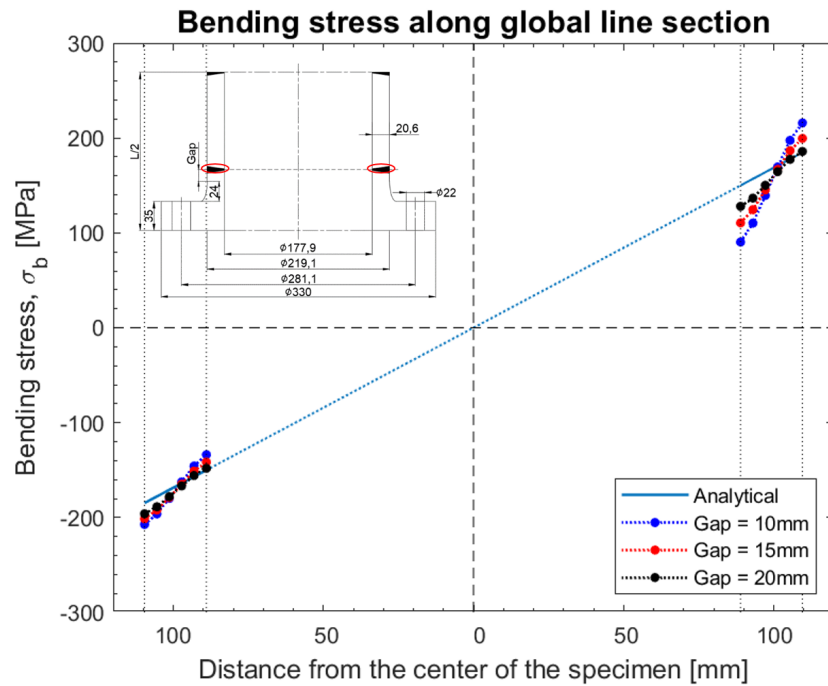


Figure 6.35: Bending stress at the middle cross section with several different 'Gap' values under fixed length of specimen

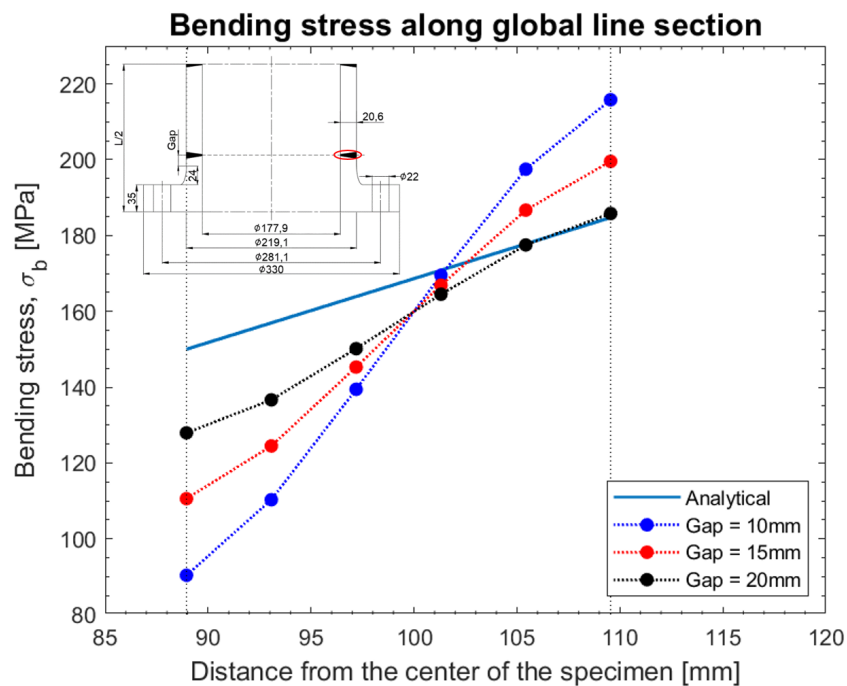


Figure 6.36: Zoomed plot of Figure 6.35

From the Figure 6.36, it is apparent that the increasing gap value leads to a very similar response as of the middle. In Figure 6.37, larger gap shows much lower stress concentration between two hot-spot locations. And similar as Figure 6.21, SCFs become convergent from the specimen length of 400 [mm] around double of the pipe diameter. The total specimen length of 400 [mm] and gap value of 20 [mm] which is similar to the pipe wall thickness are considered for the following fatigue resistance comparison between two fatigue sensitive locations.

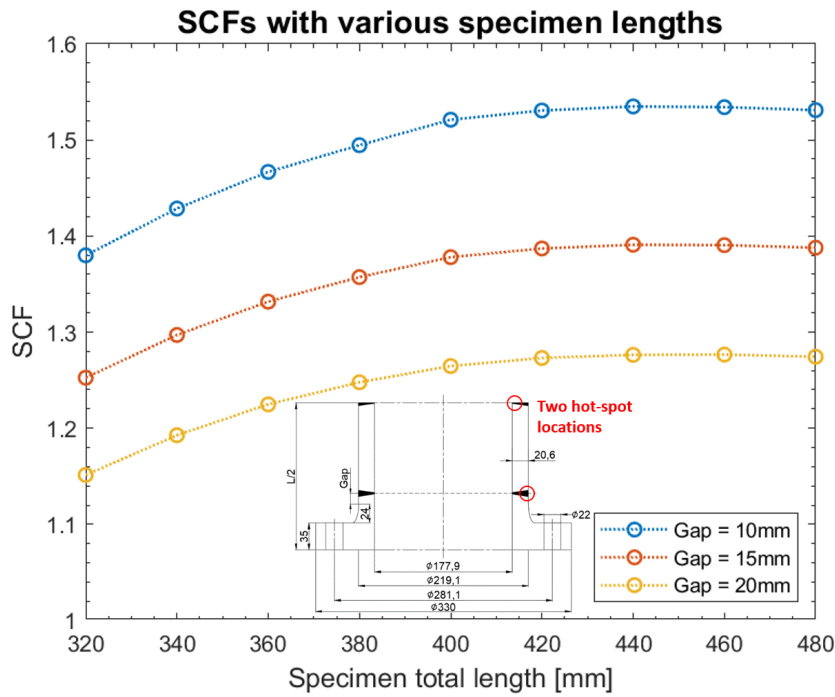


Figure 6.37: SCFs with various specimen lengths

Fatigue resistance

Similar to the previous design, the fatigue resistance comparison between the weld toe of the flange-pipe connection and weld root of the middle girth weld is required. Similarly, hot spot stress S-N curves of girth weld toe and root from DNV can be adopted[12].

S-N curve comparison From the DNVGL-RP-C203 [12], girth weld root with small misalignment is classified as FAT80 and girth weld toe is assigned as FAT90. Both S-N curves are based on as-welded and hot-spot stress, see Figure 6.38.

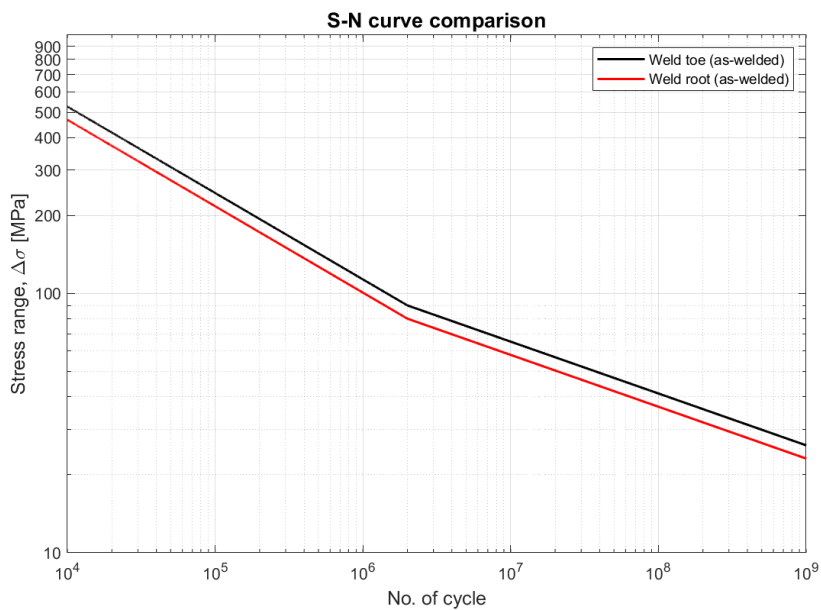


Figure 6.38: S-N curves of girth weld toe and root based on hot-spot stress

From the FE analysis, structural stress of 151.5 [MPa] at the weld root location and 189.1 [MPa] at the weld toe of flange-pipe connection girth weld are obtained. Taking the structural stress of weld root as reference stress then SCF at the weld toe of flange-pipe connection becomes 1.26. Same as the first design, a comparison between two S-N curves, S-N curve without correction for the weld root and factored S-N curve by SCF for the weld toe, is performed for flange-pipe connection, see Figure 6.39.

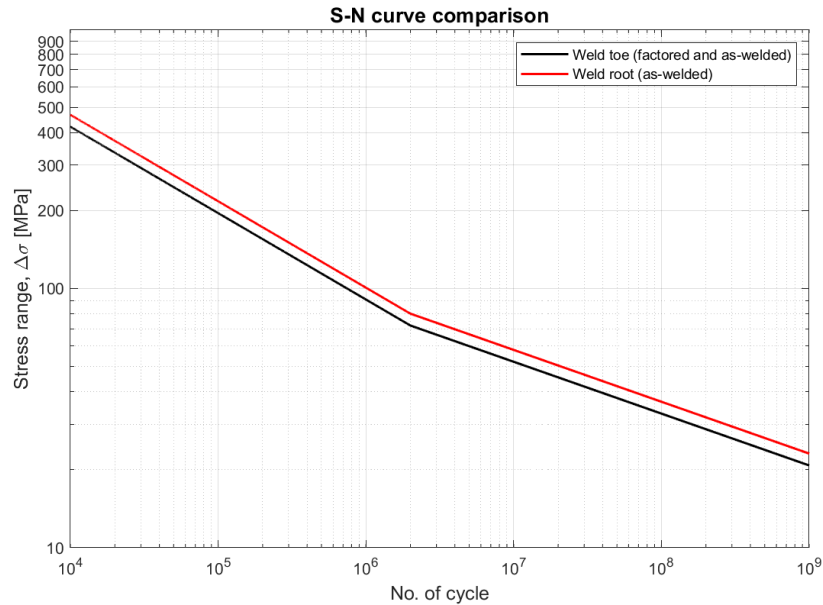


Figure 6.39: Factored S-N curve by SCF

The girth weld at the flange-pipe connection is slightly weaker than the girth weld at the middle of the specimen. Fortunately, the difference is rather small so post weld improvement can manage it. Most of the post weld improvement methods provide better fatigue resistance at the flange-pipe connection. Preferable methods are grinding and TIG dressing because they do not have a limitation with the stress ratio.

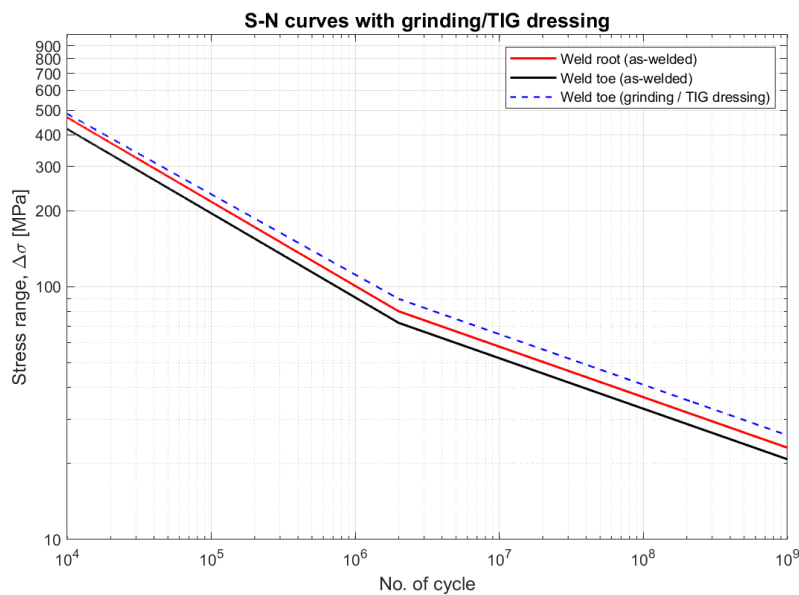


Figure 6.40: Modified S-N curve with grinding/TIG dressing

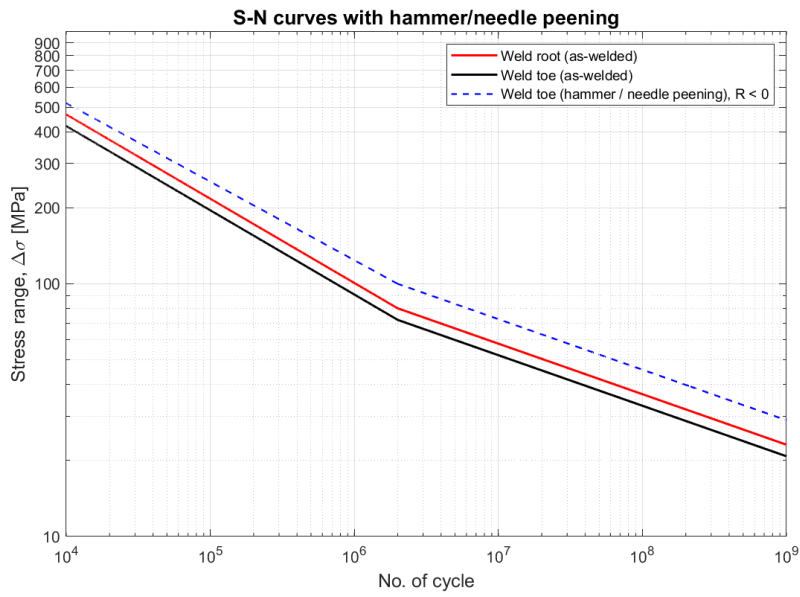


Figure 6.41: Modified S-N curve with hammer/needle peening

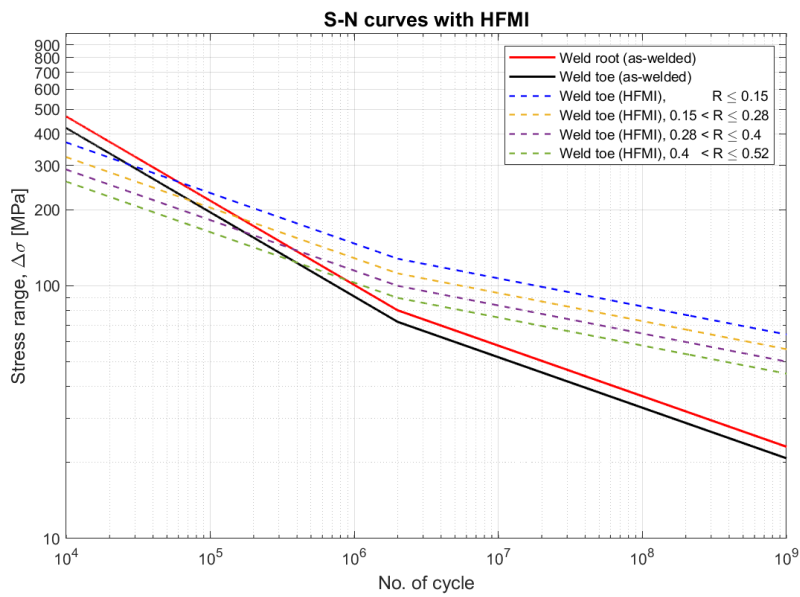


Figure 6.42: Modified S-N curve with HFMI for various stress ratios

Based on the investigation, it can be concluded that option 2 is fit for specimen design. The recommended specimen length is 400 [mm], similar to double of the diameter, and the gap length is 20 [mm], equal to the pipe wall thickness. Additionally, weld improvement technique like grinding or hammer peening must be performed both at weld toe and weld root side of the flange-pipe weld.

7

Conclusions

The weld load carrying stress is a characteristic one and unique for each weld notch. Also, it is the only unknown for the complete stress distribution through the thickness direction with the semi-analytic solution by Den Besten [9]. Especially the weld load carrying stress for the welded double-sided longitudinal attachment has been evaluated with two different methods the double weld element beam model and the parametric method.

The double weld element beam model for the DS longitudinal attachment has been developed based on the original double weld element beam model of the DS T-Joint and DS cruciform joint [17, 45]. It was possible to define the formulas for the weld load carrying stress coefficients C_{bm} and C_{bb} with the result of the beam model at particular nodes. The semi-analytic results of the weld toes stress distribution and the stress intensity factor using the C_{bw} from the double weld element beam model show reasonably good match with the solid FE results.

The parametric study concludes that the weld load carrying stress of the DS longitudinal attachment is only the function of the weld notch angle $f(h_w/l_w)$. Meaning the self equilibrating stress (V-shaped notch stress and the weld load carrying stress) is governed by the weld notch angle and the base plate thickness, i.e. size effect. The self equilibrating stress dominates the peak stress and the stress gradient near the weld notch related to the crack initiation and the micro crack growth. It is well known that the crack initiation life generally dominates the fatigue life of the intact structure. In this perspective, the base plate thickness t_b is a dominant parameter for the fatigue life of the DS longitudinal attachment rather than the attachment length l_a has been referred as the governing parameter in IIW recommendation. The attachment length l_a is still important because it is relating to the stress concentration which amplifies the equilibrium equivalent structural stress a.k.a. far field stress.

The published fatigue resistance data are performed with the nominal stress, the structural hot spot stress, and the total stress concept. Remarkably, the structural hot spot stress does not perform noticeable improvement compared to the nominal stress concept. Because the structural hot spot stress involves the attachment length effect, but it does not contain the thickness effect which is also a governing factor for the fatigue of the DS longitudinal attachment. The total stress concept performs a significant improvement, and it is apparent because the total stress concept considers the full stress distribution which contains the size effect, the structural stress which contains the attachment length effect, the mean stress effect, the notch affected micro crack growth, and the far field affected macro crack growth behaviours as well.

The FSS containing the critical single sided butt joint has been designed as well. The published fatigue test data for the SCR are generally from the resonance bending test performed with unrealistic mean stress and variable amplitude loading. For the realistic fatigue resistance data, dedicated specimen design is proposed for the Hexapod. Two design options are evaluated with FE solid models. The first option attaching flange by full penetration weld to the pipe segment is not relevant for the bending fatigue test even though considering the post weld improvement. The second option attaching the machined flange component to the pipe segment by the girth weld provides the critical fatigue resistance at the intended weld root location than the flange-pipe connection. A sufficient specimen length, double of the diameter, is necessary to avoid the stress

disturbance at the middle of the specimen due to the existence of the flange. Also, enough gap distance, equal to the pipe wall thickness, is needed between the end of the machined curvature and girth weld of flange-pipe connection. However, the post weld improvement is necessary to ensure the unintended fatigue failure appears at the flange-pipe connection.

Bibliography

- [1] AMOG. *Deep Water Installation of Steel Catenary Risers*. URL: <https://amog.consulting/verification/riser-system-design-verification>. Accessed: 26-04-2019.
- [2] API. "5L, Specification for Line Pipe". In: *Edition March* (2004).
- [3] Atzori, B., Lazzarin, P., and Meneghetti, G. "Fatigue strength assessment of welded joints: From the integration of Paris' law to a synthesis based on the notch stress intensity factors of the uncracked geometries". In: *Engineering Fracture Mechanics* 75.3-4 (2008), pp. 364–378.
- [4] Berto, F. "Crack Initiation at V-Notch Tip under In-Plane Mixed Mode Loading: A Review of the Fictitious Notch Rounding Concept". In: *Physical Mesomechanics* 18.4 (Oct. 2015), pp. 273–282. ISSN: 1990-5424. DOI: 10.1134/S1029959915040013. URL: <https://doi.org/10.1134/S1029959915040013>.
- [5] Berto, F., Lazzarin, P., and Radaj, D. "Fictitious notch rounding concept applied to sharp V-notches: Evaluation of the microstructural support factor for different failure hypotheses: Part II: Microstructural support analysis". In: *Engineering Fracture Mechanics* 76.9 (2009), pp. 1151–1175.
- [6] Cui, W. "A state-of-the-art review on fatigue life prediction methods for metal structures". In: *Journal of marine science and technology* 7.1 (2002), pp. 43–56.
- [7] Deguchi, T. et al. "Fatigue strength improvement for ship structures by Ultrasonic Peening". In: *Journal of marine science and technology* 17.3 (2012), pp. 360–369.
- [8] Den Besten, H. "Fatigue damage criteria classification, modelling developments and trends for welded joints in marine structures". In: *Ships and Offshore Structures* 13.8 (2018), pp. 787–808.
- [9] Den Besten, J. H. "Fatigue resistance of welded joints in aluminium high-speed craft: A total stress concept". PhD thesis. TU Delft, Delft University of Technology, 2015.
- [10] Den Besten, J. H. *Fatigue and Fracture in Marine Structures*. Feb. 2017.
- [11] Dimitrakis, S. and Lawrence, F. "Improving the fatigue performance of fillet weld terminations". In: *Fatigue & Fracture of Engineering Materials & Structures* 24.6 (2001), pp. 429–438.
- [12] DNVGL. "Fatigue Design of Offshore Steel Structures". In: *DNVGL-RP-C203* (2016).
- [13] DNVGL. *Structural Design of Offshore Floaters Day 4 – Fatigue Design*. 2016. URL: https://www.dnvgl.us/Downloads/TW16-OffshoreFloater_Fatigue_tcm14-80893.pdf. Accessed: 26-04-2019.
- [14] Dong, P. "A structural stress definition and numerical implementation for fatigue analysis of welded joints". In: *International Journal of Fatigue* 23.10 (2001), pp. 865–876.
- [15] Dong, P., Hong, J., and Cao, Z. "Stresses and stress intensities at notches: 'anomalous crack growth' revisited". In: *International journal of fatigue* 25.9-11 (2003), pp. 811–825.
- [16] Dong, P. et al. "Master SN curve method for fatigue evaluation of welded components". In: *Welding Research Council Bulletin* 474 (2002).
- [17] Donk, R. *Weld load carrying stress estimate for double sided cruciform joints*. TU Delft, Delft University of Technology, 2018.
- [18] Eurocode. "3, Design of steel structures - Part 1-9: Fatigue". In: EN 1993-1-9 (2005).
- [19] Fricke, W. "Recommended Hot Spot Analysis Procedure for Structural Details of FPSOs and Ships Based on Round-Robin FE Analyses". In: *11th Int. Offshore Polar Eng. Conf.* IV.9 (2001), pp. 1098–6189.
- [20] Hobbacher, A. *Recommendations for fatigue design of welded joints and components*. Springer, 2016.
- [21] Huo, L., Wang, D., and Zhang, Y. "Investigation of the fatigue behaviour of the welded joints treated by TIG dressing and ultrasonic peening under variable-amplitude load". In: *International journal of Fatigue* 27.1 (2005), pp. 95–101.

- [22] Janssen, M., Zuidema, J., and Russell, W. *Fracture Mechanics(2nd ed.)* Delft University Press, 2002, p. 312. ISBN: 90-407-2221-8.
- [23] Kainuma, S. et al. "Fatigue behaviour of out-of-plane gusset joints with one-side fillet weld". In: *Welding International* 29.12 (2015), pp. 913–921.
- [24] Kang, S. and Kim, W. "A proposed SN curve for welded ship structures". In: *WELDING JOURNAL-NEW YORK*- 82.7 (2003), 161–S.
- [25] Kawano, H. and Inoue, K. "A local approach for fatigue strength evaluation on ship structures". In: *Technical Research Centre of Finland, Fatigue Design 1992, Volume 1*. Vol. 1. 1992.
- [26] Kim, I.-T. "Fatigue strength improvement of longitudinal fillet welded out-of-plane gusset joints using air blast cleaning treatment". In: *International journal of fatigue* 48 (2013), pp. 289–299.
- [27] Kim, I.-T. et al. "Fatigue Resistance Improvement of Welded Joints by Bristle Roll-Brush Grinding". In: *International Journal of Steel Structures* (2018), pp. 1–8.
- [28] Kim, W. and Lotsberg, I. "Fatigue test data for welded connections in ship-shaped structures". In: *Journal of Offshore Mechanics and Arctic Engineering* 127.4 (2005), pp. 359–365.
- [29] Lazzarin, P. and Tovo, R. "A unified approach to the evaluation of linear elastic stress fields in the neighborhood of cracks and notches". In: *International Journal of Fracture* 78.1 (1996), pp. 3–19.
- [30] Lazzarin, P. and Tovo, R. "A notch intensity factor approach to the stress analysis of welds". In: *Fatigue & fracture of engineering materials & structures* 21.9 (1998), pp. 1089–1103.
- [31] Lee, C.-H. et al. "Effect of weld geometry on the fatigue life of non-load-carrying fillet welded cruciform joints". In: *Engineering Failure Analysis* 16.3 (2009), pp. 849–855.
- [32] Maddox, S. et al. "Improving the fatigue performance of welded stainless steels". In: *EUR* 22809 (2007), pp. 1–190.
- [33] Maddox, S. J., Doré, M., and Smith, S. D. "A case study of the use of ultrasonic peening for upgrading a welded steel structure". In: *Welding in the World* 55.9-10 (2011), pp. 56–67.
- [34] Marquis, G. "Long life spectrum fatigue of carbon and stainless steel welds". In: *Fatigue & Fracture of Engineering Materials & Structures* 19.6 (1996), pp. 739–753.
- [35] Marquis, G. B. and Barsoum, Z. *IIW recommendations for the HFMI treatment*. Springer, 2017.
- [36] Neuber, H. *Kerbspannungslehre (Theory of notch stresses: principles for exact stress calculation)*. 1937.
- [37] Niemi, E. *Stress determination for fatigue analysis of welded components*. Woodhead Publishing, 1995.
- [38] Niemi, E., Fricke, W., and Maddox, S. J. *Fatigue analysis of welded components: Designer's guide to the structural hot-spot stress approach*. Woodhead Publishing, 2006.
- [39] Ohta, A. "Fatigue strength improvement of box welds by low transformation temperature welding wire and PWHT". In: *Welding in the World* 44.3 (2000), pp. 52–56.
- [40] Palkar, S. *Steel Catenary Riser endurance examination*. Technical report. TU Delft, Delft University of Technology, 2017.
- [41] Pascual, F. G. and Meeker, W. Q. "Estimating fatigue curves with the random fatigue-limit model". In: *Technometrics* 41.4 (1999), pp. 277–289.
- [42] Peterson, R. "Methods of correlating data from fatigue tests of stress concentration specimens". In: *Stephen Timoshenko Anniversary Volume* (1938), p. 179.
- [43] Pook, L. *Why Metal Fatigue Matters*. Springer, 2007.
- [44] Qin, Y. *Weld load carrying level determination formula*. Technical report. TU Delft, Delft University of Technology, 2019.
- [45] Qin, Y., Den Besten, H., and Kaminski, M. "Rapid calculation of stress intensity factors". In: *Ships and Offshore Structures* (submitted).
- [46] Radaj, D., Sonsino, C. M., and Fricke, W. *Fatigue assessment of welded joints by local approaches*. Woodhead publishing, 2006.
- [47] Schijve, J. *Fatigue of structures and materials*. Springer Science & Business Media, 2001.

- [48] Sonsino, C. et al. "Notch stress concepts for the fatigue assessment of welded joints—Background and applications". In: *International Journal of Fatigue* 34.1 (2012), pp. 2–16.
- [49] Sshimokawa, H. et al. "Fatigue strengths of large-size gusset joints of 800 mpa class steels". In: *Doboku Gakkai Ronbunshu* 1985.356 (1985), pp. 279–287.
- [50] subsea7. *Deep Water Installation of Steel Catenary Risers*. 2012. URL: <https://www.subseauk.com/documents/presentations/installation%09%20of%20scrs%20subsea%20asia%203rd%20oct%202012.pdf>. Accessed: 26-04-2019.
- [51] Sun, C. and Jin, Z.-H. *Fracture Mechanics*. 2012, p. 312. ISBN: 9780123850010.
- [52] Tada, H., Paris, P., and Irwin, G. *The Stress Analysis of Cracks Handbook (3rd ed.)* ASME Press, 2000. ISBN: 9780791801536.
- [53] Togasaki, Y. et al. "Effect of UIT on fatigue life in web-gusset welded joints". In: *Journal of Solid Mechanics and Materials Engineering* 4.3 (2010), pp. 391–400.
- [54] Uchida, D., Mori, T., and Sasaki, Y. "Influence of grinding depth on fatigue strength of out-of-plane gusset joints with finished weld toes". In: *Kou koushou rombunshuu* 23.89 (2016), pp. 51–58. DOI: 10.11273/jssc.23.89_51.
- [55] Weich, I. "Fatigue behaviour of mechanical post weld treated welds depending on the edge layer condition (Ermüdungsverhalten mechanisch nachbehandelter Schweißverbindungen in Abhängigkeit des Randschichtzustands)". PhD thesis. Technischen Universität Carolo-Wilhelmina, 2008.
- [56] Williams, M. "Stress singularities resulting from various boundary conditions in angular corners of plates in extension". In: *Journal of applied mechanics* 19.4 (1952), pp. 526–528.
- [57] Xiao, Z.-G. and Yamada, K. "A method of determining geometric stress for fatigue strength evaluation of steel welded joints". In: *International Journal of Fatigue* 26.12 (2004), pp. 1277–1293.
- [58] Yamada, K. et al. "Fatigue analysis based on crack growth from toe of gusset end weld". In: *Proceedings of the Japan Society of Civil Engineers*. Vol. 1980. 303. Japan Society of Civil Engineers. 1980, pp. 31–41.
- [59] Yildirim, H. C., Marquis, G. B., and Barsoum, Z. "Fatigue assessment of high frequency mechanical impact (HFMI)-improved fillet welds by local approaches". In: *International Journal of Fatigue* 52 (2013), pp. 57–67.

